Environmental Influences on the Frequency and Intensity of North Indian Ocean Tropical Cyclones

Krishna Mohan. K. S

Department of Atmospheric Sciences

Cochin University of Science and Technology

Thesis submitted in partial fulfilment for the award of

Doctor of Philosophy

in

Atmospheric Sciences

Under the

Faculty of Marine Sciences

February 2013

Declaration

I herewith declare that the thesis entitled **Environmental Influences on the Frequency and Intensity of North Indian Ocean Tropical Cyclones** is an authentic record of research work carried out by me under the supervision and guidance of Prof. (Dr). K. Mohanakumar, Department of Atmospheric Sciences, Cochin University of Science and Technology, towards the partial fulfilment of the requirements for the award of Ph.D degree under the Faculty of Marine Sciences and no part thereof has been presented for the award of any other degree in any University/Institute.

Krishna Mohan. K. S
Registration Number: **3708**
Department of Atmospheric Sciences
Cochin University of Science & Technology
Cochin - 682016
India

Certificate

This is to certify that this thesis entitled **Environmental Influences on the Frequency and Intensity of North Indian Ocean Tropical Cyclones** is an authentic record of research work carried out by Mr. Krishna Mohan. K. S, under my supervision and guidance at the Department of Atmospheric Sciences, Cochin University of Science and Technology, towards the partial fulfilment of the requirements for the award of Ph.D degree under the Faculty of Marine Sciences and no part thereof has been presented for the award of any other degree in any University/Institute.

Prof. (Dr). K. Mohanakumar
Supervising Guide
Department Atmospheric Sciences
Cochin University of Science & Technology
Cochin - 682016
India

Acknowledgements

I take this opportunity to express my profound gratitude and deep regards to my guide Prof. (Dr). K. Mohanakumar, Department of Atmospheric Sciences, Cochin University of Science and Technology, for his guidance, constant encouragement and support, which enabled me to complete this thesis. I am especially grateful to him for the freedom given to me to select the topic and methodology to be adopted. Without his guidance, support and encouragement, this thesis would not have materialized.

I am deeply indebted to Prof P. V Joseph, Emeritus Professor, Department of Atmospheric Sciences, for his great support during the course of this thesis work. He has been a great mentor, with his never ending enthusiasm, encouraging attitude has consistently inspired and motivated my approach to the research. His support and endless insight, during the the course of this thesis work have been invaluable.

I acknowledge all the support and help rendered to me by Dr. C. A. Babu Head, Department of Atmospheric Sciences, for his valuable advices and for providing the necessary facilities and encouragement throughout the course of research. I extend my thanks to Prof. H. S, Ram Mohan, Dr. K. R Santosh, Sri. B. Chakrapani and Dr. V. Madhu Department of Atmospheric Sciences for their support.

I sincerely thank Dr. K. Kerala Varma, Department of Physical Oceanography, for his encouragement and providing critical insights towards improvement of the thesis. I extend my thanks to Dr. R. Sajeev, Dr. A. N. Balchand and Sri. P. K. Saji of Department of Physical Oceanography.

I would like to express my heartfelt gratefulness to Alice teacher, wife of Dr. P. V. Joseph, for her care and hospitality. My thanks are due to Dr. Mrudula, Dr Venu. G. Nair, Dr. Sreedevi, and Dr. G. Bindu for their support all occasions. I thank the Mr Yeshodharan, Mr. Rajesh and other non-teaching staffs of Department of Atmospheric Sciences for their help.

My heartfelt thanks to my dearest friends Vijith, Phiros Shah, Akhilesh Vijay, Shaiju, Gireeshkumar, Deepu, Sarin, Hasseb, Jayesh, Raneesh, Hari Krishnan,

Arun, Asha Babu and Niroop for the warm friend ship and love which has been a pillar of strength in all the challenges during these years.

I am indebted to Jayaram Chiranjivi and Johnson Zacharia for the academical and personal support they extended during the years. I extend my thanks to my lab-mates Dr. Prasanth. A. Pillai, Dr. Rajesh, Dr. Lorna, Dr. Abish, Jayakrishnan, Sivaprasad, Dr. Nithin Vishwambharan, Vijayakumar, Reshmi, Shinu and Sudeep for their support and encouragement. My sincere thanks to Dr. Thara and Gopika of Department of Physical Oceanography for their support during the course of the thesis.

I sincerely thank the support extended by my seniors and juniors of Cochin University of Science and Technology, hostel-mates, M.Sc classmates, B.Sc classmates and all other friends for the moral support, encouragement and help they rendered throughout my career.

I thank Cochin University of Science and Technology for providing me with all the facilities and Council of Scientific and Industrial Research, Government of India for providing me the financial support through its fellowship.

I gratefully acknowledge the providers of scientific datasets who put in untiring efforts to bring out quality data products used in this thesis. I extend my thanks to the providers of the scientific softwares used in this thesis.

I express my gratefulness towards my mother, my brother, my grandmother, my uncle and other family members who gave me unconditional love and support throughout my life and have enabled me to achieve this goal. I would like to make a special mention of my wife Aswathy, for her moral support and encouragement during the course of my work.

Last but not the least my sincere gratitude to everyone who reads the thesis. This gives me a sense of accomplishment that all my efforts were not in vain.

Preface

Tropical cyclones genesis, movement and intensification are highly dependent on its environment both oceanic and atmospheric. This thesis has made a detailed study on the environmental factors related to tropical cyclones of North Indian Ocean basin. This ocean basin has produced only 6% of the global tropical cyclones annually but it has caused maximum loss of human life associated with the strong winds, heavy rain and particularly storm surges that accompany severe cyclones as they strike the heavily populated coastal areas.

Atmospheric factors studied in the thesis are the moisture content of the atmosphere, instability of the atmosphere that produces thunderstorms which are the main source of energy for the tropical cyclone, vertical wind shear to which cyclones are highly sensitive and the Sub-Tropical westerly Jetsteram and its Asian high speed center. The oceanic parameters studied are sea surface temperature and heat storage in the top layer of the ocean. A major portion of the thesis has dealt with the three temporal variabilities of tropical cyclone frequency namely intra-seasonal (mainly the influence of Madden Julian Oscillation), inter-annual (the relation with El Nino Southern Oscillation) and decadal variabilities. Regarding decadal variability, a prominent four decade oscillation in the frequency of both tropical cyclones and monsoon depressions unique to the Indian Ocean basin has been brought out.

The thesis consists of 9 chapters. The first chapter 'Introduction' has given a detailed review of the available literature on tropical cyclones as relevant to this thesis. The climatology of tropical cyclones and the environmental parameters of North Indian Ocean basin have been described. Details of the datasets used in this thesis are given in chapter-2. The temporal variabilities associated with tropical cyclones are studied in chapters 3 to 5. The influence of Madden-Julian Oscillation of period ranging from 30 to 60 days on the genesis of tropical cyclones is discussed in chapter-3. One of the main findings is that the cyclone genesis preferentially occurs in the convective phase of Madden-Julian Oscillation. One of the major global factors creating inter-annual variations in atmospheric circulation and climate is the El Nino Southern Oscillation phenomenon whose period

ranges from 2 to 7 years. The inter-annual variations in the tropical cyclones particularly its genesis, movement and intensity associated with El Nino Southern Oscillation have been studied in chapter-4. A very important finding of the thesis is the establishment of a four decade oscillation in the tropical cyclones and monsoon depressions unique to the North Indian Ocean basin. Its association with sea surface temperature and the lower tropospheric wind particularly the low level Jetstream of the monsoon season has been brought out.

Cyclones intensify through several stages like severe cyclone, very severe cyclone (hurricane intensity) and super cyclones. The maximum potential intensity (MPI) of a tropical cyclone is dependent on the characteristics of the oceanic and atmospheric environment. Chapter-6 has studied the MPI of tropical cyclones of North Indian Ocean and the actual intensification of the cyclones with respect to MPI. Several factors are found related to the intensification of the cyclones of this basin like sea surface temperature, vertical wind shear in the atmosphere, temperature of the cyclone outflow region in the upper troposphere, translation speed of the cyclone over the ocean which controls the absorption of heat and moisture fluxes from the ocean and lastly very important for the land locked North Indian Ocean basin, the life duration of the cyclone.

Cyclone Gonu became a super cyclone on 4th June 2007 when it was located in the Arabian Sea. It is the first cyclone which attained super cyclone intensity in the Arabian Sea during the period of available observations spanning more than a century. Chapter-7 has given a detail case study of the intensification process of cyclone Gonu which occurred along with the summer monsoon onset over India that year. Positive sea surface height anomalies (SSHA) which are areas of high heat storage in the top layer of the ocean is found important for the rapid intensification of cyclone Gonu. The heat storage in these warm SSHA eddies are extracted by the deep moist convection in the central region of the cyclone that helped in the rapid intensification of the cyclone.

The Sub Tropical Jetstream (STJ) and the troughs associated with it have been studied in several ocean basins as associated with the movement and intensification of tropical cyclones. There are very few studies on the association of the high speed center (HSC) of STJ in the intensification of the cyclones. Chapter-8 has studied the important role played by the Asian HSC on the intensification of

northward moving cyclones of Bay of Bengal. As the cyclone moves north over the Bay, two features happen (a) the intensification of the cyclone when it enters the divergent right entrance region of the HSC and (b) in turn the strengthening of the HSC winds by the interaction with the cyclone heat source. Chapter-9 has given the summary and conclusions of this thesis. Important findings of this thesis have been highlighted in this chapter.

To ...My family, teachers and friends...

Contents

List of Figures

List of Tables

Abbreviations

ENSO - El Nino Southern Oscillation

EMPI - Emanuel Maximum Potential Intensity

FDO - Four-Decadal Oscillation

GPI - Genesis Potential Index

HSC - High Speed Center

HFP - High Frequency Period

IOD - Indian Ocean Diople

LLJ - Low Level Jetstream

LFP - Low Frequency Period

MJO - MaddenJulian Oscillation

MPI - Maximum Potential Intensity

MMPI - Modified Maximum Potential Intensity

NIO - North Indian Ocean

OLR -OLR Outgoing Longwave Radiation

SST - Sea Surface Temperature

SSHA - Sea Surface Height Anomaly

STJ - Sub Tropical Jetstream

TEJ - Tropical Easterly Jetstream

VIM - Vertically Integrated Moisture

VWS - Vertical Wind Shear

Chapter 1

Introduction

1.1 General details

Tropical cyclones are synoptic scale low pressure systems which form over the warm tropical oceans characterized by strong cyclonic winds and organized convection with heavy rainfall. These warm core systems are driven by the latent heat energy released in the convective clouds in their central regions. A tropical cyclone generates surface winds which exceed 17 ms^{-1} (33 knots); in extreme cases winds reach 90 ms^{-1} (175 knots). Tropical cyclone with its tremendous fury and destructive power has been a disastrous event for the people in coastal areas and ships on high seas throughout the history of human race.

Tropical cyclones can impact over a wide area with its strong winds, heavy rains and storm surges. The greatest damage to life and property is from the storm surges associated with the cyclone, where as the storm approaches the coast, sea level raises rapidly and the sea enters land. Death toll in a single cyclone has reached very high figures, for example a cyclone in November 1970 which had landfall over Bangladesh coast killed nearly 300,000 people. In areas such as north Bay of Bengal, high storm surges occur due to the prevailing bathymetry. Eight of the ten deadliest tropical cyclones globally have occurred in the Bay of Bengal and the Arabian Sea with five impacting Bangladesh and three making landfall in India (WMO, 2010). In the recent years, during the 2005 Atlantic hurricane season, tropical cyclones *Katrina*, *Rita* and *Wilma* dev-

astated the North American continent causing about 4000 deaths; these storms were accompanied by huge damage in the coastal areas.

The life duration of tropical cyclones range from several days to several weeks. A typical mature tropical cyclone has a low pressure central region called the 'core' region which in a severe cyclone develops an 'eye' of radius 5 to 30 km surrounded by a ring of cumulonimbus clouds of radial width 10-15 kms called the 'wall cloud' (see figure 1.1). In the severest of cyclones the atmospheric pressure inside the eye is about 10% lesser than that outside the cyclone at sea level. With the friction in the atmospheric boundary layer winds are forced to flow inward cyclonically (anti-clockwise in Northern Hemisphere and clockwise in Southern Hemisphere) spiralling up to the wall cloud in the lower levels of the atmosphere. At the wall cloud there is strong upward motion field which takes the warm moist air upward in cumulonimbus clouds. In the upper troposphere the mass flux from the central region of the cyclone is outward. The strongest radial inflow of the cyclone occurs in the layer between surface and 850 hPa, while the strongest outflow occurs between 300 and 100 hPa. The inflowing air creates spiral bands of cumulonimbus clouds from a radial distance of about 300 kms to the wall cloud. Maximum wind and rainfall in a tropical cyclone is in the wall

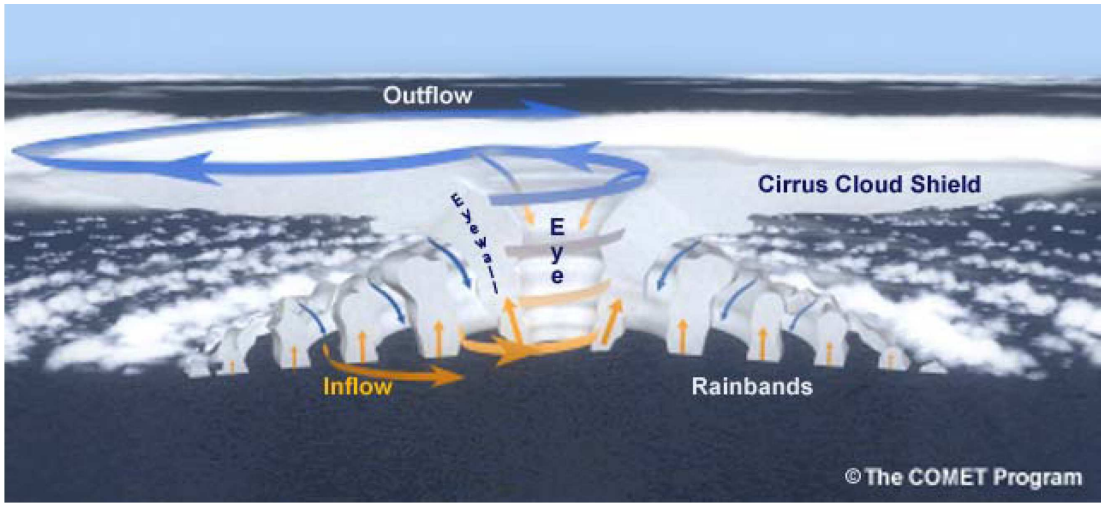

Figure 1.1: Vertical cross-section of a typical tropical cyclone; image source *The Comet Program*.

cloud region. In the troposphere, the cyclonic winds can extend more than 1000 km from the center of the cyclone. Tropical cyclones have radii ranging from 800 to 1500 kilometers. Cyclones of North Indian Ocean are smaller in radial size (typically 800 kms) compared to those in the Atlantic and Pacific Oceans. The outflow layer (300 to 100 hPa) consists of a small cyclonic central region of radius 200 to 300 kms surrounded by a large anticyclonic vortex. The central region of the tropical cyclone has a warm core with the eye having the highest temperature. The measured temperature anomaly in the eye region compared to the mean tropical atmosphere is about 10°C in the lower troposphere and 15° to 18°C in the upper troposphere in very severe cyclones.

Tropical cyclones are classified into different categories according to the maximum sustained surface wind speed attained in the core region (wall cloud) or the minimum pressure reached in the eye of the cyclone (pressure drop of the cyclone). The generic name *tropical cyclone* is used when the observed maximum sustained wind speed is 17 ms^{-1} (34 knots) or more. For measuring the maximum sustained wind speed, different averaging time periods are used around the world. The World Meteorological Organization (WMO) convention is to measure 10 minute average surface wind speed but the United States is following a 1 minute averaging. For the North Indian Ocean Cyclones India Meteorological Department uses a 3 minute averaging.

1.2 Classification of low pressure systems

Differences exist in nomenclature of tropical low pressure systems in different ocean basins. In general tropical low pressure systems with maximum sustained surface wind below 34 knots are called *tropical depressions*. If the maximum wind is 34 knots and above, the system is referred as a *tropical storm* in North Atlantic and North Pacific but is called as a *cyclonic storm* in the North Indian Ocean and a *moderate tropical storm* in the Southwest Indian Ocean. Once the system reaches maximum wind of 64 knots and more, it is called *hurricane* in the Atlantic, *Typhoon* in the Western North Pacific and *Very Severe tropical cyclones* in North Indian Ocean. Tropical cyclones in North Indian Ocean are classified into four major categories based on maximum sustained surface wind

Table 1.1: Classification of low pressure systems in North Indian Ocean

Type	MWS (knots)	T number
Low Pressure Area	< 17	1.0
Depression	17-27	1.5
Deep Depression	28-33	2.0
Cyclonic Storm	34-47	3.0
Severe Cyclonic Storm	48-63	3.5, 4.0
Very Severe Cyclonic Storm	64-119	4.0, 6.0
Super Cyclonic Storm	119>	6.0 >

by India Meteorological Department (IMD). They are *cyclonic storm* (CS) when the wind speed ranges from 34 to 47 knots, *severe cyclonic storm* (SCS) from 48 to 63 knots, *very severe cyclonic storm* (VSCS) from 64 to 119 knots and *super cyclonic storm* (SUCS) above 119 knots.

Tropical cyclones in all the ocean basins show great similarities in their structure and organisation. By comparing characteristics of the central cloud area, the eye and the spiral cloud bands of cyclones as abstracted from satellite cloud pictures with the reconnaissance aircraft measurements of maximum wind speed of the cyclone, Dvorak (1975) derived a method of estimating the intensity of a tropical cyclone on a T-number scale of 1 to 8. Each T-number has a corresponding maximum wind speed. For a cyclone of maximum wind speed 34 knots the T-number is 2.5, for a very severe cyclone (hurricane intensity) it is 4 and a super cyclone has a T-number of 6.5. A few North Indian ocean cyclones have reached intensity of T-7 (maximum wind speed=140 knots) in the last 100 years; that is the highest for this ocean basin. In Atlantic and Pacific oceans cyclones have reached intensity of T-8 (maximum wind speed=170 knots). The complete list of the classification followed by IMD of low pressure systems is given in table 1.1 which also give the associated T number.

1.3 Tropical cyclone climatology

A detailed climatology of the tropical cyclones in the global ocean basins was prepared by Gray (1979). He found that in a year about 80 tropical cyclones form globally of which half to two thirds reach hurricane strength (maximum sustained winds greater than 33 ms^{-1}). About two thirds of all cyclones occur in the Northern Hemisphere. Similarly about two thirds of tropical cyclones form in the eastern (which includes North Indian Ocean) as compared to the Western Hemisphere. Only about 13% of the cyclones form pole-ward of 20° latitude and nearly all these occur in the Northern Hemisphere. Cyclone genesis generally does not occur near the equator in the latitude belt 5°S to 5°N. Gray (1979) found that globally tropical cyclones occur in 7 ocean basins - Northeast Pacific, Northwest Pacific, Northwest Atlantic, North Indian Ocean, South Indian Ocean, Australian Seas and South-west Pacific (of which 4 are in the Northern Hemisphere). Figure 1.2 represents the global distribution of tropical cyclone genesis, one dot for each cyclone of a 20 year period (1970 - 1989) taken from Wallace and Hobbs (2006). Figure 1.3 gives the tracks of cyclones of a 60 year period from 1947 to 2007 (Knapp et al, 2010). After their genesis cyclones move westwards initially and then re-curve towards the poles of each hemisphere. The distribution of the mean annual number of cyclones (about 80) among the 7 ocean basins are given in table 1.2. North Indian Ocean accounts for only about 6% of the global cyclones but human fatalities have been maximum in this basin.

1.4 Environmental parameters influencing cyclone genesis

Formation of a tropical cyclone depends on mesoscale and synoptic scale interactions. The essential conditions for tropical cyclone genesis were analysed by Gray (1968, 1975, 1979) who identified 6 parameters that are important for cyclone genesis, of which 3 are thermodynamic parameters

1. *Sufficient Ocean thermal energy (A warm ocean surface layer with temperature above 26° C extending to a depth of 60m from the ocean surface)*

Table 1.2: Ocean basin-wise variation of tropical cyclones by from 1958-1977 (Gray, 1979)

Year	SH.	NW Atl.	NE Pac.	NW Pac.	N Indian	S Indian	Aust.	S Pac.	Total
1958	1958-59	12	13	22	5	11	11	7	81
1959	1959-60	11	13	18	6	6	13	2	69
1960	1960-61	6	10	28	4	6	8	8	70
1961	1961-62	11	12	29	6	12	7	4	81
1962	1962-63	6	9	30	5	8	17	3	78
1963	1963-64	9	9	25	6	9	7	7	72
1964	1964-65	13	6	39	7	6	9	4	84
1965	1965-66	5	11	34	6	12	7	4	79
1966	1966-67	11	13	31	9	5	5	6	80
1967	1967-68	8	14	35	6	11	9	8	91
1968	1968-69	7	20	27	7	8	7	8	84
1969	1969-70	14	10	19	6	10	7	6	72
1970	1970-71	8	18	23	7	11	12	3	82
1971	1971-72	14	16	34	6	7	14	6	97
1972	1972-73	4	14	28	6	13	12	10	87
1973	1973-74	7	12	21	6	4	16	8	74
1974	1974-75	8	17	23	7	6	10	3	74
1975	1975-76	8	16	17	6	8	16	5	76
1976	1976-77	8	18	24	5	9	12	9	85
1977	1977-78	6	17	19	5	6	7	7	67
Total		176	268	526	121	168	206	118	1583
Average		8.8	13.4	26.3	6.4	8.4	10.3	5.9	79.1

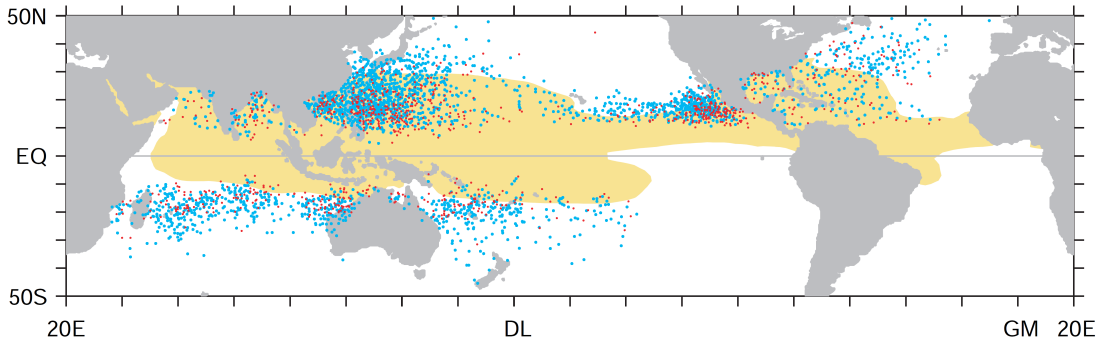

Figure 1.2: A climatology of tropical cyclones with peak surface wind velocities in excess of 32 ms^{-1}, based on the years 1970-1989. Red dots indicate the genesis regions (i.e., the positions of the cyclones on the first day during which their peak winds exceeded 32 ms^{-1}) and blue dots indicate the positions of the same cyclones on all subsequent days (on which their peak winds exceeded 32 ms^{-1}). The shading indicates oceanic regions with sea surface temperatures in excess of 27°C. Adapted from Wallace and Hobbs (2006).

2. *Conditional (convective) instability in the atmosphere for thunderstorm generation.*

3. *High mid-troposphere (700 to 500 hPa) relative humidity.*

and 3 are dynamic parameters, viz;

1. *High lower troposphere relative vorticity (pre-existing).*

2. *Weak vertical shear of the horizontal wind between 950 and 200 hPa.*

3. *High value of Coriolis parameter in the genesis area.*

Although these parameters are not completely independent of each other (Frank, 1987), their existence provide favourable conditions for cyclogenesis over the ocean basins. Palmen (1948) suggested that sea surface temperature (SST) greater than 26°C are favourable for tropical cyclone formation. Warm ocean water provides water vapour and sensible heat required for the formation of the initial disturbance. This is the reason why majority of the cyclogenesis occur

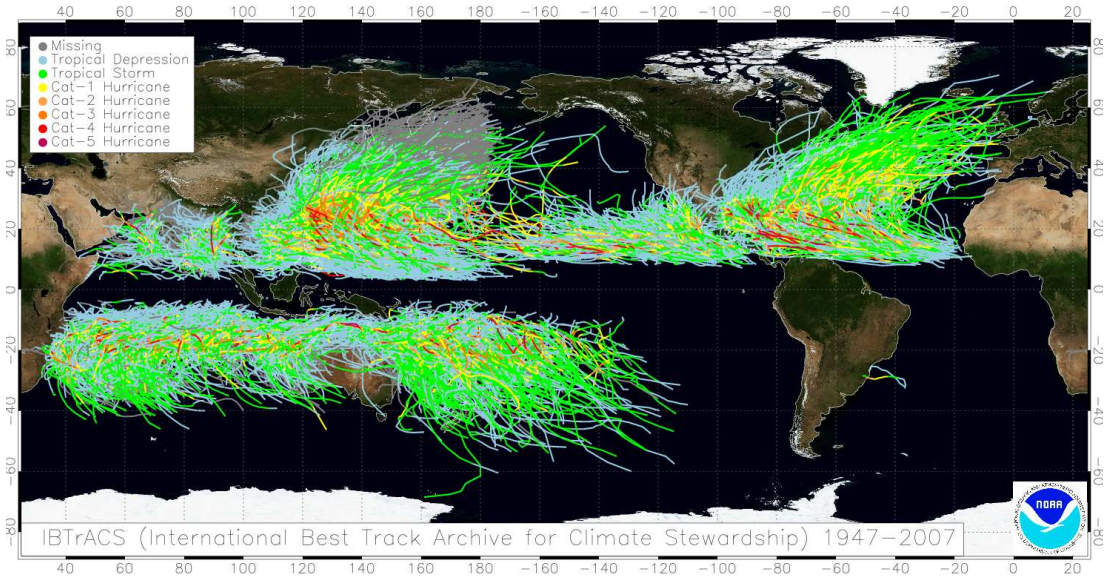

Figure 1.3: Observed tropical cyclone tracks and intensity for all known storms over the period 1947 to 2008. Tracks are produced from the IBTrACS dataset of NOAA/NCDC (Knapp et al, 2010).

in the tropical ocean compared with cold mid-latitude waters and cold tropical oceans like South Atlantic and South-east Pacific. According to Gray (1979) when a cyclone forms, the top oceanic layer gets mixed due to the strong winds and unless the ocean thermal energy in the top 60 meters above 26°C is large, there is little chance for cyclone formation. Conditional instability in the atmosphere (high convective available potential energy CAPE) provides favourable conditions for formation of cumulonimbus clouds, the latent heat release from which is the main energy (heat) source for tropical cyclones. To maintain high intensity levels for tropical cyclone, large amounts of latent heat release (rain) is needed within the cyclone and this is possible only if the middle troposphere is sufficiently moist.

Considering the dynamical parameters, pre-existence of positive lower tropospheric vorticity is required for cyclone genesis. Lower troposphere with large pre-existing cyclonic vorticity provides a favourable environment for the spin up of the tropical cyclone to high vorticity values in the central region. Another

major dynamic factor contributing to the cyclone spin up to large vorticity values is the existence of an initial non-negligible value of Coriolis parameter. Thus cyclone genesis generally does not occur within 5° north and south of the equator and usually forms over the 5° to 20° latitude belt. In order for an initial cyclonic disturbance to intensify, the atmospheric environment must be such that the latent heat released in the cumulonimbus clouds by the converging moisture must remain in the core of the system. Low vertical wind shear (VWS) between 950 and 200 hPa levels reduces the 'ventilation effect' of latent heat released in the cumulonimbus clouds in the core region of the cyclone (Gray, 1979). It is observed that cyclones do not form if the wind shear exceeds 12.5 ms^{-1} (Zehr, 1992). Thermodynamic factors change slowly and may remain favourable for cyclogenesis for the entire season. But the dynamic factors, other than Coriolis parameter, can change dramatically within days (Gray, 1975; McBride 1981).

1.5 Intensification of tropical cyclones

The intensification of a tropical cyclone after its genesis is dependent on both thermodynamic and dynamic parameters. In addition several other parameters have been identified such as the cyclones internal dynamics, translational speed, life duration, interaction with the upper troposphere, regional influences of individual basins like dry air advection from land and passage over oceanic heat anomaly regions. Majority of studies on cyclone intensification have concentrated on the role of SST in modulating tropical cyclone intensity. Holland (1997) suggested that the role of the ocean is to initially contribute a favourable environment for the development and then to provide the additional energy required for the intensification into a high intensity cyclone. He also pointed out that ocean surface with SST below 26°C provides insufficient energy for development of a tropical cyclone. Rather than a direct predictor of intensity, SST acts as a capping function of the intensity of a tropical cyclone (Merrill, 1988).

The interaction of tropical cyclone with SST can be considered as a feedback mechanism for the intensification of the cyclone. As explained by Ginis (1994), SST feedback mechanism is favourable for tropical cyclone intensification in the initial development stages. As tropical cyclone intensifies, the increasing wind

speed enhances the evaporation rate and the increased moisture supply in-turn increases the latent heat energy released and causes further intensification of the tropical cyclone. As the tropical cyclone intensifies, the wind stress associated with the surface wind generates strong turbulent mixing over the upper oceanic layer which results in the entrainment of cooler sub surface waters into the surface layer. This deepens the ocean mixed layer and SST decreases. Thus a reduction of total heat flux from the ocean occurs which leads to the decrease in the storm intensity. This SST feedback process is thus considered as a negative feedback to the intensification of tropical cyclone. Using numerical models, Schade and Emanuel (1999) showed that the SST feedback effect can reduce a typical hurricane intensity by more than 50%. Price (1981) found that entrainment is the primary mechanism that lowers the SST beneath a moving hurricane and air-sea heat exchange plays only a minor role.

Tropical cyclones convert large amounts of available ocean thermal energy into mechanical energy which drives the entire system. Thus the total energy of a tropical cyclone depends on the energy availability from the ocean which is a direct function of its SST. Emmanuel (1999) observed that the evolution of hurricane intensity depends on the initial intensity, thermodynamic profile of the atmosphere and the heat exchange between tropical cyclone and upper ocean. Other factors such as VWS and dynamic interactions with the environment appear influencing the storm during the formative stages when the storm is comparatively weak. Emmanuel (1986, 1991) found that the energy in a tropical cyclone comes from a cyclone heat engine performing a Carnot cycle. By this theory, a tropical cyclone is regarded as an ideal Carnot heat engine gaining energy from the disequilibrium between the atmospheric boundary layer and the ocean surface and losing energy in the upper-level outflow layer. If the heat source at the ocean surface at temperature is T_S (SST) and heat sink in the lower stratosphere is at a much colder temperature T_0, then the efficiency ε of the cyclone heat engine is given by the expression

$$\varepsilon = \sqrt{\frac{T_S - T_0}{T_S}} \tag{1.1}$$

An important problem here is the upper bound of cyclone intensity i.e. the maximum potential intensity (MPI) a cyclone can reach in a given environmental condition. Emanuel (1987) defined a MPI based on SST, temperature of the upper troposphere temperature and the thermodynamic structure of the atmosphere. This air-sea interaction theory of the tropical cyclone intensity has been further elaborated subsequently by Emanuel (1988, 1991, 1995). He formulated equations to calculate the MPI of cyclones in terms of maximum sustained wind speed as

$$V_{max} = \sqrt{\frac{T_S}{T_0} - \frac{C_K}{C_D} \left(CAPE^* - CAPE\right)_m} \tag{1.2}$$

where C_K is the exchange coefficient for enthalpy, C_D is a drag coefficient, $CAPE^*$ is the convective available potential energy of air lifted from saturation at sea level in reference to the environmental sounding, and CAPE is that of boundary layer air. High SST allows for higher rate of energy transfer from the ocean, which in turn increases the MPI. Studies by DeMaria and Kaplan (1994), Schade and Emanuel (1999) pointed out that even though SST is important in tropical cyclone intensification, the heat content of the ocean mixed layer must be considered. Accurate prediction of hurricane intensity requires accurate measurements of upper ocean thermal structure ahead of the storm (Emanuel, 1999).

In order to resist the weakening due to the negative feedback from the ocean, a warm upper ocean layer is also an essential condition for the intensification of the cyclone (Gray, 1968; Leipper and Volgenau, 1972; Gray, 1978). The extent of interaction of tropical cyclone with the upper ocean also depends on the translation speed of the tropical cyclone over the ocean. Chang and Anthes (1979) commented that appreciable weakening of a hurricane due to the negative SST feedback will not occur if it is translating at typical speed. Price (1980) proposed that the SST response is a lively function of hurricane strength and translation speed and of the initial mixed layer depth and the upper thermocline temperature gradient. Black (1983) suggested that the maximum SST decreases were primarily a function of the storm translation speed and the storms moving faster (slower) than 3 ms^{-1} produce a SST change of 1°C to 3°C (3°C to 5°C) within one-half day after storm passage. For rapidly moving storms, if the oceanic mixed

layer is deep, then the SST feedback effect has only minor importance (Schade and Emanuel, 1999).

Although there is an observed relation of tropical cyclone intensity with SST, it cannot exclusively determine the total intensity (Merrill, 1988; Evans, 1993; DeMaria and Kaplan 1994). Tropical cyclones are found to weaken in the environment with high vertical shear of horizontal winds. To an extent the uncertainties in the proper prediction of tropical cyclone intensity is caused due to uncertainties in the forecast of VWS (Emmanuel et al, 2004). According to Gray (1979) in an environment of high VWS, heat and moisture will be ventilated away from the system. Resistance of tropical cyclones to VWS depends on the size (Wong and Chan, 2004) and intensity of the tropical cyclone. Although the critical values of VWS can vary in different ocean basins (Ritchie, 2002), it is observed that generally VWS below 12 ms^{-1} favours cyclone intensification (Zehr, 1992; DeMaria and Kaplan, 1994; Whitney and Hobgood,1997; and Gallina and Velden, 2002).

Upper tropospheric divergence which maintains the mass balance in the cyclone has a role in the intensification of cyclones. Gray (1979, 1998) found that for proper maintenance and intensification, tropical cyclone must be developing in areas where upper tropospheric anticyclonic flow is significant. Studies by Sadler (1976), Hanley et al (2001) explained the positive influence of tropical upper tropospheric trough (TUTT) on cyclone intensification. This is further analysed by Wu and Cheng (1999) in an observational study of the environmental influences on the intensity changes of Typhoons *Flo* and *Gene* (1990). They pointed out that the influence of upper level environmental feature like upper level eddy flux convergence (EFC) has a major role in tropical cyclone intensification.

1.6 Tropical cyclone climatology over North Indian Ocean

North Indian Ocean is divided into two sub-basins namely Bay of Bengal and Arabian Sea. Bay of Bengal is more productive than Arabian Sea in respect of tropical cyclones. North Indian Ocean is bounded by land to the north, west and east which limits the lifetimes of cyclones in this basin. Tropical cyclone frequency

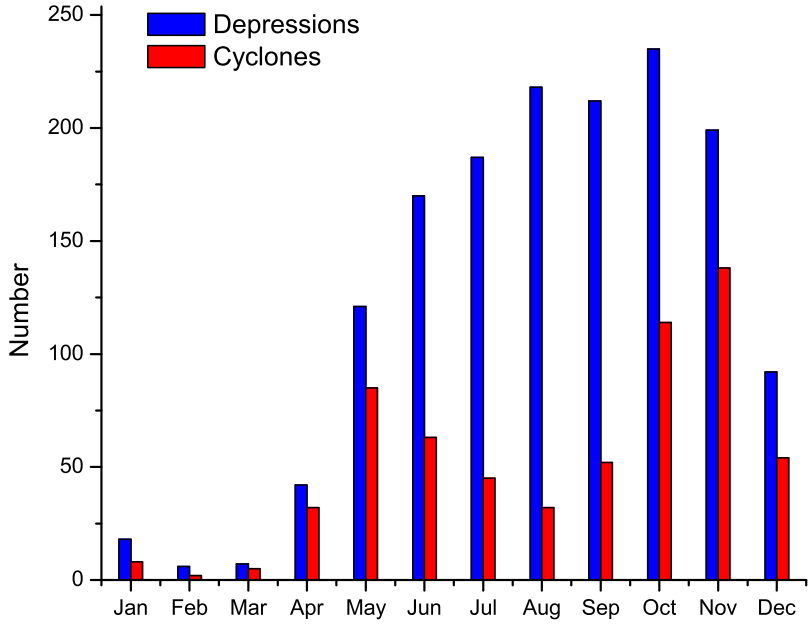

Figure 1.4: Number of depressions and tropical cyclones in North Indian Ocean in each month using data of 1891 to 2011 (data from IMD).

in North Indian Ocean is known to have a bimodal structure (figure 1.4). They occur from mid-September to December with a primary maximum in November and from April to mid June with a secondary maximum in May. During the Asian summer monsoon season (June-September), adverse conditions, especially high VWS reduce cyclogenesis over North Indian Ocean. During this season, winds in the North Indian Ocean are dominated by the Tropical Easterly Jetstream (TEJ) (Koteswaram, 1958) in the upper troposphere with wind maximum in the 150 to 100 hPa level and the westerly Low Level Jetstream (LLJ) in the lower (Joseph and Raman, 1966; Findlatter, 1969; Joseph and Sijikumar, 2004) with wind maximum around 850 hPa level. Thus high VWS prevails over the region making it difficult for the genesis of tropical cyclones.

During the Asian summer monsoon season another type of low pressure system known as Monsoon Depression forms over North Bay of Bengal. Monsoon Depressions are cyclonic disturbances weaker than tropical cyclones in wind and central surface pressure anomaly that form over the North Bay of Bengal and hav-

ing a northwestward track over the Indian subcontinent. They are one of the main rain producing systems of the monsoon. Also the genesis of monsoon depression is close to the coast (head Bay of Bengal) and the vortex rapidly moves over to land which is another factor other than VWS that does not allow intensification of monsoon depression into tropical cyclone intensity. There is significant difference in the structure of monsoon depressions when compared to that of tropical cyclones. Lower tropospheric wind field of monsoon depression is highly asymmetric around the centre of the vortex with maximum winds and vorticity to the south of the monsoon depression vortex center. In the south west sector temperatures are low at 850 and 700 hPa and high in the northwest sector (Joseph and Chakravorty, 1980). Thus advection of vorticity and temperature control rainfall dynamics in monsoon depression in addition to boundary layer friction. Heavy rainfall occurs in the south west sector of monsoon depression. The vertical axis of monsoon depression vortex slopes towards southwest considerably, whereas the axis of tropical cyclone remains vertical.

1.7 Spatial variability of the environmental parameters over North Indian Ocean

With the presence of the Asian summer monsoon system, North Indian Ocean basin has considerable seasonal variability in the atmospheric circulation. Seasons over North Indian Ocean basin are classified into four; Pre-monsoon (March to May -MAM), Monsoon (June to September- JJAS), Post-monsoon (October to December-OND) and Winter (January to February - JF). With the changes in the seasons most of the environmental parameters show large variations. The environmental parameters and their variations in the North Indian Ocean basin are discussed in this section.

Lower tropospheric circulation features over the North Indian Ocean basin for the four seasons are depicted in figures 1.5 and 1.6 which shows the 850 hPa wind and vorticity, composited for the years 1948 to 2010 using NCEP/NCAR reanalysis data. During the JF season, the North Indian Ocean is dominated by easterly winds. Cyclonic vorticity exists close to the equator. During MAM, westerly flow

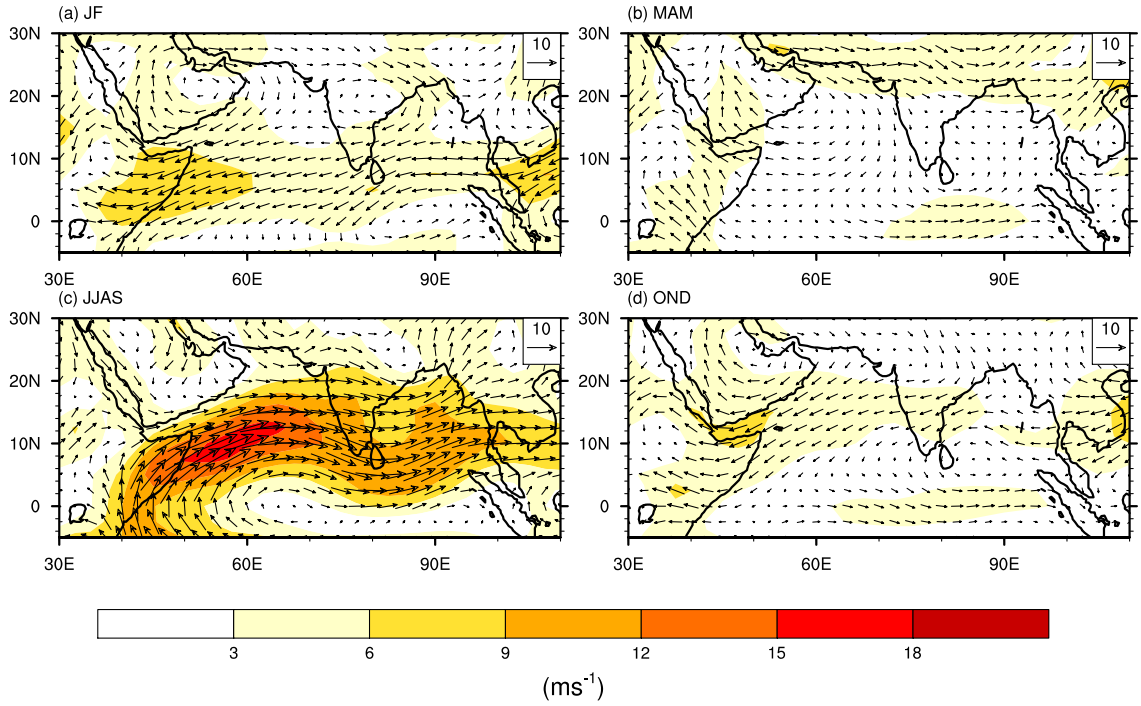

Figure 1.5: Composites of 850 hPa wind for (a) January-February (b) March to May (c) June to September (d) October to December.

is established near the equator and a region of cyclonic vorticity is found north of the equator. During JJAS, Asian monsoon exists over south Asia along with a cross-equatorial LLJ with strong westerly winds over the North Indian Ocean with a region of high cyclonic vorticity north of the LLJ axis in Arabian Sea and the Bay of Bengal. Compared with the pre-monsoon, the strength of the westerly flow is more during the OND and thus the cyclonic vorticity is also more.

Upper tropospheric features are analysed using the 200 hPa wind and mean for the period 1948 to 2010 is given in figure 1.7 for the four seasons. During the JF and MAM, the Sub-Tropical Jetstream (STJ) is strong over the high latitudes of North Indian Ocean (Krishnamurthi, 1961). The strength of STJ is highest during JF. The scenario changes during the Asian monsoon season where a strong TEJ gets established over the entire North Indian Ocean. During this period the STJ gets shifted to a position north of Himalayas. The core of TEJ lies close to and north of the equator during the season. During MAM and OND, STJ axis

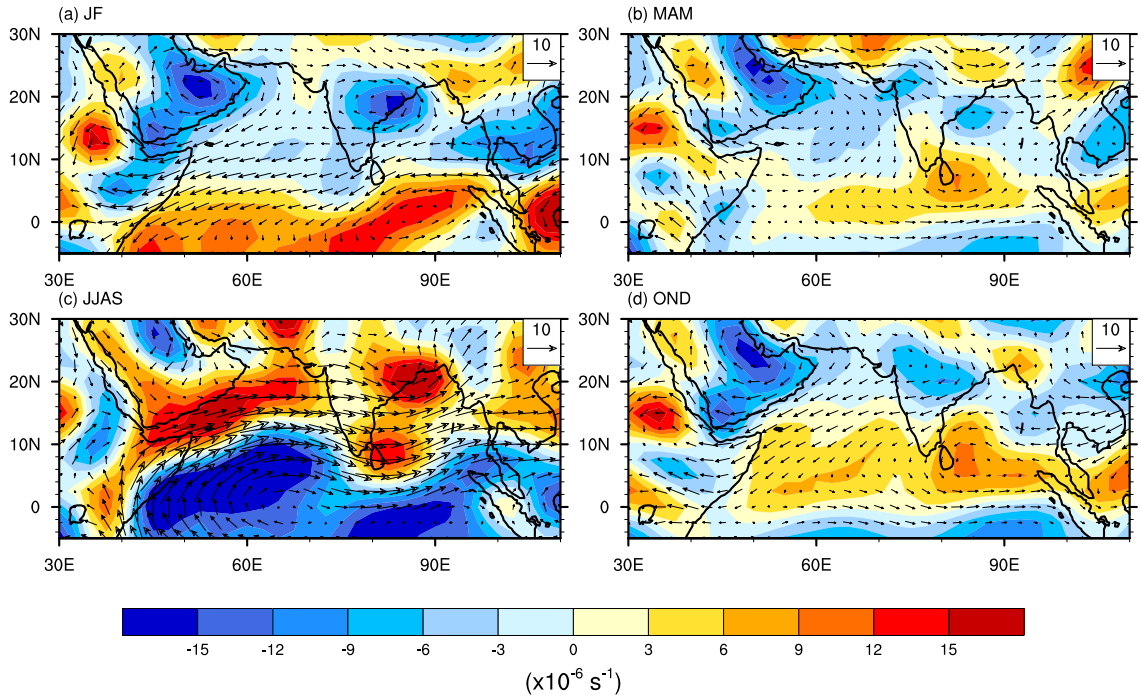

Figure 1.6: Same as figure 1.5 but for vorticity

lies south of the Himalayas as in the JF season, but is weaker. The existence of TEJ and STJ in the upper troposphere and LLJ in the lower troposphere provide a highly variable VWS environment over North Indian Ocean. It is found that during the MAM and OND seasons cyclones while they move northwards, at times enter the high VWS region associated with the STJ and they weaken or die. Figure 1.8 gives the VWS between 850 and 200 hPa for the 4 seasons as average of the period 1948 to 2010. A large and strong VWS area covers the whole of North Indian Ocean during JJAS which precludes genesis of tropical cyclone. During this season the VWS over north Bay of Bengal is much weaker which permits formation of systems of intensity lower than tropical cyclone like monsoon depressions.

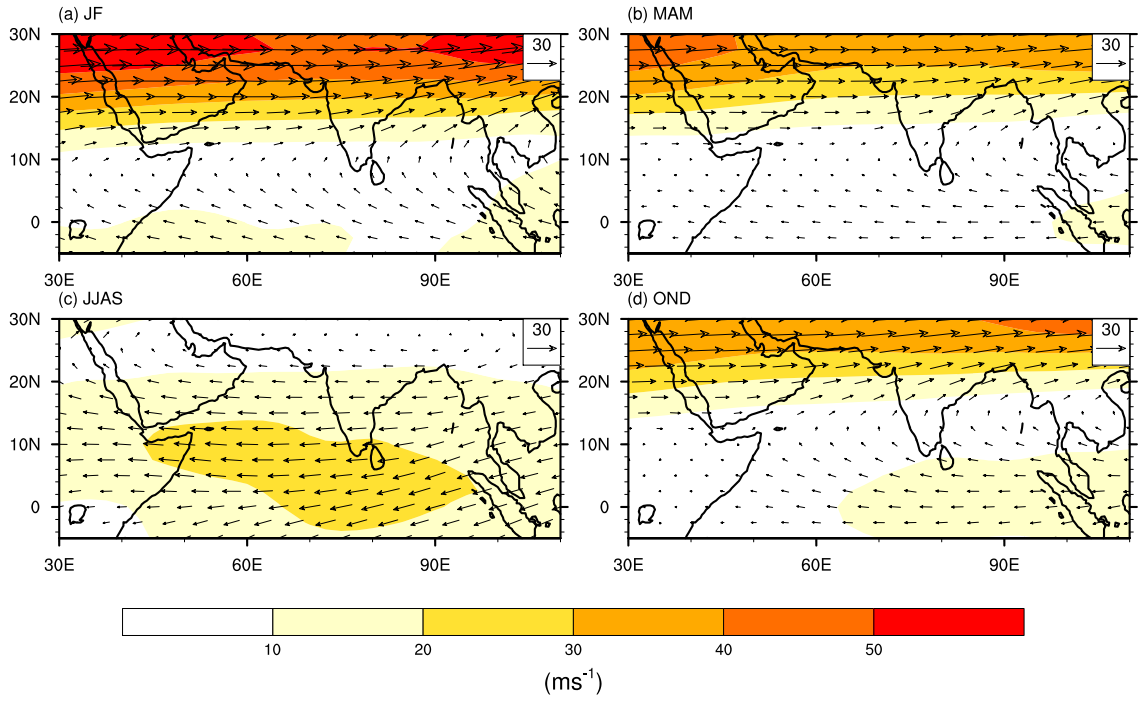

Figure 1.7: Same as figure1.5 but for 200 hPa wind.

1.8 Temporal variability of tropical cyclones

Tropical cyclones show large temporal variability globally in their genesis and intensity since the environmental parameters show large variations in intra-seasonal, inter-annual and decadal time scales.

1.8.1 Intraseasonal variations

Since about 90% of the tropical cyclone genesis occur within the tropical belt 20°S to 20°N latitudes, genesis events are highly modulated by the equatorial waves that propagate zonally (Frank and Roundy, 2006). Roundy and Frank (2004) analysed the contributions to the total variance in Outgoing Longwave Radiation (OLR) by each of the five prominent wave types with periods of two days or longer. These are Madden-Julian Oscillation (MJO), equatorial Rossby waves, mixed Rossby-gravity waves, Kelvin waves and westward propagating tropical depression-type wave which is referred to as easterly waves or African easterly

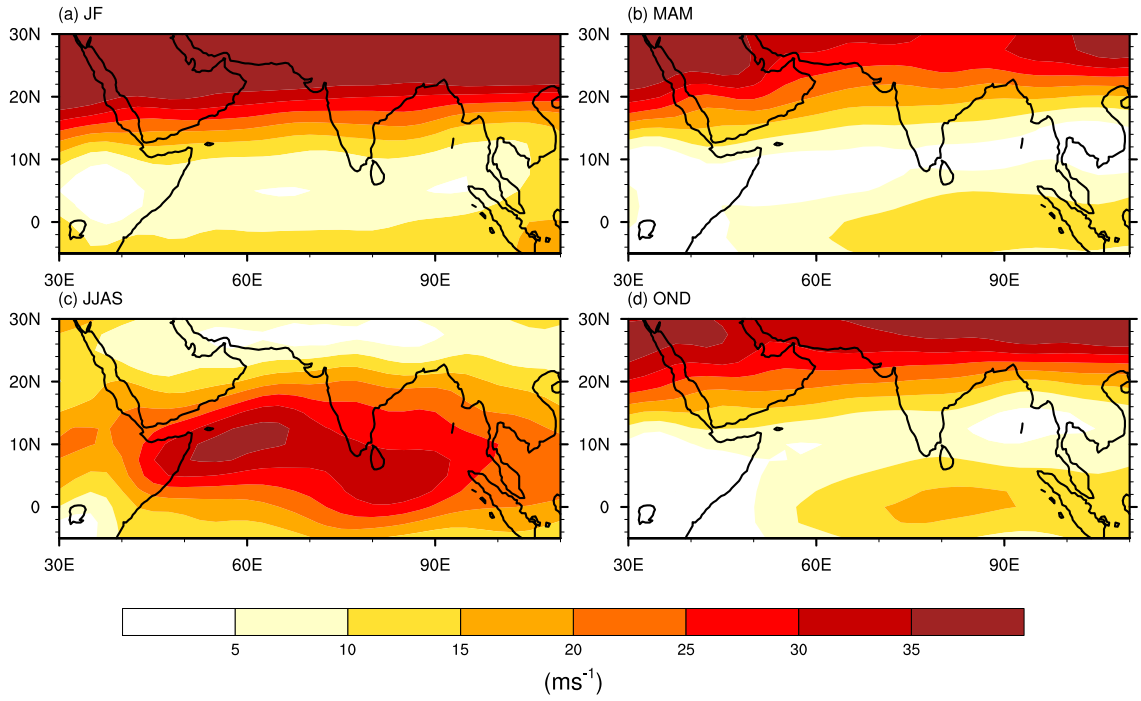

Figure 1.8: Same as figure 1.5 but for VWS.

waves. They found that MJO and equatorial Rossby waves together explain at least 15% of the total OLR variance between 20°N and 20°S latitude, and in some regions they explained at least 50% of the sub-seasonal local variance.

MJO is the largest mode of intra-seasonal variability in the tropics involving large-scale coupling between atmospheric circulation and tropical deep convection. Convection associated with MJO originates over the equatorial western Indian Ocean, propagates eastward and enters the Pacific Ocean crossing the maritime continent. This eastward propagating tropical disturbance with period in the range of 40 to 50 days was first identified by Madden and Julian (1971). Further studies showed that MJO has a broadband spectral period ranging from 30 to 60 days and has a global wave number one structure with a spatial wavelength of roughly 12000-20000 km (Nakazawa, 1988). This oscillation is associated with eastward moving convection with an enhanced convective phase followed by a non-convective (suppressed convection) phase at any one location. The low level wind fields associated with MJO are characterized by fluctuations between

easterly and westerly phases and can be observed in several other parameters such as surface pressure, upper tropospheric wind and proxies for deep convection such as OLR.

Gray (1979) found that the global tropical cyclone formation can be grouped into temporal clusters with an active period of cyclogenesis of a few weeks followed by a few weeks of relatively less cyclogenesis. The relation between MJO and tropical cyclones was analysed by Nakazawa (1986) for the year 1979 who found that the genesis and growth of tropical cyclones occur globally during the active phase of intraseasonal variations associated with the 30 to 60 day oscillations in OLR. Liebmann et al (1994) studied the relationship between tropical cyclones of the western Pacific and Indian Ocean with MJO and found that the absolute number of storms and typhoons are enhanced during the convective phase of the MJO compared with the non-convective phase. They reported that there exist more storms and typhoons because of more depressions in the convective phase. Later studies found significant relation between tropical cyclones and MJO over the global ocean basins; such as Maloney and Hartman (2000a) for Gulf of Mexico, Maloney and Hartman (2000b) for eastern North Pacific, Hall et al (2001) for the Australian region, Maloney and Hartman (2001) and Hartman and Maloney (2001) for north Pacific Ocean, Bessafi and Wheeler (2006) for south Indian Ocean, Kim et al (2008) for the western north Pacific, Klotzbach (2010) for the Atlantic Ocean and Kikuchi and Wang (2010) for North Indian Ocean. Kikuchi and Wang (2010) have studied cyclogenesis in North Indian Ocean associated with both the northward moving Boreal Summer Intra Seasonal Oscillation and the eastward moving MJO.

1.8.2 Interannual variations

Major modes of interannual variations in North Indian basin are El Nino Southern Oscillation (ENSO) and Indian Ocean Dipole (Saji et al, 1999). Interannual variability of weather systems around the world is influenced by ENSO and its associated teleconnections. The oceanic part of ENSO is characterized by warming (cooling) of equatorial eastern Pacific during El Nino (La Nina) years and

the atmospheric part is characterized by a sea-saw of reversing wind and pressure patterns between the eastern and western tropical Pacific. ENSO affects the global weather patterns through the modulation of SST, atmospheric circulation, land-surface temperatures and precipitation (Diaz et al, 2001; Alexander et al, 2002). Gray (1984) observed a decrease in tropical cyclone frequency over the Atlantic during the El Nino years. Subsequently several studies have analysed different aspects of ENSO related variabilities affecting tropical cyclone activity over the ocean basins and it is observed that the relationship between El Nino and tropical cyclone activity varies from one basin to other. A detailed review of the available literature on the modulation of tropical cyclone activity by ENSO over different ocean basins given by Camargo et al (2010) is reproduced in table 1.3.

Table 1.3: Summary of the ENSO impacts on tropical cyclone activity in the different regions, including references (Camargo et al, 2010).

Basin	**Characteristic**	**ENSO**	**Change**	**References (e.g.)**
Western North Pacific	Number of TCs	Strong EN	increase	Wang and Chan (2002)
	Number of TCs	Summer following EN	decrease (1992),	Chan (1985), Wu and Lau Chan (2000)
	Mean genesis location	EN/LN	Displacement to the Southeast/ Northwest	Chan (1985), Chen et al. (1998), Wang and Chan (2002), Chia and Ropelewski (2002)
	Lifetime	EN/LN	Increase/decrease	Wang and Chan (2002), Camargo and Sobel (2005)
	Number of intense typhoons and ACE	EN/LN	Increase/decrease	Camargo and Sobel (2005), Chan (2007)
	Track types	EN	Long tracks, recurve northeastward and reach more northern latitudes	Wang and Chan (2002), Wu and Wang (2004), Camargo et al. (2007e)
Eastern North Pacific	Number of intense TCs	EN/LN	Increase/decrease	Gray and Sheaffer (1991), Frank and Young (2007)
	Mean genesis location	EN	Westward shift	Irwin and Davis (1999), Kimberlain (1999)
	Tracks	EN	Longer westward direction	Chu (2004), Camargo et al. (2008a)
Central North Pacific	Number of TCs	EN	Increase	Wu and Lau (1992), Chu and Wang (1997), Clark and Chu (2002),

Continued on next page

Table 1.3 – *Continued from previous page*

Basin	Characteristic	ENSO	Change	References (e.g.)
				Camargo et al. (2007a)
Atlantic	Number of TCs, number of hurricanes, number of intense hurricanes, number of hurricane days, number of tropical storms, ACE	EN/LN	Decrease/Increase	Gray (1984a); Gray et al. (1983); Landsea et al. (1999); Bell et al. (2000)
	US landfalls	EN/LN	Decrease/increase	OBrien et al. (1996); Bove et al. (1998); Pielke and Landsea (1998); Larson et al. (2005)
North Indian	Number intense TCs	EN	Decrease (Bay of Bengal)	Singh et al. (2000)
South Indian	Number of TCs east of 70°E	LN	Increases	Kuleshov (2003)
	Peak of the season	EN/LN	February/January	Kuleshov (2003)
	Start of the season	LN	1 month earlier	Kuleshov (2003)
	Mean genesis location	EN	Westward shift increase (decrease) west (east) of 75°E	Ho et al. (2006)
	Tracks	EN	Movement further east	Ho et al. (2006), Kuleshov et al. (2008)

Singh et al (2000) found that the North Indian Ocean tropical cyclones shows a prominent ENSO scale variation with a reduction in the number of tropical cyclone in May and November during the warm phases of ENSO. The effect of dynamical factors related with ENSO on the cyclogenesis in North Indian Ocean was analysed by Ng and Chan (2011) by taking the number of tropical cyclones, severe cyclones and the Accumulated Cyclone Energy (ACE) for the years 1983 to 2008. El Nino is influencing the post monsoon Bay of Bengal cyclogenesis during October-November-December (OND) by variations in the atmospheric flow patterns and moist static energy that are apparently forced largely by the El Nino (Ng and Chan, 2011).

Indian Ocean Dipole is a coupled ocean and atmosphere phenomenon in the equatorial Indian Ocean that affects the climate of the countries that surround

the Indian Ocean basin. Positive (negative) IOD is characterized by anomalous cooling (warming) of SST in the south eastern equatorial Indian Ocean and anomalous warming (cooling) of SST in the western equatorial Indian Ocean. It is commonly measured by an index that is the difference of SST; the western (50°E to 70°E and 10°S to 10°N) minus the eastern (90°E to 110°E and 10°S to 0°S) equatorial Indian Ocean. This index is also called Dipole Mode Index (DMI). A possible relation between IOD and tropical cyclone is suggested by Singh (2008) who showed that the circulation patterns associated with negative IOD is favourable for cyclone genesis in Bay of Bengal. During the positive (negative) phase of IOD, an anomalous anticyclonic (cyclonic) circulation is created over the Bay of Bengal. Thus the anomalous cyclonic circulation during the negative phase may support the formation of cyclones over the Bay of Bengal as the anomalous cyclonic vorticity triggers the genesis of cyclones. Although Ng and Chan (2011) could not find a strong relationship between IOD and North Indian Ocean cyclogenesis, they concluded that IOD may affect the relationship between tropical cyclone activity and ENSO by influencing the large-scale parameters.

1.8.3 Decadal variations

Tropical cyclone frequency over the ocean basins have shown long-term trends and multidecadal oscillations. Multidecadal modes of tropical cyclone activity are associated with climatic oscillations like Pacific Decadal Oscillation (PDO), Atlantic Multidecadal Oscillation (AMO), North Atlantic Oscillation (NAO) etc., which influence directly or through global teleconnections. Variations in tropical cyclone frequency and intensity in a decadal scale were reported by several studies especially in Pacific (Chan and Shi, 1996; Chu and Clark, 1999; Chu, 2002; Matsura et al, 2003) and Atlantic (Elsner et al, 2000; Goldenberg, 2001; Bell and Chelliah, 2006). Aiyyer and Thorncroft (2011) analysed the interannual to multidecadal variabilities in VWS and associated tropical cyclone activity over the global oceans and observed that apart from interannual variations associated with El Nino, the major variability is accounted by Pacific Decadal Oscillation (PDO) and Atlantic Multidecadal Oscillation (AMO). Interdecadal variations of monsoon depression of North Indian Ocean basin has been studied by Kumar

and Dash (2001) and Dash et al (2004) and they found that monsoon depression frequencies are decreasing from the decade 1969-1978 till the most recent decade. Singh et al (2000) and Singh (2007) found statistically significant increasing trend in the frequency of severe cyclonic storms of the Bay of Bengal during the period 1887 to recent years. Jadav and Munnot (2008) have shown that in the recent decades monsoon depression frequency has shown a decreasing trend while SST over the area of their genesis has shown increasing trend.

Singh et al (2000) used 122 years (1877-1998) data of tropical cyclone over North Indian Ocean and analysed the significant oscillations which affect it. They showed that the number of tropical cyclone forming over the Bay of Bengal in November and May have a significant increasing trend although Arabian Sea has not shown any significant trend. They have shown that Bay of Bengal cyclone data shows a 29 year oscillation in the May and a 44 year oscillation during November and Arabian Sea shows significant 13 year and 10 year periodicity during May-June and November respectively. Joseph and Xavier (1999) identified a decadal oscillation in the number of tropical cyclones and monsoon depressions occurring in the North Indian Ocean basin with a period close to 36 years. In the case of monsoon depression this 36 year oscillation is superposed on the long-term decreasing trend in the annual frequency of monsoon depression. The reason for the decreasing trend in monsoon depressions was studied by Dash et al (2004) who attributed it to the weakening of the atmospheric dynamical parameters which favor formation of monsoon depressions. Pattanaik (2005) using 113 years of data (1891-2003) studied the long term variations in the tropical cyclone characteristics. The data is divided into high frequency period (HFP) and low frequency period (LFP) and analysed the change in the dynamical and thermodynamic parameters related to them. The HFP is from 1969 to 1978 and LFP is from 1993 to 2002 which is almost consistent with Joseph and Xavier (1999).

1.9 Tropical cyclones in a warming environment

Changes in tropical cyclone number and intensity during a warming environment is a matter of current debate and is extensively studied in the recent liter-

ature. Variability due to both anthropogenic and natural causes tends to modify the environment in which a tropical cyclone has genesis and intensification. Very limited (in time) and accurate records available from global cyclone basins restricts the studies on natural climate variability to the recent decades only. It is a well accepted fact by the scientific community that the human induced anthropogenic warming by the increase in the amount of greenhouse gases is a reason for the observed increase in global mean surface temperature of the atmosphere and ocean. The Intergovernmental Panel on Climate Change (IPCC) report (Solomon et al, 2007) concludes that most of the globally averaged temperature increase since the mid-20th century is very likely (>90% chance) due to the observed increase in human-generated greenhouse gas concentrations. Several studies pointed out that the associated changes can also be observed in global mean ocean temperature. The SST over most tropical ocean basins has increased by 0.25° to 0.5 °C in past 50 years (Kumar et al, 2004; Webster et al, 2005; Santer et al, 2006).

Webster (2005) reported an increase in the global tropical cyclone intensity in the recent decades although Landsea (2006) questioned the reliability of the data used due to false intensity estimations caused by problems in observational methods. Emmanuel (2005) defined a potential destructive index (PDI) which is the cube of the maximum winds of a cyclone integrated over its life-time. He showed that this index has been increasing markedly since the mid-1970s for the West Pacific and Atlantic Ocean basins. Vecchi and Soden (2007) found that, apart from a uniform increase in global temperature, regional SST structures are also important in long-term variations in potential intensity of tropical cyclones. Based on these and other studies several assessment reports are available discussing the changes in tropical cyclone intensity (Henderson-Sellers et al, 1998; WMO, 2006; Solomon et al, 2007). Henderson-Sellers et al (1998) concluded that although substantial multidecadal variability is found in some regions, there is no clear evidence of long-term trends in tropical cyclone activity. Later assessments by WMO (2006) and Solomon et al (2007) concluded that the detection of a reliable trend in the tropical cyclone activity cannot be accepted with confidence in the present scenario.

An approach to study the future changes in the intensity and frequency of tropical cyclones is to use the climate models with respect to the increased CO_2 concentrations. The main restricting factor is the horizontal resolution of the current generation of global climate models which is insufficient to simulate the complex inner core structure of intense tropical cyclones. With this limitation, many studies have reported the climatic changes associated with the simulated tropical cyclone like disturbances in climate models (Sugi et al, 2002; Oouchi et al, 2006; Yoshimura et al, 2006; Bengtsson et al 2007). A net increase in the intensity of tropical cyclones is predicted by models in an environment with higher amount of CO_2 (Henderson-Sellers et al; 1998, Knutson et al; 1998, Knutson and Tuleya; 1999, Knutson et al; 2001). A critical review on future changes in tropical cyclone by Knutson et al (2010) reported that although the models project a reduction in the global averaged frequency of tropical cyclones, there is a possibility that the storms may shift into stronger intensity categories.

Chapter 2

Data

2.1 General

Tropical cyclone data from India Meteorological Department (IMD) and International Best-track Archive for Climate Stewardship (IBtRACS) have been used for studying the frequency and intensity variations of tropical cyclones of North Indian Ocean. Monsoon depression frequency data provided by IMD are also used. Daily and monthly wind and humidity data from National Centers for Environmental Prediction/National Center for Atmospheric Research (NCEP/NCAR) Reanalysis; daily fields from European Centre for Medium-Range Weather Forecasts interim reanalysis (ERA-interim) and NCEP FNL analysis; Outgoing Long wave Radiation (OLR) data from National Oceanic and Atmospheric Administration (NOAA); Hadley Centre Sea Ice and Sea Surface Temperature (HadISST) data and Extended Reconstructed Sea Surface Temperature (ERSST) data; SST from NOAA Optimum Interpolated Sea Surface Temperature (OISST) data; SST and Vertical Integrated Moisture data from TMI; Sea surface height Anomaly (SSHA) data from AVISO are used in the thesis. Available indices such as ENSO index from NOAA-Climate Prediction Center, IOD index from Japan Agency for Marine-Earth Science and Technology (JAMSTEC) and MJO index from Bureau of Meteorology (BOM), Australia are also used. The details regarding the datasets are given in the following sections.

2.2 Tropical cyclone datasets

The process of understanding the tropical cyclone structure and intensity started long before the satellite era where routine ship and aircraft observations in a number of basins enabled the scientists to study the basic structure, dynamics and energetics of the system. There is still a debate about the quality of tropical cyclone data prior to the satellite era since only a few cyclone basins were properly monitored at that time. Adopting proper monitoring tools enabled the scientific community to observe the tropical cyclones closely, starting from the ship reports and land-based observations to the unmanned drones flying into the cyclones. These platforms include radiosondes, dropsondes, radar, satellite and aircraft reconnaissance depending on the parameters measured. Inhomogeneities in quality of data occurs since there are large regional variations in the observation methods in different ocean basins.

Before 1940s the only observations available on cyclones were based on available ship records and land-based stations. Many cyclones formed over open ocean which did not affect any coastal region and thus went undetected before the satellite era (Landsea, 2004). Aircraft reconnaissance of tropical cyclones started over western North Pacific and North Atlantic regions beginning around 1945 and improved the storm detection and monitoring. The detection rate reached close to 100% only after 1970s when satellite observations became available. Geostationary satellites can provide continuous observations of different types of images in high temporal resolution of about 15 to 30 minute intervals. Along with the low earth orbiting satellites which provides high resolution spatial data, satellites are one of the most important tools for tropical cyclone observation. Also by using Dvorak (1975) method the cyclone intensity can be estimated from geostationary satellites by analysing the visible and infrared images and deriving a T-number. Currently organized aircraft reconnaissance, coastal radar network, and weather satellites with visible and infrared sensors are used to monitor cyclone track, eye, wall cloud, maximum wind speed and other storm parameters accurately.

World Meteorological Organization (WMO) has designated certain centers as the official warning centers with forecasting capabilities. There are six tropical cyclone Regional Specialized Meteorological Centres (RSMCs) together with

five Tropical Cyclone Warning Centres (TCWC) around the world. The RSMC-tropical cyclones New Delhi operated by India Meteorological Department is the official warning center for North Indian Ocean.

2.2.1 India Meteorological Department data

The cyclone atlas (IMD, 1979) and later atlases published by the India Meteorological Department were used to obtain the numbers of tropical cyclones, severe tropical cyclones and depressions formed over North Indian Ocean from 1891. Cyclone and monsoon depression data of recent years have been collected from *Mausam* which is the quarterly research journal of India Meteorological Department. The frequency data of monsoon depressions is highly reliable (1891 to date) since the monsoon depressions form near the coast and move quickly into the land which has a dense network of observatories (Joseph and Xavier, 1999).

The basic data for MD and tropical cyclone of North Indian Ocean basin were taken from the atlas (Atlas IMD, 1979) of *"Tracks of storms and depressions in the Bay of Bengal and the Arabian sea 1877-1970"* and other sources as described above. In the introduction portion of this atlas is given the following.

> *From the India Weather Review it was found that 1150 cyclonic disturbances occurred over the area during the period (1891 to 1970). Of these about 250 disturbances where either stationary or short lived (less than 1 day) or had no well-defined tracks and as such were left out from the atlas.*

Cyclonic disturbances as mentioned in the atlas are of 3 categories, depressions, tropical cyclone and severe tropical cyclone. Monthly frequencies of these three categories are given in table 1 of the atlas. Appendix 1 at the end of the atlas has given the list of only the cyclonic disturbances whose tracks are given in the atlas. In the earlier decades, the frequencies of cyclonic disturbances with tracks drawn in the atlas are much less than the frequencies of cyclonic disturbances as shown in table 1 of the atlas.

For a climate change studies, cyclonic disturbances which are short lived or those without track cannot be omitted. Rao (1976) has given the total number

Table 2.1: Decadal distribution of monsoon depressions reported and those without tracks or short lived.

Decade	No. of MD (a)	No of MD with full tracks (b)	(b/a) x 100 (%)
1891-1900	115	77	67
1901-1910	107	55	51
1911-1920	87	55	63
1921-1930	105	76	72
1931-1940	92	84	91
1941-1950	99	92	93
1951-1960	73	69	95
1961-1970	76	76	100
1971-1980	78	78	100
1981-1990	52	52	100
1991-2000	31	31	100
2001-2009	34	34	100

of monsoon depressions during each monsoon season, whether track is marked in the IMD atlas or not. The numbers of monsoon depressions and tropical cyclones given in IMD atlas is same as that of Rao (1976). Bhalme (1972) and Joseph and Xavier (1999) have also used similar counts in their studies. This makes a very significant difference for the decades of the period 1891 to 1960 as may be seen from the table 2.1 in respect of monsoon depression frequency. In the thesis the number of monsoon disturbances as given in table 2.1 of the IMD atlas and other later sources is used.

2.2.2 International best Track Archive for Climate Stewardship data

Tropical cyclone data from the International best Track Archive for Climate Stewardship - IBTrACS (Knapp et al, 2010) version v02r01 from 1979 to 2008 is used in the study. For the Indian Ocean basin, this data set is derived from

various sources like Joint Typhoon Warning Center (JTWC) (Pearl Harbour, Hawaii) and the Regional Specialized Meteorological Center (RSMC) New Delhi. The data discrepancy between different sources used in IBtRACS dataset is discussed in Knapp and Kurk (2010). Tropical cyclone data from IBtRACS-WMO which includes data only from the WMO RSMCs is also used for the cyclone intensification study for years from 1990 to 2010 (21 years).

2.3 National Centers for Environmental Prediction/National Center for Atmospheric Research reanalysis data

The NCEP/NCAR reanalysis data (Kalnay et al, 1996; Kistler et al, 2001) is a joint venture by the National Centers for Environmental Prediction (NCEP) and National Center for Atmospheric Research (NCAR) in order to produce a retroactive record global analyses of atmospheric fields. This data set is available from 1948 with a resolution of 2.5° latitude-longitude grids and with vertical resolution of 17 standard pressure levels (from surface to 10 hPa). Temporal resolution of the data is 6 hours. Daily and monthly means are also available. Reanalysis uses an atmospheric general circulation model which is coupled to a data assimilation system. Reanalyses are particularly suited for the detection of long-term changes or oscillations in the atmosphere and are widely used. As the reanalysis data includes assimilation of data products from different sources, long-term studies have to take into account the possible introduction of artificial jumps and trends into the reanalysis by changes in observing systems (Trenberth et al, 2001; Marshall, 2002; Bengtsson et al, 2004). There were major concerns about the changes regarding the use of satellite data (especially satellite radiances) in reanalysis (Kanamitsu et al, 1997) after the mid- 1970s, when reliable satellite data became available. Kanamitsu et al (1997) observed that use of radiance in the analysis has a very large impact on the analysis which tends to enhance horizontal temperature gradients and disturbance intensity where other observations are not available. Also inclusion of satellite data was particularly useful over the

southern hemisphere where reanalysis skills were much more improved by the use of satellite observations (Mo et al, 1995; Kistler et al, 2001).

The accuarcy and bias of the output variables are different. The gridded variables have been classified into three classes (Kalnay et al, 1996): type A variables, which are generally strongly influenced by the available observations and are therefore the most reliable product of the reanalysis including upper air temperatures, rotational wind, and geopotential height. Type B variables, which are influenced both by the observations and by the model, and are therefore less reliable including moisture variables, divergent wind, and surface parameters. Type C variables are completely determined by the model such as surface fluxes, heating rates, and precipitation and should be used with caution when compared with model-independent estimates.

In the present study NCEP/NCAR data has been used to analyse the different aspects of environmental conditions modulating topical cyclone activity over North Indian Ocean. Daily and monthly mean data such as wind, air temperature, specific humidity at different atmospheric levels and surface pressure have been used for analysis and for other computations.

2.4 European Centre for Medium-Range Weather Forecasts – Interim Reanalysis data

ERA-Interim (Simmons et al, 2006) is the latest global atmospheric reanalysis produced by the European Centre for Medium-Range Weather Forecasts (ECMWF) which was actually prepared as an 'interim' reanalysis in preparation for the next-generation extended reanalysis to replace ERA-40. It has several advantages compared with ERA-40 reanalysis such as use of 12 hour 4D-Var assimilation system, better (T255) horizontal resolution, Better formulation of background error constraint, new humidity analysis, improved model physics, variational bias correction of satellite radiance data, more extensive use of radiances and improved fast radiative transfer model. The data is available from 1979 to present day with a spatial resolution of 1.5° x 1.5° lattitude-longitude grid and 6 hourly data is available from ECMWF data server.

2.5 National Center for Environmental Prediction Final Analysis data

Objectively analyzed data of final analysis (FNL) is given by National Center for Environmental Prediction (NCEP). This data has 1° x 1° latitude-longitude horizontal resolution and a vertical resolution of 26 levels. It is available from July-1999 to present at 6 hour time intevals.

2.6 National Oceanic and Atmospheric Administration Outgoing Long-wave Radiation data

Outgoing Long-wave Radiation (OLR) data (Liebmann and Smith, 1996) from National Oceanic and Atmospheric Administration (NOAA) is used in the thesis. The data is measured by Advanced Very High Resolution Radiometer (AVHRR) aboard the NOAA Polar Orbiting satellites available from 1974 onwards with gaps filled with temporal and spatial interpolation. The data contains a major gap of several months during 1978 due to the failure of satellite. The data has a spatial resolution of 2.5° latitude-longitude grids and monthly and daily fields are available. Generally geostationary-derived OLR data is suitable for cyclone studies requiring high temporal resolution, but they lack global coverage. Compared with it NOAA interpolated OLR provide better accuracy, global coverage and have multi-decade record which makes it suited for studies of low-frequency variability.

2.7 Hadley Centre Sea Ice and Sea Surface Temperature data

Hadley Centre sea ice and sea surface temperature data (Rayner et al, 2003) version 1.1 (HadISST V1.1) developed at the Met Office Hadley Centre for Climate Prediction and Research is used in this thesis. The data has global coverage with a resolution of 1° x 1 ° latitude-longitude grid and is available from 1871. Gaps in the SST data have been interpolated. Care has to be taken when using

HadISST-1 for studies of climatic variability, particularly in some data sparse regions, because of the limitations of the interpolation techniques (Rayner et al, 2003).

2.8 Extended Reconstructed Sea Surface Temperature data

The extended reconstructed sea surface temperature (ERSST) (Smith and Reynolds, 2003) was constructed based on the International-Comprehensive Ocean-Atmosphere Data Set (I-COADS). ERSST Version 3 (Smith and Reynolds, 2008) is used in this thesis. The data has a spatial resolution of 2 ° latitude-longitude and monthly means are available. Although there are differences due to both the use of different historical bias corrections as well as different data and analysis procedures, the large-scale variations of ERSST are broadly consistent with those associated with the HadISST (Smith and Reynolds, 2003). Each month the ERSST analysis is updated with the available GTS ship and buoy data. The anomalies are computed with respect to 1971-2000 month climatology (Xue et al, 2003). ERSST version 2 was an improved extended reconstruction of ERSST version 1. However ERSST version 3 differs form ERSST version 2 by the inclusion of satellite data.

2.9 Optimum Interpolated Sea Surface Temperature data

Daily high resolution SST data from NOAA Optimum Interpolated Sea Surface Temperature Version-2 (OISST-V2) (Reynolds et al, 2007) is used for analysing the daily oceanic conditions. The data have a spatial grid resolution of 0.25° x 0.25° latitude-longitude grid and a temporal resolution of 1 day. NOAA OISST has two versions; one uses the Advanced Very High Resolution Radiometer (AVHRR) infrared satellite SST data and other uses AVHRR and Advanced Microwave Scanning Radiometer (AMSR) on the NASA Earth Observing System satellite SST data. Both products also use in situ data from ships and buoys and include

a large-scale adjustment of satellite biases with respect to the in situ data. The AVHRR-only product was used in the thesis. The AVHRR-only product uses Pathfinder AVHRR data and operational AVHRR data from 2006 onwards.

2.10 Tropical Rain Measuring Mission Microwave Imager data

Tropical Rain Measuring Mission (TRMM) is a joint NASA Japan Aerospace Exploration Agency (JAXA) mission. TRMM Microwave Imager (TMI) is a passive microwave sensor on-board TRMM which measures the intensity of radiation at five separate frequencies 10.7, 19.35, 22.235, 37.0 and 85.5 GHz to estimate the SST, rain rate, vertical integrated moisture, near surface wind speed and cloud liquid water content. These data are acquired on a 0.25° x 0.25° latitude-longitude grid resolution globally from 39°S to 39°N latitudes and the data is available since November 1997. Daily ascending and descending passes and three day averaged data can be obtained from remote sensing systems (http://ssmi.com).

2.11 Aviso Sea Surface Height Anomaly Data

Merged Sea Surface Height Anomaly (SSHA) is the data in which sea surface height from satellites Jason1, Envisat and GFO (Geosat Follow On) are merged together. This data is available on 1/3 ° mercator grid horizontal resolution. The near real time merged SSHA data from SSALTO/DUACS which is distributed by Aviso and available at http://www.aviso.ocean.obs.com is used in this thesis. Details of the satellite data merging process is given in SSALTO/DUACS handbook (2010). Combining data from different satellites significantly improves the estimation of mesoscale signals in SSHA (Le Traon and Dibarboure, 1999; Le Traon et al, 2001; Pascual et al, 2006).

2.12 Madden Julian Oscillation index

The real-time multivariate MJO index (RMM) developed by Wheeler and Hendon (2004); available at http://cawcr.gov.au/staff/mwheeler/maproom/RMM/ is used in this thesis. This index is developed based on the first two empirical orthogonal functions (EOF) of the combined fields of equatorially averaged 850 hPa zonal wind, 200 hPa zonal wind, and OLR. The two leading principal components (PC) corresponding to the two EOFs, known as Real-Time Multivariate MJO series 1 and 2 (RMM1 and RMM2 respectively) is used to calculate the phase and amplitude of eastward MJO propagation. The amplitude and the phase of MJO for each day in the entire time period are provided in the dataset.

2.13 National Oceanic and Atmospheric Administration - Climate Prediction Center Nino 3.4 index

The monthly Nino 3.4 SST indices obtained from the NOAA Climate Prediction Center (CPC) website (CPC, 2011) is used for defining the El Nino and La Nina years. The index is created from ERSST version 3b and the SST anomalies are calculated for the Nio 3.4 region (5°N − 5°S, 120° − 170°W) based on centered 30-year base periods updated every 5 years. El Nino (La Nina) years are defined such that the October-December averaged SST anomaly of the region is above (below) a threshold value of 0.5°C and the condition should persist for a minimum of 5 consecutive over-lapping months.

2.14 Indian Ocean Dipole index

The IOD index, also known as Dipole Mode Index (DMI) is obtained from Japan Agency for Marine-Earth Science and Technology (JAMSTEC) website (JAMSTEC, 2011). Intensity of the IOD is represented by anomalous SST gradient between the western equatorial Indian Ocean (50°E−70°E and 10°S−10°N) and the south eastern equatorial Indian Ocean (90°E−110°E and 10°S−0°N).

When the DMI is positive then, the phenomenon is refereed as the positive IOD and when it is negative, it is refereed as negative IOD. The index used in the thesis is derived from HadISST and monthly index is available from 1958.

Chapter 3

The Influence of Madden Julian Oscillation in the Genesis of North Indian Ocean Tropical Cyclones

3.1 Introduction

The relation between MJO and tropical cyclones can be attributed to the deep convection in the convective phase and the associated strengthening of equatorial lower tropospheric westerly wind towards the west of the area of convection (Rui and Wang, 1990). Such a situation leads to an increase in cyclonic vorticity in the atmospheric boundary layer of the low latitude regions north and south of the equator. MJO is also characterized by enhanced upper level divergence associated with the convective phase.

Liebmann et al (1994) observed that the cyclones preferentially occur during the convective phase of MJO, and cluster around the low-level cyclonic vorticity and upper level divergence anomalies that appear poleward and westward of the large-scale convective anomaly along the equator. Later studies have shown the importance of eddy kinetic energy associated with the convective phase of MJO in the formation of cyclones. Maloney and Hartman (2001) noticed that when 850 hPa wind anomalies of MJO are westerly, small-scale slow-moving eddies

grow through barotropic eddy kinetic energy conversion from the mean flow and these growing eddies, together with strong surface convergence, 850 hPa cyclonic wind shear (vorticity) and high mean SST, create a favourable environment for tropical cyclone formation. Leroy and Wheeler (2008) developed a statistical scheme to predict the tropical cyclone activity in the southern hemisphere using five predictors in which two represents the eastward propagation of the MJO, two represents the leading patterns of interannual SST variability in the Indo-Pacific Oceans and one represent the climatological seasonal cycle of tropical cyclone activity in each zone. They found that inclusion of indices of the MJO as predictors leads to increased skill out to about three weeks.

Roundy (2008) discussed in detail the interaction of convectively coupled Kelvin wave with MJO in North Indian Ocean basin and has shown that the MJO phase modulates the intensity of moist deep convection associated with the Kelvin waves. The role of convectively coupled waves like MJO, convectively coupled equatorial Rossby, Kelvin, and mixed Rossby-gravity waves in the modulation of south Indian Ocean tropical cyclones were analysed by Besafi and Wheeler (2006) who studied the dynamical controls of these waves on tropical cyclone through wave-induced perturbations to the dynamical fields of low-level vorticity, vertical shear, and deep convection. They have shown that large-scale atmospheric variability caused by MJO and equatorial Rossby waves is important for the modulation of tropical cyclones in south Indian Ocean and can be used for prediction purposes extending up to few weeks.

The cyclones having their genesis in the area bounded by latitudes 0° to 15°N and longitudes 60°E to 100°E has been studied as outside this area very few cyclones have their genesis in the pre-monsoon and post-monsoon seasons. In the Indian summer monsoon season (June to September) monsoon depressions (cyclonic systems weaker than tropical cyclones) are formed and their genesis area is north of the area chosen for the study. During the monsoon season very few of the cyclonic systems formed develop into cyclone intensity due to the prevailing high VWS in the environment, with LLJ in the lower troposphere and the TEJ in the upper troposphere.

3.2 Methodology

The MJO days can be clustered into 8 phases (P1, P2, P3,..., P8 hereafter) depending on the phase angle variations in the phase space created by the RMM1 and RMM2 indices (Wheeler and Hendon, 2004). Each phase represents the geographical location of the enhanced convection of the MJO with respect to the phase space. On this, the phases P1, P2, P3 and P4 represent the convective phase of MJO where the equatorial Indian Ocean is dominated by convection. Similarly the phases P5, P6, P7 and P8 represent the period when convection is suppressed in the equatorial Indian Ocean. The genesis dates of cyclones are clustered into these 8 groups based on the MJO phase in which a cyclone genesis date resides. The genesis date of a cyclone is defined as the first day of the cyclone reported in the IBTrACS dataset. Following Hall et al (2001) a statistical analysis of the significance of the number of tropical cyclone in each MJO category is done. Here a Z statistic is calculated for the 8 phases of MJO taking the null hypothesis that cyclones are equally distributed in all the phases. The statistic is given as

$$Z = \frac{P - P_0}{\sqrt{P_0\left(1 - \frac{P_0}{N}\right)}} \tag{3.1}$$

Where P and P_0 are expected and observed proportion of cyclogenesis days within a particular MJO category respectively and N is the number of days in the category. It was tested at the 95%, 98% and 99% levels, using a two-tailed test, with critical values of Z = $\pm$ 1.96, $\pm$ 2.326 and $\pm$ 2.576 respectively.

3.3 Results and discussion

3.3.1 Genesis and distribution of cyclones

From IBTrACS cyclone data, cyclonic systems with maximum sustained wind speed of 34 knots or above, which is the criteria used by India Meteorological Department for North Indian Ocean cyclones; are used in the study. Using this criteria, 118 cyclones were identified which satisfy the intensity criteria for North Indian Ocean basin from 1979 to 2008. Out of the 118 cyclones selected, 96

Table 3.1: Summary of the distribution of cyclones from January to December. Here the first row represents the total 118 cyclones formed during the period of study (1979 to 2008). The second row shows the distribution of 96 cyclones which formed in the genesis area selected for the study (0-15°N, 60°E-100°E).

Total	Jan	Feb	Mar	Apr	May	Jun	Jul	Aug	Sep	Oct	Nov	Dec
118	4	0	3	5	21	10	1	1	7	21	34	11
96	4	0	2	5	17	6	0	0	3	16	32	11

cyclones had their genesis in the study region. Figure 3.1 gives the distribution of the genesis points of cyclones in which the area inside the box (0-15°N and 60°E-100°E) represents the area of cyclogenesis selected for the study. Figure 3.1a represents the total 118 cyclones formed and figure 3.1b gives the cyclones which originated during June to September (JJAS). It can be seen that majority of the JJAS cyclones had their genesis outside the study area. The month-wise distribution of the total 118 cyclones selected and the 96 cyclones having their genesis located in the study region are given in table 3.1. It may be seen that during the monsoon season (June to September) very few cyclones have formed. Similarly there are few cyclones in February and March. Cyclone prone months are April and May and October to December which account for the majority of cyclogenesis in the area.

A phase space diagram is created using the RMM1 and RMM2 index to represent the different phases of MJO. The phase space diagram along with the distribution of cyclones is given by figure 3.2. In figure 3.2 the circle in the center of phase space with radius 1 represents days with MJO amplitude 1 and less. The back dots represent the date of cyclogenesis. Any day falling inside this circle is considered as a weak MJO day. From the phase-space diagram, it can be seen that cyclogenesis dates are clustered on the convective phase of MJO (P1 to P4). Although cyclogenesis occurred in the suppressed convection phases of MJO, majority of the days are under MJO amplitude 1.

The distributions of cyclones in different MJO categories were studied by setting different amplitudes of MJO. The MJO amplitudes, total number of cyclones

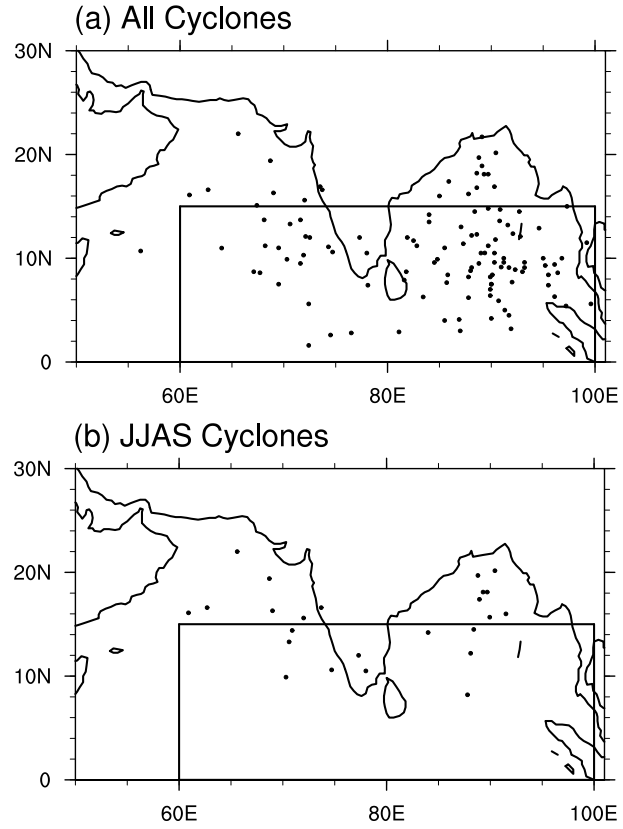

Figure 3.1: Tropical cyclone genesis location (dots) for the three decades from 1979 to 2008. The rectangular area marked in the figure shows the region selected for the study (0-15°N, 60°E-100°E) (a) Total 118 cyclones formed during 1979 to 2008 (b) Cyclones which formed from June to September.

formed under each amplitude and distribution of cyclones in each MJO phase are given in table 3.2. The first column in table 3.2 represents the MJO amplitude and the second column gives the total number of cyclones for the corresponding phase. Columns from 3 to 10 give the distribution of genesis days within the eight phases of MJO. The MJO amplitude 0.5 covers approximately 89% of the total days selected which include the majority of the cyclogenesis days and accounts for 83 cyclones out of the total 96 cyclones formed in the study area. Out of this 83 cyclones, 7 (8.4%) formed in P1, 15 (18%) in P2, 22 (26.5%) in P3, 20 (24.1%) in P4. For MJO amplitude 1, which includes approximately 61% of the total days, 54 cyclones are formed. Out of this 54 cyclones, 5 (9.3%) formed in P1, 10

Table 3.2: Summary of the distribution of tropical cyclone genesis days in the different categories of MJO for the various amplitudes taken. Here the first column represents the MJO amplitude and the second column gives the total number of cyclones for the corresponding amplitude. Columns from 4 to 7 give the distribution of genesis days with in the four categories of MJO.

MJO Amplitude	No. of Cyclones	P1	P2	P3	P4	P5	P6	P7	P8
0.5	83	7	15	22	20	8	4	5	2
1	54	5	10	13	16	5	2	2	1
1.5	27	3	4	8	8	2	1	0	1

(18.5%) in P2, 13 (24.1%) in the P3, 16 (29.3%) in the P4. Convective phase of MJO (P1, P2, P3 and P4) accounts for 44 (81.5%) of cyclones formed under MJO amplitude 1. Using the statistic defined earlier the number of cyclones phases P3 and P4 are found to be significantly high at 98% significance level. For MJO amplitude of 1.5 which includes 33.4% of the total days 27 cyclones formed. Here 22 out of 27 cyclones originated in the convective phase of MJO. In all cases, it is seen that the number of cyclogenesis days are more in the convective phase of compared with the suppressed convection phases.

The month wise distribution of the tropical cyclone genesis in each phase is given in table 3.3. As seen from table 3.3, the monthly distributions of cyclones within the MJO phases are also showing the bimodal structure similar to the general North Indian Ocean cyclone variability. As we can see the bimodal peak has its largest amplitude during November to December which accounts for 25 cyclones followed by May-June accounting 20 cyclones. For P3 more number of cyclones formed in May-June period; but for P4, majority of cyclones are formed in November-December period. Thus we have two distinct periods (May-June and November-December) of cyclogenesis for each MJO phase which is used to analyze the prevailing synoptic conditions for the phases.

The spatial distribution of cyclogenesis with the genesis points and tracks of tropical cyclones in each MJO phases are shown in figure 3.3. Here only the days with MJO amplitude 1 or above is considered. Figure 3.3a to figure 3.3d

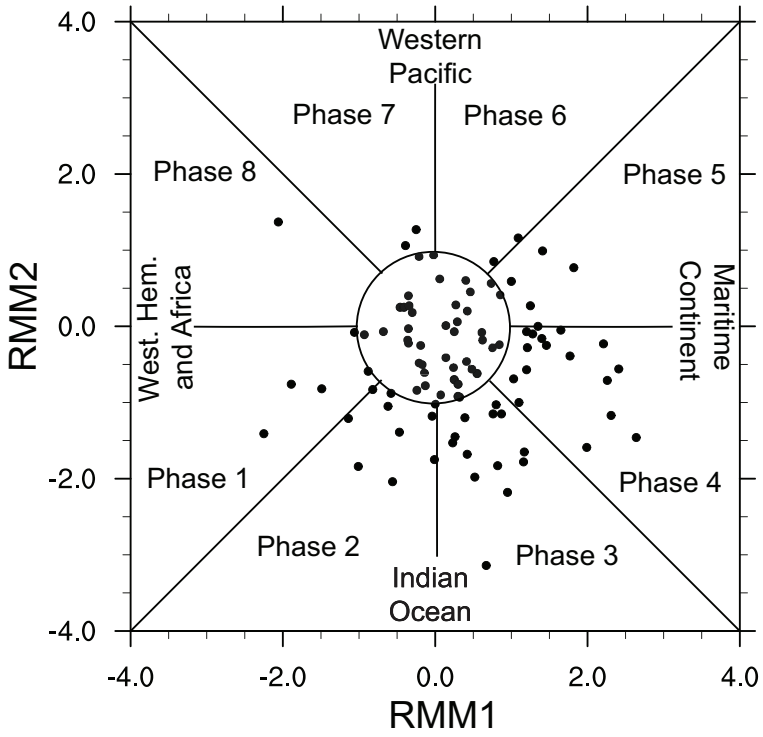

Figure 3.2: Phase amplitude diagram constructed with the principal components RMM1 and RMM2 of MJO from 1979 to 2008. The black dots represent the cyclogenesis days. Eight categories are defined according to the phase angle in which a day resides. The circle in the center with amplitude 1 represents days with weak MJO activity.

represents the convective phases of MJO and figure 3.3e to figure 3.3h represents the suppressed convection phase. For phases P1 and P2 although the number of tropical cyclones are less, they are distributed almost equally in the Arabian Sea and Bay of Bengal. But for phases P4 and P5, more cyclones are formed in the Bay of Bengal comparing with Arabian Sea. For phases P5 to P8 the cyclogenesis occurred mainly in the Bay of Bengal. The spatial distributions of cyclones are found to be highly influenced by the synoptic conditions associated with the MJO categories. A detailed discussion about the synoptic conditions leading to cyclogenesis and distribution during the phases are given in the following section.

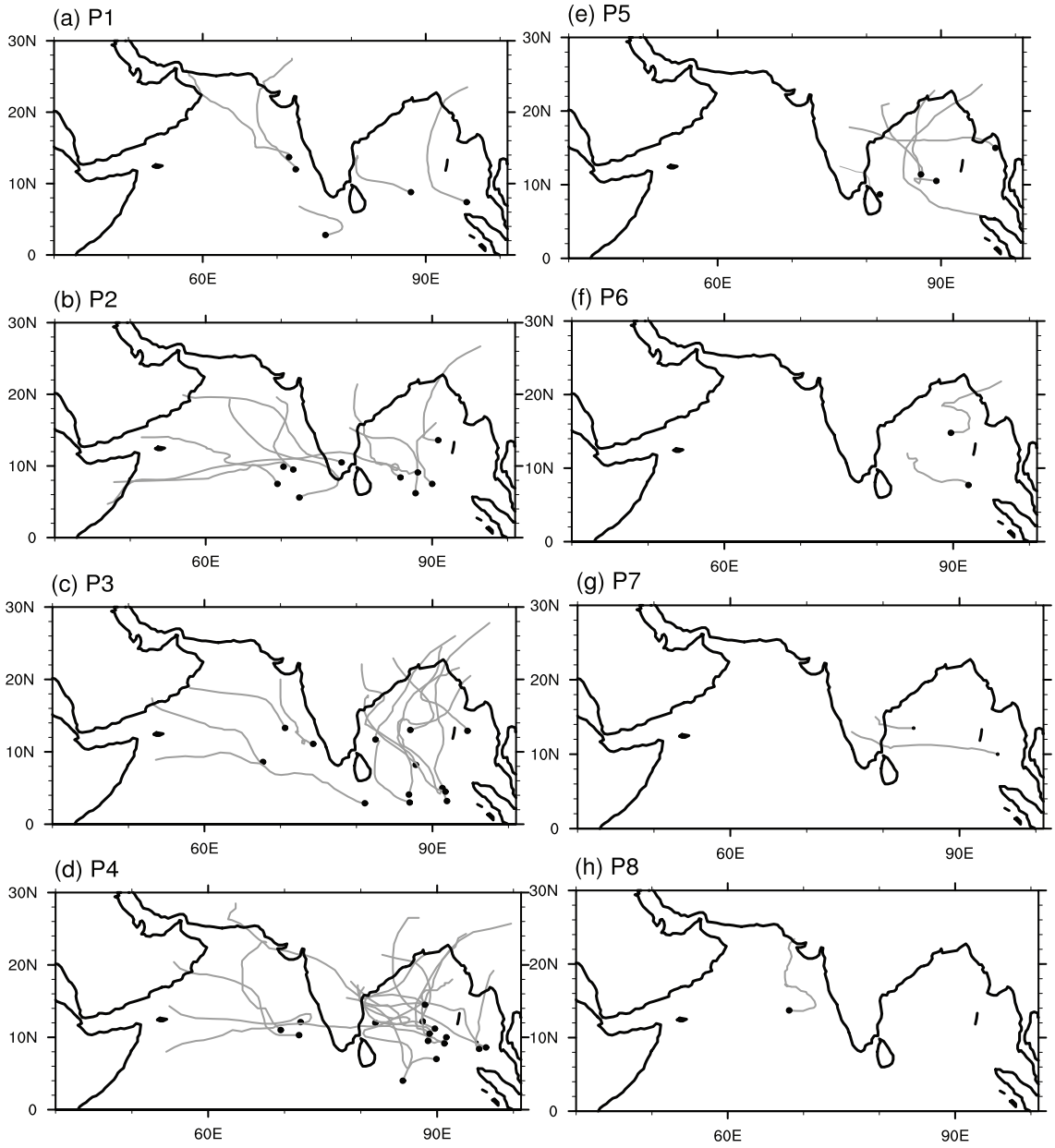

Figure 3.3: Tropical cyclone genesis location (dots) and tracks (lines) for different MJO Phases.

Table 3.3: Month wise distribution of cyclones in each phase of MJO. Here the first column represents the MJO Phase. Columns from 2 to 13 give the distribution of genesis days with in the eight categories of MJO. The last row gives the total distribution of cyclones (above MJO 1 amplitude) in the 12 months.

Phase	Jan	Feb	Mar	Apr	May	Jun	Jul	Aug	Sep	Oct	Nov	Dec
1	–	–	–	1	2	–	–	–	–	–	2	–
2	–	–	1	–	2	1	–	–	1	1	4	–
3	2	–	–	–	6	2	–	–	–	–	1	2
4	–	–	–	1	3	2	–	–	–	–	9	1
5	–	–	–	–	–	–	–	–	–	–	4	1
6	1	–	–	–	1	–	–	–	–	–	–	–
7	–	–	–	–	–	–	–	–	–	1	1	–
8	–	–	–	–	1	–	–	–	–	–	–	–
Total	3	0	1	2	15	5	0	0	1	2	21	4

3.3.2 Synoptic conditions

Synoptic conditions associated with each phase of MJO are studied by compositing the different parameters related with cyclogenesis such as OLR, SST, 850 hPa wind flow, 850 hPa vorticity and the VWS between 200 hPa and 850 hPa. SST of the study region has remained higher than 28°C in all the MJO phases during November-December. In May-June SSTs are still higher. Our study has shown that SST is not an important factor for cyclogenesis in the study region with respect to the phases of MJO. However, the large scale circulation patterns and associated changes in environmental parameters such as 850 hPa relative vorticity and VWS are important in modulating the tropical cyclone activity over the ocean basins (Chand and Walsh, 2009; Belanger et al, 2010). Composites of these fields were analysed in the study to bring out the favourable conditions which led to cyclogenesis. For each phase, the days having MJO amplitude 1 or above is composited for the months under consideration. The anomalies were calculated from these fields by subtracting the climatological mean of the months from 1979 to 2008.

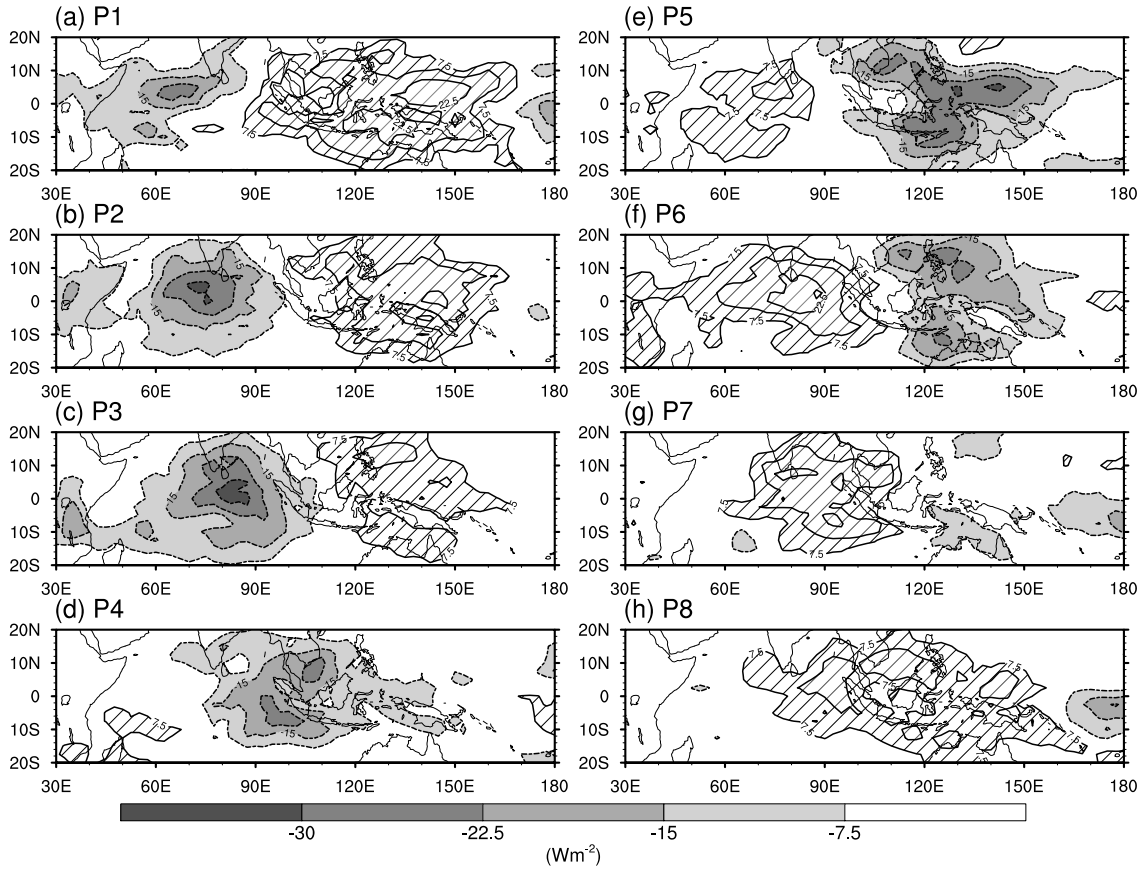

Figure 3.4: OLR anomaly composites of November-December associated with MJO phases 1 to 8. The negative contours are shaded and the positive anomaly contours are hatched. The contour interval is 7.5 Wm^{-2}.

The OLR anomaly patterns for November-December are given in figure 3.4. The eight phases of MJO convection is depicted in the figure which shows the temporal varying patterns for the season. It is seen that during the phases P1 to P4, the area of convection is located over the Indian Ocean. During P1 the convection is in its initial phase with a small patch extends over the Arabian Sea. During P2 the convection has shifted to central Indian Ocean and from there it has shifted to eastern Indian Ocean during P3. This convection further extends in P4 covering the entire eastern Indian Ocean and maritime continent. During P5 the convection over maritime continent strengthens but there is suppressed convection

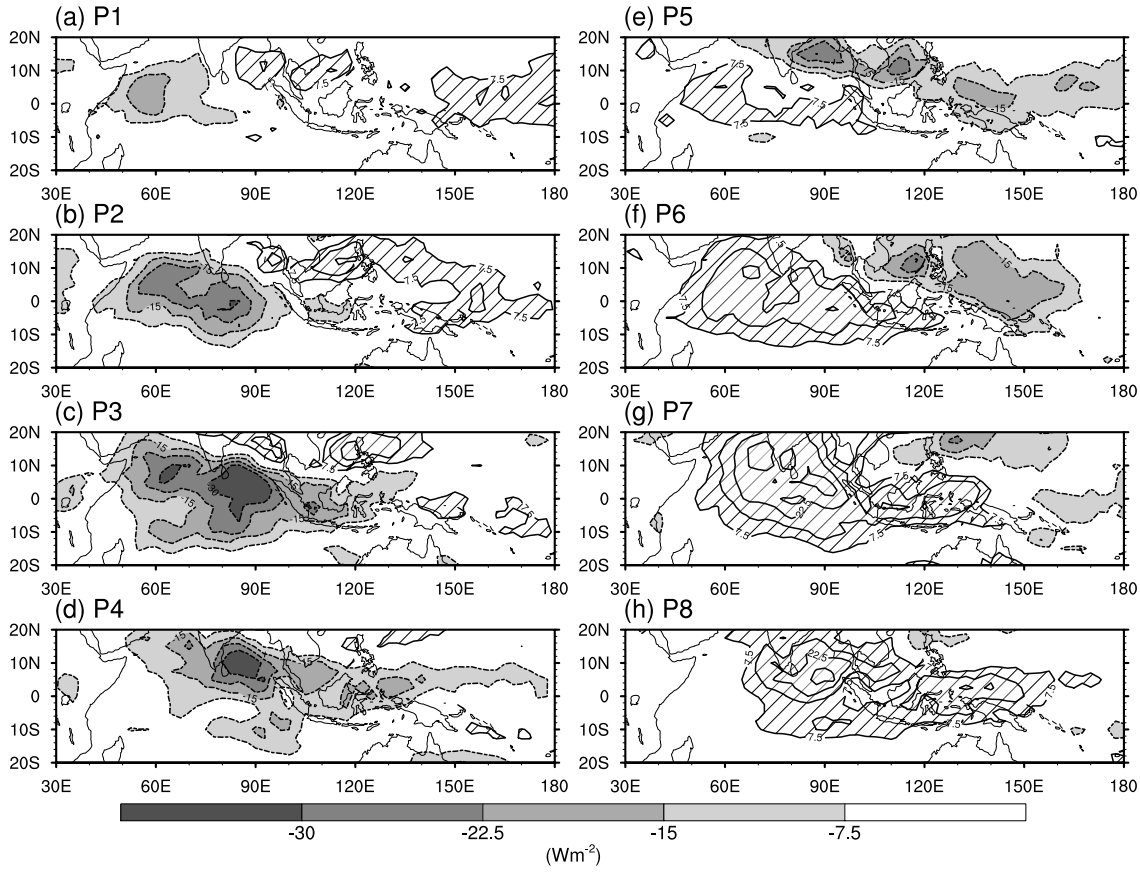

Figure 3.5: Same as figure 3.4, but for May-June.

generating over the western Indian Ocean. This suppressed convection follows the same development pattern as in the convective phase of MJO by subsequent development of suppressed convection from P5 to P8. The May-June convection patterns for the same phases are given in figure 3.5 which is identical with those given in Wheeler and Hendon (2004). Similar to P1 of November-December, the first phase (P1) of MJO consists of weak convection over the Arabian Sea. During P2 this further extends into central Indian Ocean. In P3 convection covers the entire Indian Ocean and reaches up to the maritime continent. This convection moves further eastward during P4 with a slight northward movement with an elongated patch reaching Western Pacific and covering the entire Indian Ocean. From P5 to P8, suppression phase of MJO exists over the Indian Ocean with its

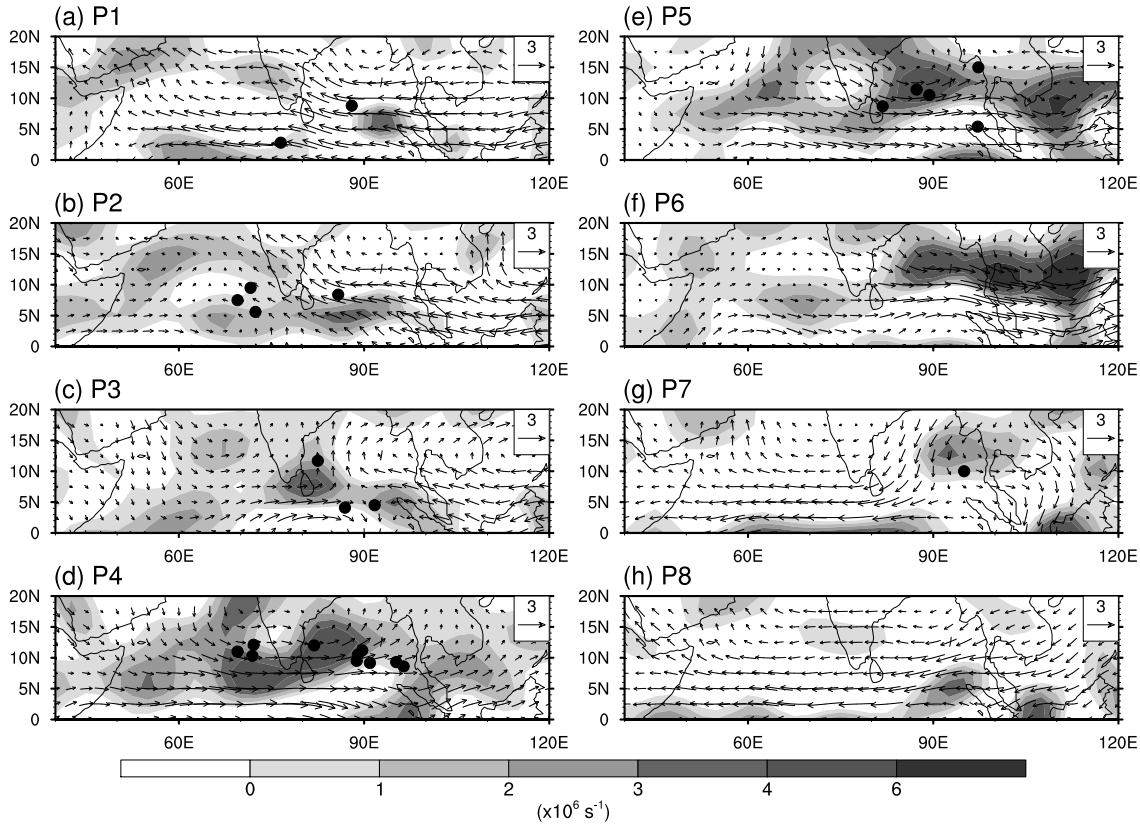

Figure 3.6: Composite 850 hPa wind and vorticity anomalies of November-December associated with MJO phases. Wind magnitude and direction is shown by the arrows. Reference vector is given in the upper right corner. Contours of cyclonic vorticity are also shown as shaded. Vorticity values are scaled by $1x10^{-5}$ and the contour interval is $1x10^{-5}s^{-1}$. The cyclogenesis points are given as black dots.

development patterns similar to the convective phases.

Wind anomaly patterns associated with the MJO convection during November-December is given in figure 3.6. The cyclone genesis points are also given in the figure for each phase as black dots. Only the positive vorticity anomaly (cyclonic vorticity) regions are shown in the diagram as shaded regions. It is seen that the cyclones are clustered around the cyclonic vorticity anomaly formed during the passage of MJO convection. In P1, as the convective region is generated over Arabian Sea, easterly wind anomaly exits over the North Indian Ocean. Two cy-

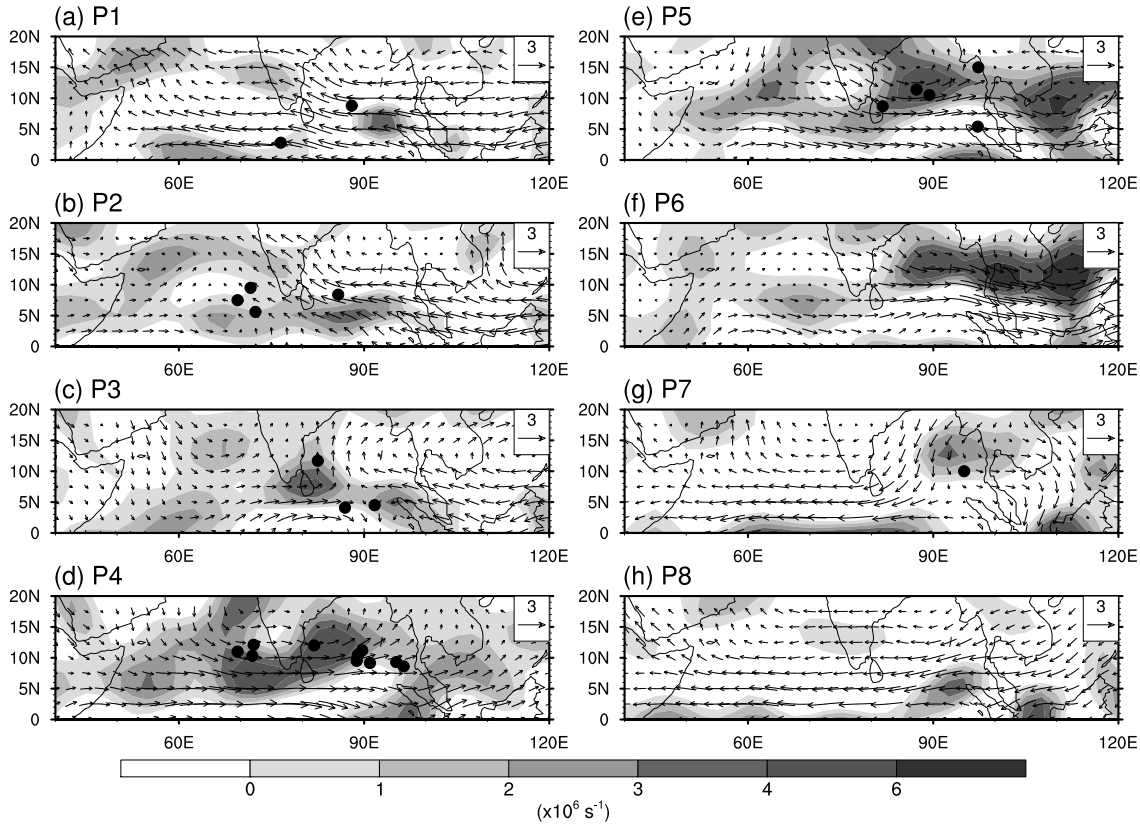

Figure 3.7: Same as figure 3.6, but for May-June.

clones had genesis in the equatorial Arabian Sea and Bay of Bengal near areas of cyclonic vorticity. As the convection moves eastward in P2, anomalous westerly flow is generated in the North Indian Ocean especially in Arabian Sea and the cyclones get formed in the cyclonic vorticity region associated with this. As the MJO convection shifts further eastward during P3 the westerly flows enter the Bay of Bengal creating a favourable vorticity region for the genesis of cyclones there. The anomalous westerly flow is strengthened further in the entire North Indian Ocean during P4, which account for 10 cyclones formed in its cyclonic vorticity region. As the convection moves to the western Pacific the westerly wind strengthens over the Bay of Bengal and 5 cyclones are formed. Thus P5 is favourable for cyclogenesis in North Indian Ocean particularly the Bay of Bengal although the convection is suppressed there. In effect the phases P1 to P5

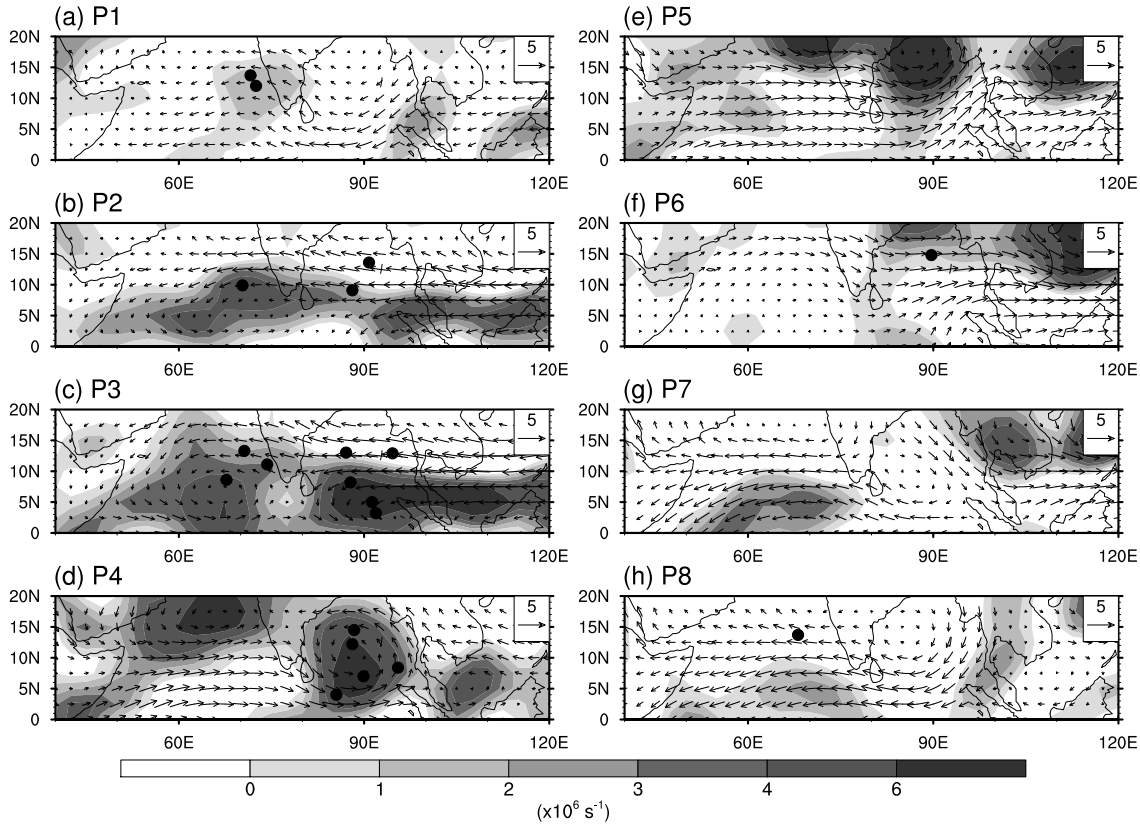

Figure 3.8: Composite VWS associated with MJO phases during November-December. The cyclogenesis points are given as black dots.

favours cyclogenesis in North Indian Ocean. From P6 to P8 although vorticity is favourable, the other environmental factors like suppressed convection and VWS (discussed later) inhibit cyclogenesis in North Indian Ocean.

Composites for May-June are shown in figure 3.7. Similar to November-December, the westerly wind anomalies are generated which moved eastwards along with the convection. Westerly wind maximum occurs during the phases P3 and P4 which accounts for the maximum cyclogenesis in North Indian Ocean. During P3 vorticity maximum exits over the Arabian Sea and Bay of Bengal accounting for 8 cyclones. In P4 the vorticity maximum region shifts eastwards and 5 cyclones are formed in the Bay of Bengal. During the phase P5, cyclonic vorticity is strong over Bay of Bengal but there is no cyclogenesis. In phases P5

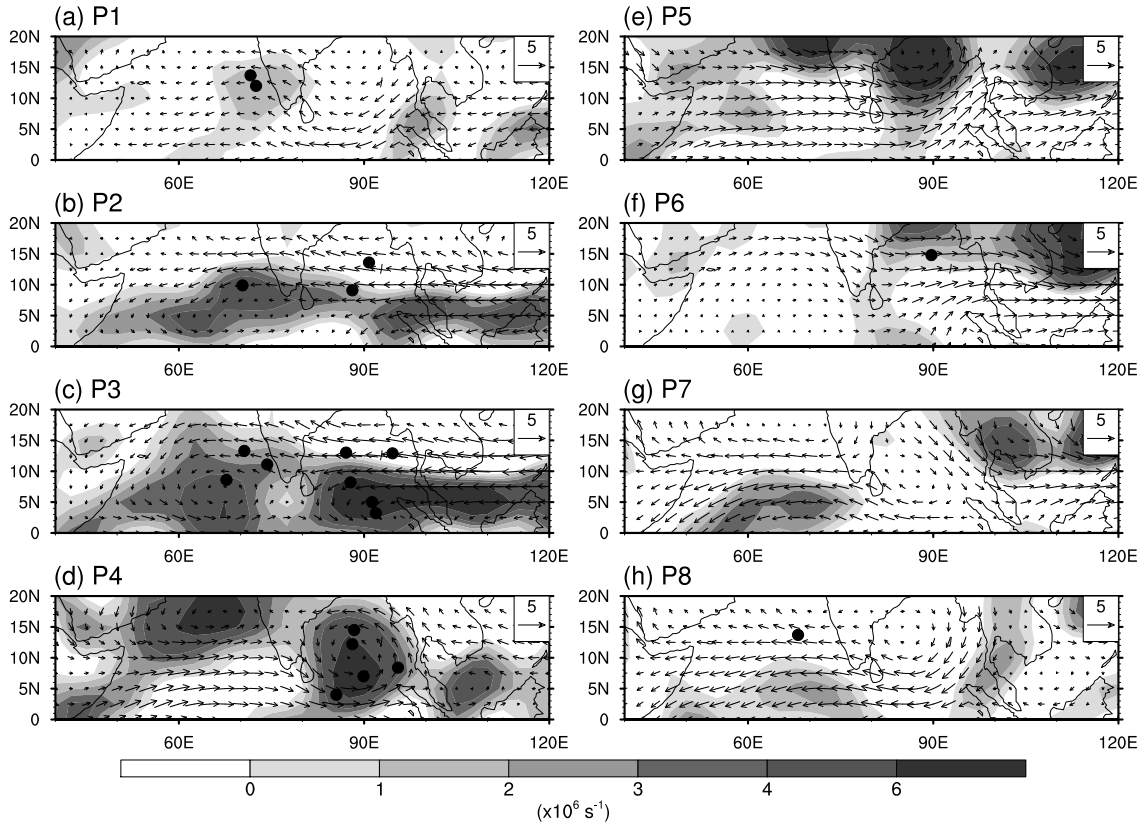

Figure 3.9: Same as figure 3.8, but for May-June.

to P8 there is little cyclogenesis as both vorticity and VWS (discussed later) are unfavourable along with the suppressed convection existing over North Indian Ocean.

Figure 3.8 and figure 3.9 represents the VWS composites for November-December and May-June seasons respectively. During November-December the VWS is found to be favourable for the study region in MJO phases P2 to P5 and cyclogenesis occures with VWS less than 8 ms^{-1}. In the other phases VWS is more that 8 ms^{-1} and there is very little cyclogenesis in the study area. Comparing with November-December, the VWS over the study region is higher during the May-June. Cyclones have occurred in large numbers during the phases P3 and P4. In these phases VWS is in the order of 8 to 16 ms^{-1}. Cyclones have occurred with these high shear values in this season, most likely due to the high

cyclonic vorticity available there at 850 hPa (See figure 3.7).

3.4 Conclusion

Formation of cyclonic storms over North Indian Ocean in the area bounded by latitudes 0 and 15°N and longitudes 60°E and 100°E during the period 1979 to 2008 have been studied with respect to the eastward passage of Madden-Julian Oscillation. In this study, MJO intensity with amplitude 1 and above is considered, which includes 61.24% days of the whole period. There were a total of 118 cyclones in the three decades out of which 96 formed in the study region. The relationship between these cyclones with the different phases of MJO has been studied.

The cyclones are clustered in eight phases of MJO and have been analysed by selecting different amplitude criteria. The number of the MJO days for each amplitude varies significantly from one to another. However irrespective of the amplitudes chosen, it is observed that cyclogenesis over North Indian Ocean basin preferentially occurred during the convective phase of MJO (P1 to P4). By selecting MJO amplitude 1 and above 81.5% of the cyclones formed was under the convective phase of MJO. Further increasing the amplitude to 1.5, convective phase of MJO dominates by accounting 22 out of the 27 cyclones formed. The study has also shown that P3 and P4 of MJO have the highest favourable environment for cyclogenesis in Bay of Bengal.

The spatial distribution of the cyclogenesis is seen to be highly associated with the synoptic conditions existing over the North Indian Ocean during the phases. Phases P1 and P2 are associated with the initial phase of the MJO cycle where active convection occurs over equatorial Indian Ocean. This active convection area will induce strong equatorial westerlies to its west and associated cyclonic vorticity. The cyclogenesis location is seen to be distributed in the Arabian Sea and Bay of Bengal almost equally. In the next three phases of the MJO cycle (P3 to P5) the equatorial area of active convection has moved to the Bay of Bengal and the adjoining western Pacific and the associated westerlies in the lower troposphere cover the whole of equatorial Indian Ocean and is particularly strong over the equatorial areas south of Bay of Bengal. These phases are thus

most favourable for cyclogenesis in the Bay of Bengal. The cyclogenesis locations are seen to be distributed more in the Bay of Bengal comparing with Arabian Sea. In phases P6 to P8 the equatorial convection has moved further east and the subsiding motion in the North Indian Ocean leads to suppressed convection and thereby develops unfavourable conditions for cyclogenesis.

The cyclogenesis parameters were composited and analysed for the different phases of MJO particularity 850 hPa wind and vorticity. The cyclonic vorticity appearing the north and south of the flow induced by the westerly phases of MJO are significantly influencing the cyclogenesis. The axis of the 850 hPa wind maxima particularly the zonal component is seen to be shifting from Arabian Sea to Bay of Bengal changing the location of cyclogenesis. Vertical shear of zonal wind is found to be favorable during the P3 and P4 phases of November-December and May-June seasons which account for the maximum number of cyclone formation in those phases.

In this study intensification trends or the direction of movement of tropical cyclones in any category were not examined. Although the convective phase of MJO is found to be favourable for cyclogenesis, further studies are needed for using MJO as an effective predictor of cyclogenesis in North Indian Ocean.

Chapter 4

Interannual Variations of Tropical Cyclone Activity over the North Indian Ocean

4.1 Introduction

For the Indian Ocean basin, inter-annual climate variability is highly influenced by ENSO. Variability of Indian summer monsoon rainfall (ISMR) in interannual timescales is modulated by ENSO (Sikka, 1980; Pant, 1981; Ashok et al, 2001) although the relationship varies between decades (Kumar et al, 1999). Indian Ocean Dipole (IOD) (Saji et al, 1999), which is another mode of interannual variability in Indian Ocean, characterized by east-west SST anomaly over Indian ocean is highly related with ENSO. A large percentage of positive IOD (negative IOD) years are El Nino (La Nina) years (see table 4.1). Available literature on ENSO-tropical cyclone interaction over North Indian Ocean is mainly concentrated on the Bay of Bengal cyclones during the post-monsoon (October-December) season (Gupta and Muthuchami, 1991; Ng and Chan, 2011; Girishkumar and Ravichandran, 2012). Gupta and Muthuchami (1991) observed that during El Nino years tropical cyclones formed over Bay of Bengal landfalls south of 17°N and the numbers of these storms are highly correlated with the southern oscillation indices. Singh et al (2000) found that the frequency of tropical cyclones in North Indian Ocean during May and November reduces during warm phases of ENSO. Ng and

Chan (2011) showed that apart from the local SST, moist static energy and atmospheric flow patterns forced by ENSO modulates the interannual variability of tropical cyclones over Bay of Bengal during the post-monsoon season. Using 30 years of IBtRACS cyclone data, interannual variations in genesis region, direction of movement and intensity of post monsoon (October-December) tropical cyclones over north Indian Ocean basin associated with ENSO is analysed.

4.2 Methodology

Interannual variation in these cyclones have been studied with respect to, El Nino and La Nina of the years 1979 to 2008. The monthly Nino 3.4 SST indices obtained from the NOAA Climate Prediction Center (CPC) website are used for defining the El Nino and La Nina years, and are listed in table 4.1. The positive/negative IOD years obtained from JAMSTEC website are also listed in 4.1. El Nino (La Nina) years are defined such that the October-December averaged SST anomaly of the region is above (below) a value of 0.5. Thus the years 1982, 1986, 1987, 1991, 1994, 1997, 2002, 2004 and 2006 are considered as El Nino-0 years and 1983, 1984, 1988, 1995, 1998, 1999, 2000, 2005 and 2007 years are considered as La Nina years. Thus we have 9 years each of El Nino and La Nina in the 30 years 1979 to 2008. El Nino spans two consecutive years, the first year of which (warming phase) is called El Nino-0 year.

The tropical cyclone Genesis Potential Index (GPI) developed by Emmanuel and Nolan (2004) is used in the study. Camargo et al (2007) subsequently used this index to analyse the effects of ENSO on GPI over the global ocean basins. The GPI is given by

$$GPI = \left|10^5\eta\right|^{3/2} \left(\frac{H}{50}\right)^3 \left(\frac{V_{max}}{50}\right)^3 (1 + V_{shear})^{-2} \tag{4.1}$$

where η is the absolute vorticity at 850 hPa , H is the relative humidity at 600 hPa in percent, V_{max} is the potential intensity Emanuel (1995), and V_{shear} is the magnitude of the VWS between 850 hPa and 200 hPa. The value of V_{max} is calculated as

Table 4.1: List of years when El Nino or La Nina and/or negative or positive IOD occured.

Year	El Nino/La Nina	PIOD/NIOD
1979	-	-
1980	-	NIOD
1981	-	-
1982	El Nino	PIOD
1983	La Nina	-
1984	La Nina	NIOD
1985	-	-
1986	El Nino	-
1987	El Nino	PIOD
1988	La Nina	-
1989	-	-
1990	-	-
1991	El Nino	PIOD
1992	-	NIOD
1993	-	-
1994	El Nino	PIOD
1995	La Nina	-
1996	-	NIOD
1997	El Nino	PIOD
1998	La Nina	NIOD
1999	La Nina	-
2000	La Nina	-
2001	-	-
2002	El Nino	PIOD
2003	-	PIOD
2004	El Nino	-
2005	La Nina	NIOD
2006	El Nino	PIOD
2007	La Nina	-
2008	-	-

$$V_{max} = \sqrt{\frac{T_S}{T_0} - \frac{C_K}{C_D}\left(CAPE^* - CAPE\right)_m} \tag{4.2}$$

where T_S is the SST, T_0 is the mean outflow temperature (temperature at the level of neutral buoyancy), C_K is the exchange coefficient for enthalpy, C_D is a drag coefficient, CAPE* is the convective available potential energy of air lifted from saturation at sea level in reference to the environmental sounding, and CAPE is that of boundary layer air.

For analyzing the parameters related to the tropical cyclones, several parameters such as 850 hPa wind, 850 hPa vorticity, 200 hPa wind, 200 hPa divergence, SST and GPI are composited and analysed. Anomalies of these parameters are computed with respect to a climatological field, which is an averaged field of the season (October-December) from 1979 to 2008.

4.3 Results and discussion

4.3.1 Changes in lower tropospheric circulation

The ENSO is characterized by easterly-westerly fluctuations in the lower troposphere wind over the equatorial Pacific. During a La Nina year or a normal year, large area of warm water over the Western Pacific causes the wind to converge over this region, which becomes the upward limb for Indian Ocean and Pacific Walker cell. During this time, lower tropospheric winds are westerly over the Indian Ocean and easterly over the equatorial Pacific. As the westerly wind flow is established in equatorial Indian Ocean, it enhances cyclonic vorticity north and south of this flow. This will create an increase in cyclonic vorticity over the cyclogenesis region over North Indian Ocean since it is in the wind shear region of these winds. In order to analyse the lower tropospheric circulation patterns, 850 hPa wind and vorticity are composited for El Nino-0, El Nino-1, El Nino+1 and La Nina years.

The changes in lower tropospheric Indian Ocean Walker circulation patterns and their anomalies associated with ENSO are depicted in figure 4.1. During El

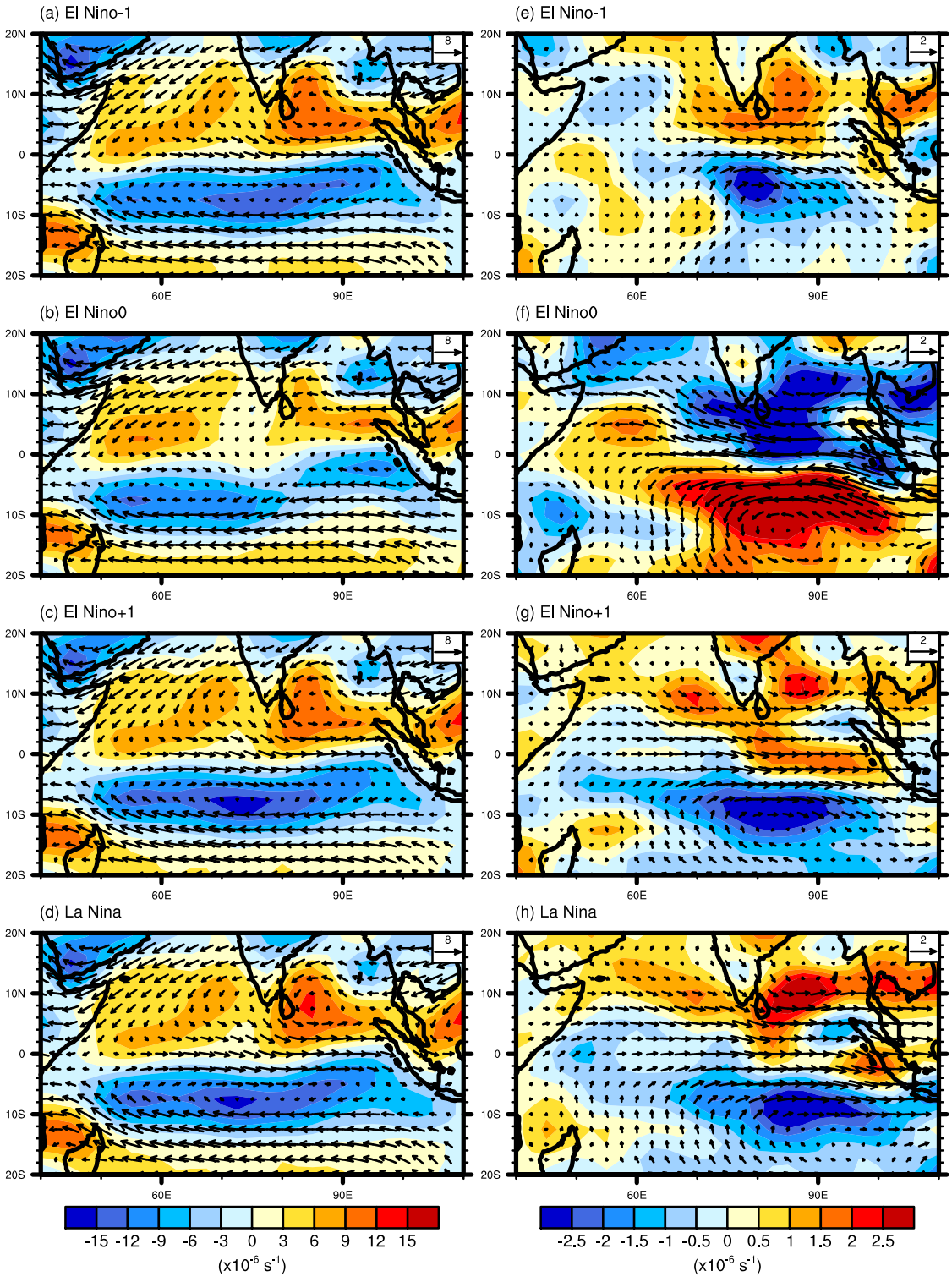

Figure 4.1: Composites of circulation and vorticity patterns and their anomalies associated with different phases of ENSO a) El Nino-1 b) El Nino-0 c) El Nino+1 and d) La Nina years.

Nino-1, El Nino+1 and La Nina years there is strong westerly wind flow over the equatorial Indian Ocean as can be seen from figure 4.1a, 4.1c, 4.1d. There is strong cyclonic vorticity over the North Indian Ocean especially in Bay of Bengal. The anomalous wind and vorticity field also shows the same features. There is strong westerly anomaly and associated increase of the cyclonic vorticity over Bay of Bengal during the non El Nino years. During the El Nino-0 years the convection is shifted to the central Pacific Ocean changing the normal circulation patterns in the whole Indo-Pacific region. Along with this shift, the upward limb of the Walker circulation over the north Indian Ocean shifts to the central Indian Ocean. These changes are depicted in figure 4.1b,4.1f where the reduction in the westerly wind and associated decrease in cyclonic vorticity over the Indian ocean are shown. The anomalies of wind and vorticity also shows the same signal in which a large negative vorticity anomaly region in over the Bay of Bengal. Thus the decrease in the available vorticity for the cyclogenesis is reduced considerably during the El Nino-0 years which lead to the reduced cyclogenesis over the region. Most of the El Nino-0 years are positive IOD years which further reduces the magnitude of the lower tropospheric westerlies over the region.

4.3.2 Changes associated with cyclogenesis

In order to differentiate the general characters of tropical cyclones between El Nino and non El Nino years, composites of tracks are made and analysed.The tropical cyclone tracks composited shows large differences in basic characteristics such as genesis, tracks and intensity of a tropical cyclone during the El Nino and non El Nino years. Figure 4.2 gives the composite of genesis points and tracks of tropical cyclones during October to December for El Nino-1, El Nino-0, El Nino+1 and La Nina years. The first reported point of the cyclone is given as black dot and the colour of the track represents maximum intensity reached by a cyclone. Cyclones are grouped into four categories; Cyclonic storms (CS) (34 to 47 knots), severe cyclonic storms (SCS) (48 to 64 knots), very severe cyclonic storms (VSCS) (64 to 119 knots) and super cyclonic storm (SUCS) (above 119 knots) based on the maximum intensity following IMD classification for Indian Ocean.

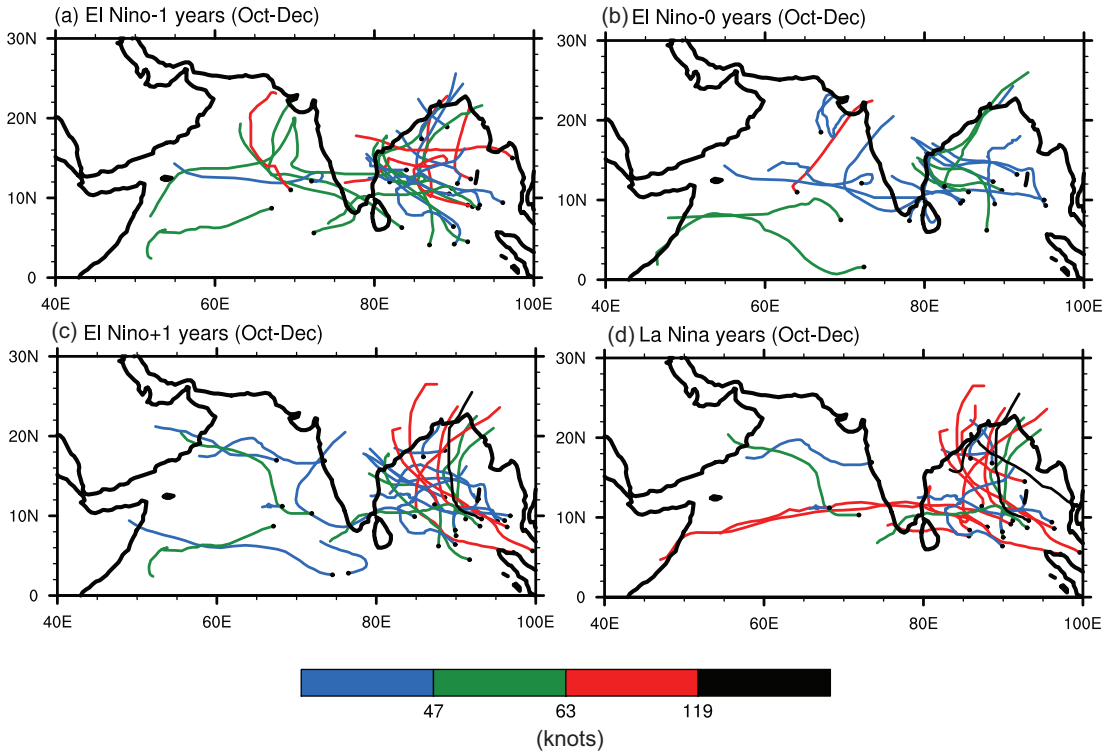

Figure 4.2: Cyclogenesis points and tracks associated with a) El Nino-1 years b) El Nino-0 c) El Nino+1 and La Nina years. The different colours in tracks represent the different intensity categories of the storm.

From figure 4.2, it can be seen that the tropical cyclone activity over the North Indian Ocean basin in comparatively low during the El Nino-0 years. Also the genesis region shifts westward during the El Nino-0 years which is consistent with the result from Girishkumar and Ravichandran (2012). During El Nino-1 and El Nino+1 and La Nina years, cyclone genesis is distributed over the entire Bay of Bengal region. But during El Nino-0 years, cyclogenesis are more constrained in the southern Bay of Bengal as seen from figure 4.2c. Camargo et al (2007) observed that there is a shifting of GPI from northern Bay of Bengal to southern Bay of Bengal during El Nino-0 years. They attributed these changes to the variations in wind shear. The genesis character over the Arabian Sea does not show much change over the years. The variations in GPI associated with ENSO will be discussed in detail on later sections.

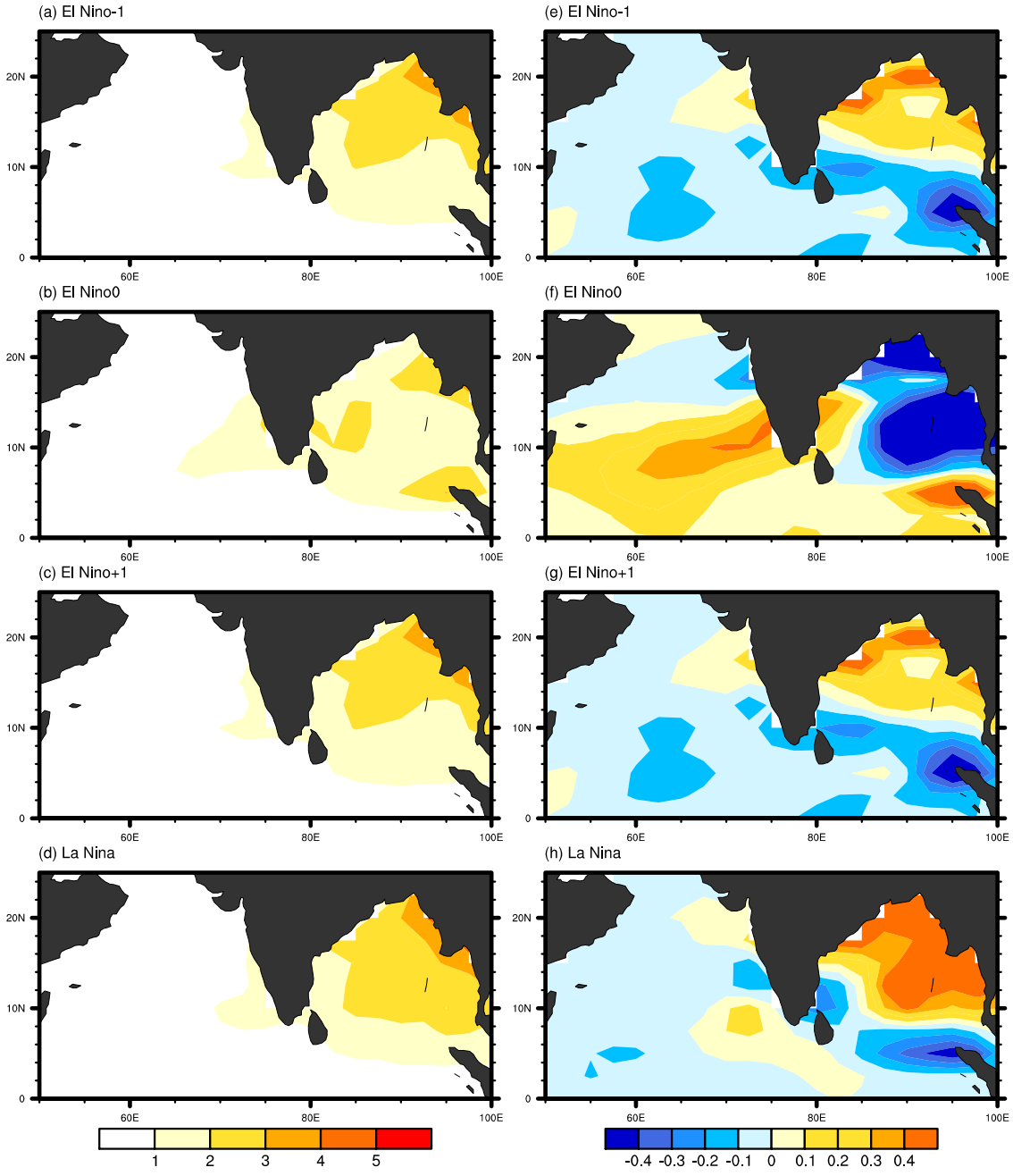

Figure 4.3: Composite GPI patterns and their anomalies associated with different phases of ENSO a) El Nino-1 b) El Nino-0 c) El Nino+1 and d) La Nina years.

4.3.3 Changes in genesis potential index

The variation in the mean genesis regions are analysed using a genesis potential index calculated from the environmental parameters. Camarago et al (2007) used this index to study the ENSO related variations in tropical cyclone genesis around the globe. Menkes et al (2012) evaluated the performance of four cyclogenesis indices in different ocean basins and found that genesis potential calculated by Emmanuel and Nolan (2004) and Tippett et al (2011) are best adjusted indices for North Indian Ocean.

The October-December GPI is composited for different phases of ENSO. Figure 4.3 depict the changes in the genesis potential index and its anomaly associated with the El Nino-1, El Nino-0, El Nino+1 and La Nina years. During El Nino+1 and La Nina years, high values of GPI are available over the North Indian Ocean especially over the Bay of Bengal region. Although there are positive GPI values over Bay of Bengal during El Nino-0 years, the values are much less compared with the La Nina years especially over the northern Bay of Bengal. The composite anomalies of GPI are given in figure 4.3e to 4.3f. During El Nino-0 years large area of negative GPI anomaly is over the Bay of Bengal. Thus the reduced cyclogenesis potential during El Nino-0 is causing the reduction in tropical cyclone activity. For La Nina years the entire pattern is opposite and there is a high value of positive GPI anomaly over Bay of Bengal. From both El Nino-0 and La Nina events it can be seen that the area of activity is enhanced over the western Bay of Bengal which explains the shift in the cyclogenesis area.

The reasons for the reduction in GPI during El Nino-0 years is examined by considering the individual parameters used for calculating the GPI. Relative contributions of each of the 4 parameters used in GPI are examined by the method given in Camarago et al (2007). For each variable, the relative contribution is analysed by recalculating GPI, taking actual varying values of one variable and for other 3 variables, long-term unvarying monthly climatological fields are used. The procedure is then repeated for all the variables. The relative contributions of the four variables are composited for El Nino-0 and non El Nino years. For all the parameters the composite anomaly for El Nino-0 and La Nina years are depicted in figure 4.4. Of the thermodynamic parameters, 600 hPa relative humidity shows

a maximum (minimum) over the eastern Bay of Bengal during the La Nina (El Nino-0) years. Maximum potential intensity parameter has not much variability between the periods. The relative contribution of vorticity at 850 hPa is showing a positive (negative) anomaly in Bay of Bengal during La Nina (El Nino-0) years. This is due to the reduced 850 hPa vorticity over Bay of Bengal during the El Nino years. During El Nino-0 years, the relative contribution from VWS shows large positive values over the southern Bay of Bengal and Arabian Sea. This favorable condition during El Nino-0 years is due to the decrease in VWS since both the lower and upper tropospheric wind over Bay of Bengal weakens during the El Nino-0 years. Thus it is inferred that the large contribution from relative humidity and 850 hPa vorticity in the eastern Indian Ocean causes the shifting of genesis region during the El Nino-0 years. Also the southward shifting of VWS component during El Nino-0 years enhances the cyclogenesis over the southern Bay of Bengal which was also observed by Camarago et al (2007).

4.3.4 Changes in intensity

There is strong interannual variation in the intensity of North Indian Ocean cyclones as observed from figure 4.2. Intensity of tropical cyclones are reduced considerably during an El Nino-0 year compared with non El Nino years. The number of tropical cyclone in each intensity category which are formed in different phases of ENSO is given in table 4.2. The total number of tropical cyclones formed during El Nino-0 years are almost equal to the La Nina years with a difference of 4 tropical cyclones. The major difference is in the intensity during the El Nino-0 years since there is a significant decrease in the tropical cyclones with intensity above VSC category. During the El Nino-0 years 95% of cyclones (18 out of 19) formed are under the VSC category but during La Nina years it is only 52% (12 out of 23) and remaining 48% (11 out of 23) are above the VSC.

The maximum potential intensity estimated by Emmanuel (1994) does not consider dynamic influences like VWS which restricts the development of the storm. From the composites of MPI (not shown) it is observed that there are not much differences between the values during El Nino-0 and La Nina years. Also during the El Nino-0 years, VWS is favourable for cyclogenesis in North

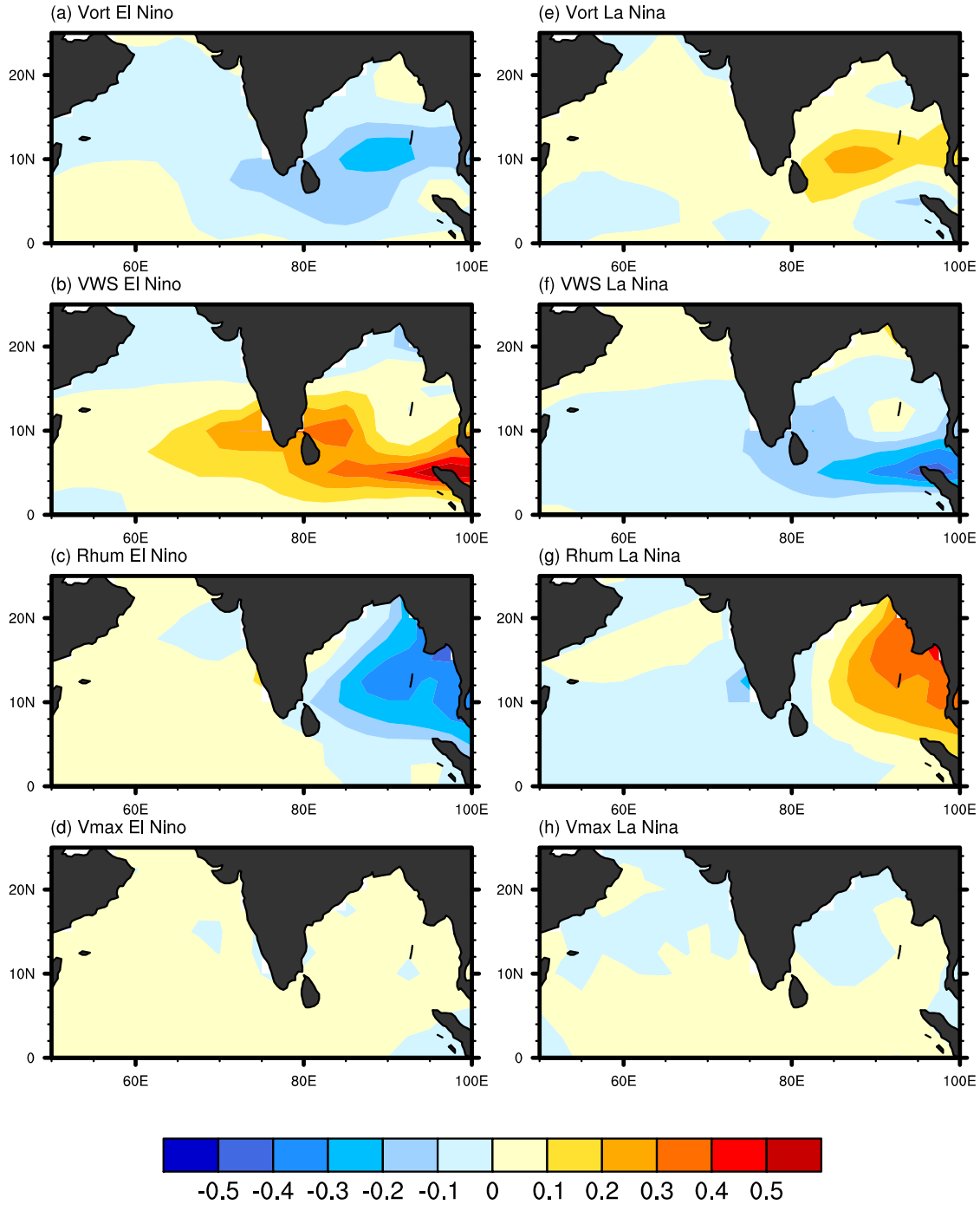

Figure 4.4: Anomalies in genesis potential index owing to the four parameters a) vorticity b) VWS c) relative humidity and d) potential intensity during El Nino-0 (left panel) and La Nina (right panel).

Table 4.2: The distribution of tropical cyclone intensity categories in the different phases of ENSO

Category	Total	CS	SCS	VSC	SUCS
El Nino-1	23	9	9	5	0
El Nino 0	19	12	6	1	0
El Nino+1	27	15	7	4	1
La Nina	23	8	4	9	2

Indian Ocean. Although VWS and thermodynamic MPI are favourable, there is a decrease in the intensity of tropical cyclones during El Nino-0 years. Since North Indian Ocean is bounded by land to the north, the change in the direction of tracks affects the intensity. This is more evident in Bay of Bengal since westward moving storms makes landfall faster than the northward moving storms. The genesis region during El Nino-0 years shifts to the eastern Bay of Bengal and the direction of movement is westward comparing with the northward moving tropical cyclones in non El Nino years. If we set 17°N as a threshold point for land fall, it is seen that most of the tropical cyclones make land fall below this in El Nino-0 years which is consistent with the observation of Gupta and Muthuchami (1991).

Tropical cyclones formed during La Nina years moves northward and makes landfall over north Bay of Bengal. As the tropical cyclones remains over the ocean for a long duration before the landfall, the intensity of the cyclones are increased. A similar type of intensification mechanism was observed in Western North Pacific by Emmanuel (2000) and Camarago et al (2007). Camarago et al (2007) found that although the potential intensity (Emmanuel, 1986) is less over the Western North Pacific, the increase in intensity of tropical cyclones during El Nino-0 years is due to the longer lifetimes that occur as a result of the eastward displacement in mean genesis location. Girishkumar and Ravichandran (2012) reported a similar intensification mechanism for Bay of Bengal cyclones. The shifting of genesis region is found to be caused by variations in vorticity, VWS and relative humidity.

4.4 Conclusion

The interannual variations in the genesis, intensity and tracks of the post-monsoon (October-December) north Indian Ocean tropical cyclones with respect to the ENSO are analysed using data of 30 years. It is observed that there is a reduction in the intensity and frequency of tropical cyclones formed over the north Indian Ocean during the El Nino-0 years compared with the non El Nino years. Due to the changes in circulation patterns associated with El Nino-0, the 850 hPa equatorial westerlies over the north Indian Ocean reduces considerably which in turn reduces the vorticity over the tropical cyclone genesis region. A southward shifting of the genesis region is observed during the El Nino-0 years along with a zonal shift towards east.

Analysis using a genesis potential index (GPI) shows that anomalous negative values of GPI exists over the northern Bay of Bengal during the El Nino-0 years which inhibit cyclogenesis over the region. The relative contribution of individual parameters are examined and it is found that low values of VWS over southern Bay of Bengal during El Nino-0 years favours the southward shift of genesis region. Vorticity and relative humidity parameters are found to be favourable for La Nina years and higher contributions of these parameters are responsible for the westward shift of mean genesis region over the Bay of Bengal. The tropical cyclone tracks are west bound during the El Nino-0 years compared with the northward moving tropical cyclones during La Nina, which is caused by the changes in upper tropospheric circulation patterns. Although the VWS is less favourable compared with El Nino-0 years, tropical cyclones during La Nina intensifies more since the duration of northward moving tropical cyclones over the oceanic region is more due to their northward motion.

Chapter 5

Decadal Variation in the Intensity and Frequency of Tropical Cyclones and Monsoon Depressions of North Indian Ocean

5.1 Introduction

The North Indian Ocean cyclones are known to have a bimodal distribution with a primary maximum around October to December and a secondary maximum around March to May (Atlas IMD, 1979; McBride, 1995). The two sub-basins of North Indian Ocean, viz., Arabian Sea and Bay of Bengal, show major differences in tropical cyclone activity. The cyclone activity is more over Bay of Bengal compared to that of Arabian Sea. In the present study we examined the variability of tropical cyclones and monsoon depressions of North Indian Ocean basin. There are two types of climatic variations (a) Type-1: decadal changes (a few decades of increased activity followed by a few decades of decreased activity) a sort of long duration oscillation, and (b) Type-2: long term increase or decrease (trends).

5.2 Results and discussion

5.2.1 Decadal variations of monsoon depressions

Several studies reported that the annual frequency of monsoon depressions has a large decreasing trend (eg: Bhalme, 1972; Joseph and Xavier, 1999; Kumar and Dash, 2001; Dash et al, 2004). Joseph and Xavier (1999) analysed the annual frequency of tropical cyclones and monsoon depressions of North Indian Ocean for the period 1891-1998 and found that the third harmonic (of period 36 years) has the largest amplitude. The present study focused on the variations in the annual frequency of occurrence of monsoon depressions from 1891 to 2009. Annual frequency of monsoon depressions from 1891 to 2009 is given in figure 5.1. There is a statistically significant and strong decreasing linear trend with a superposed multidecadal oscillation as shown by the 5-year moving average. Harmonic analysis indicates a prominent third harmonic of period 39 years as marked in the figure. We designated this feature as a Four Decade Oscillation (FDO). The frequency of monsoon depressions had reduced from a large number of occurrences ($\approx$ 12 per year) in the 1890's to a much small number (3-4 per year) in the recent years. The major part of the decrease in monsoon depressions has occurred after 1950s. Separate linear trends for the periods 1891-1960 and 1950-2009 are also shown in figure 5.1. The FDO signal has amplitude of about 1 depression above or below its mean state. In the recent period, FDO amplitude attained the maximum around 1970 and minimum around 1990. During the last 60 years (1950 to 2009) high quality re-analysed data are available (Kalnay et al, 1996). Monsoon depressions and tropical cyclones of the period 1965 to 2009 have been monitored using data obtained from weather satellites. Thus the FDO cycle from 1965 to 2009 had very reliable observational data.

Studies have attributed the changes in the frequency of monsoon depressions to the climate change in the Indian Ocean region especially the changes in SST (Rajeevan et al, 2000; Jadhav and Munot, 2008). Dash et al (2004) found a decrease in the horizontal and vertical wind shears of the mean monsoon flow over India as well as over the Bay of Bengal and decrease in the moisture and convection over the Bay of Bengal area. According to Sikka (1977) one of the

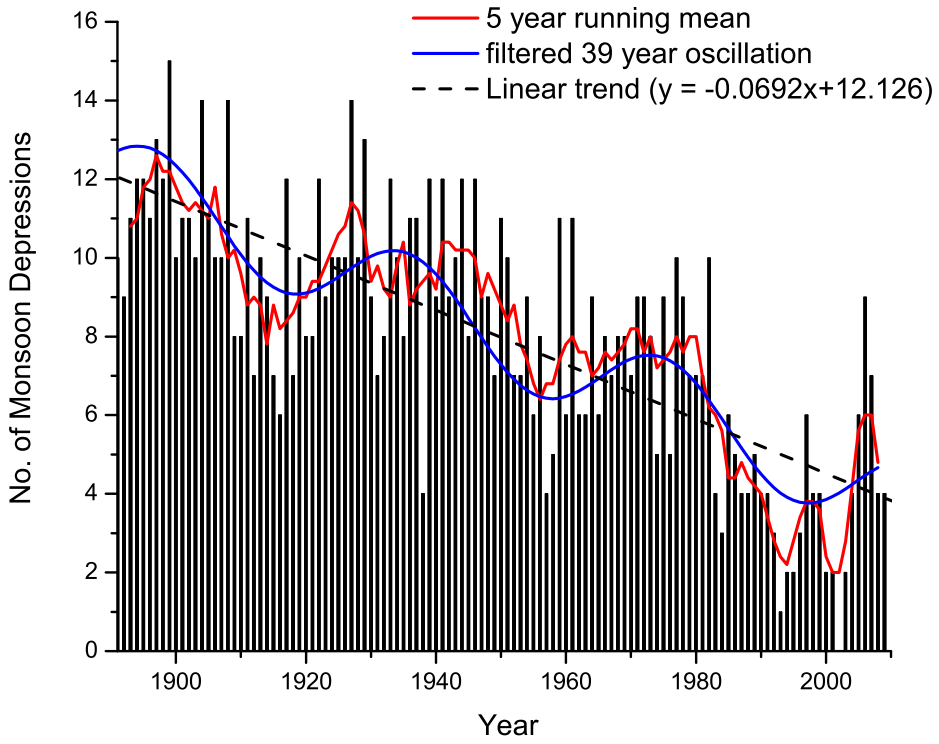

Figure 5.1: Annual frequency of monsoon depressions from 1891 to 2009.

major synoptic conditions for the genesis of monsoon depression is the strong flow of monsoon LLJ through peninsular India and Bay of Bengal. Monsoon depression is known to be formed in the cyclonic vorticity area associated with LLJ (Sikka, 1977). Studies reveal that the intensity of the LLJ had a decreasing trend during 1950 to 2002 (Joseph and Simon, 2005).

The decrease in the intensity of LLJ (June-September averaged zonal wind through an area bounded by latitudes 10°N to 20°N and longitudes 75°E to 90°E from 1950 to 2009 is shown in figure 5.2. A 5-year running mean is marked in the figure. A 35-45 year filter has been applied to the data and this variation is also marked. It is hypothesized that the FDO and decreasing trend in monsoon depressions are caused by the change in intensity of the monsoon LLJ. In order to find out the strength of the relationship, a correlation analysis has been carried out between the strength of LLJ and the frequency of monsoon depressions during each monsoon. The correlation coefficient increases from 0.35 to 0.56 when 5 year

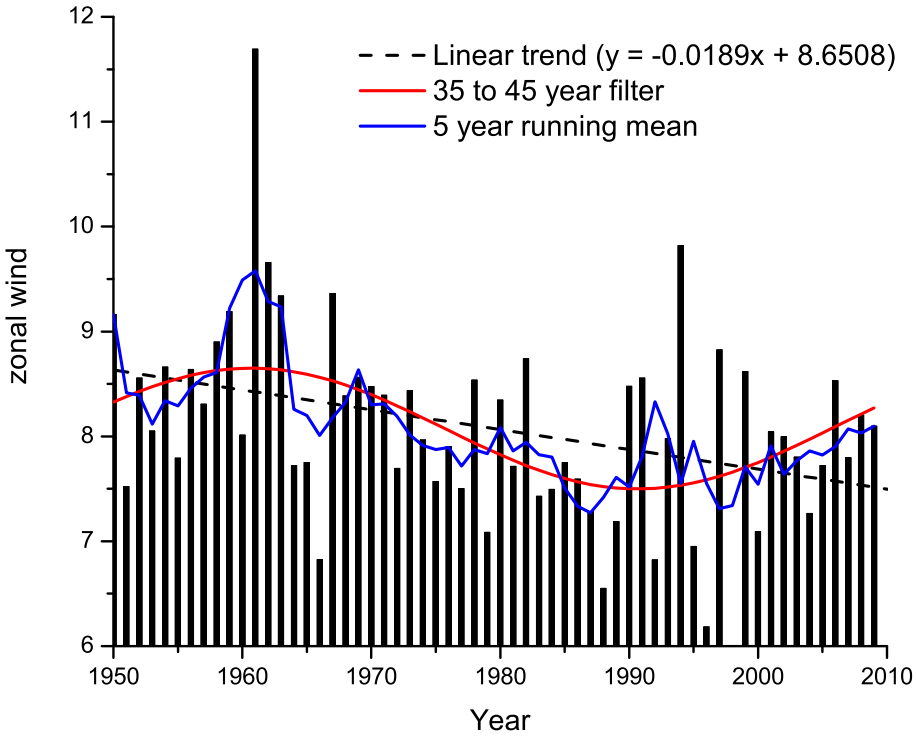

Figure 5.2: Strength of monsoon LLJ (zonal wind in ms^{-1}) averaged over an area 10°N-20°N, 75°E-90°E. The linear trend (dashed line), 5-year moving average (blue curve) and 35 to 45 year filtered data (red curve) are indicated.

running mean is considered, which is high and statistically significant.

5.2.2 Rapid warming of the Indian Ocean as related to monsoon depressions

Joseph and Sabin (2008) reported a rapid increase in the SST of the equatorial Indian Ocean during the monsoon season from 1950 which resulted in an increase in the convection over the area. This increased convection resulted in the weakening the monsoon Hadley circulation and the consequent weakening of the LLJ, TEJ and the southern hemisphere STJ (Joseph and Sabin, 2008). The weakening of the LLJ could be the possible cause for the decreasing trend in the frequency of monsoon depressions. The decrease in the intensity of TEJ associated with

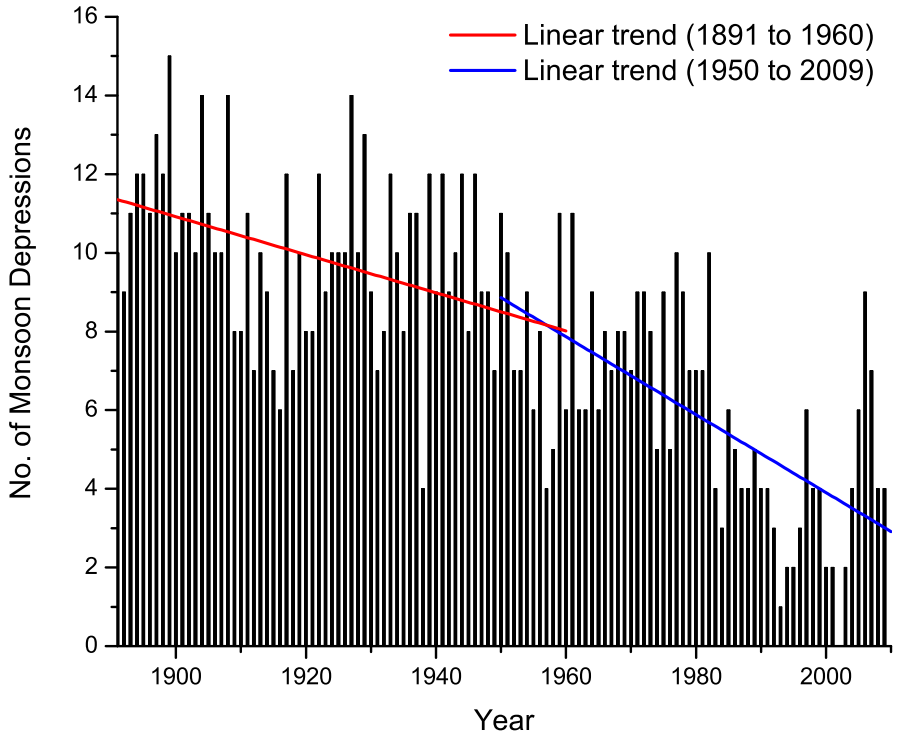

Figure 5.3: Annual frequency of monsoon depressions from 1891 to 2009.

the weakening of monsoon causes a major reduction in the VWS over the region. According to Rao et al (2008) there is a possibility of increasing intensity of the cyclonic disturbances over North Indian Ocean during the summer monsoon. In support of this view, they have shown that a super cyclone *Gonu* formed over the Arabian Sea in 2007 for the first time in the recorded history.

The rapid warming of the Indian Ocean and the corresponding changes in the frequency of monsoon depressions is shown in figure 5.3, 5.4 respectively. For SST, the June-September average over an area bounded by latitudes 5°S to 5°N and longitudes 60°E to 90°E is taken. The SST showed only a small increasing trend prior to 1950 and correspondingly monsoon depressions is also having a small decreasing trend. But after 1950, the SST showed a rapid increasing trend, whereas monsoon depressions showed a rapid decreasing trend during the corresponding period, from about 10 depressions in 1950s to about 3 in 2000s.

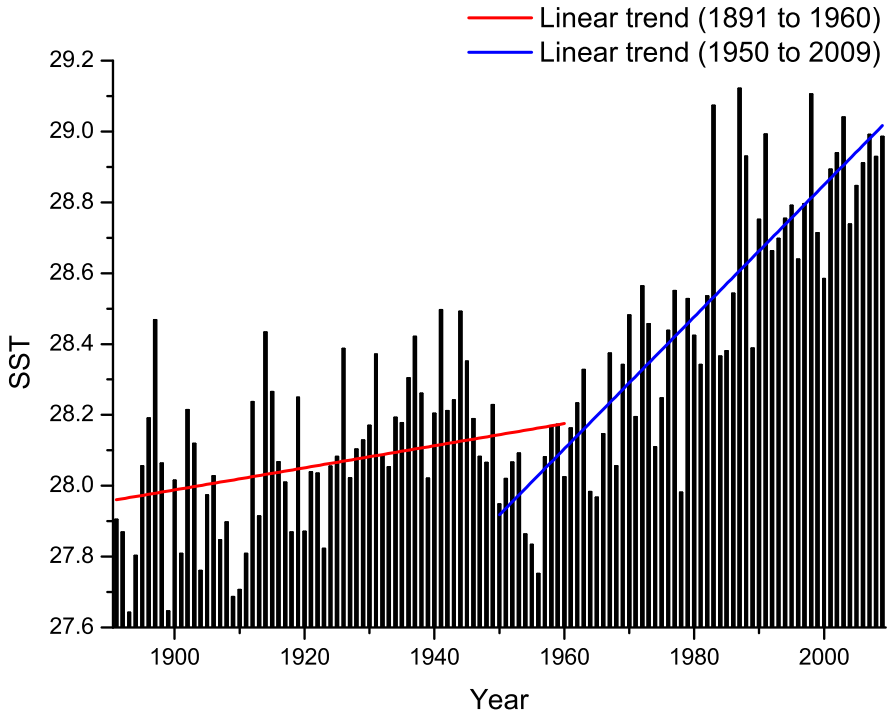

Figure 5.4: SST of equatorial Indian Ocean averaged over the area 5°S-5°N, 60°E -90°E.

5.2.3 Decadal variation in tropical cyclones

Similar to the climate change in monsoon depressions, the frequency of tropical cyclones in North Indian Ocean basin shows a long-term decreasing trend and a distinct multi-decadal oscillation. Comparing with monsoon depressions, the decreasing trend is smaller in the case of tropical cyclones. The annual frequency of tropical cyclones which formed over the North Indian Ocean basin from 1891 to 2009 is shown in figure 5.5. The filtered 39 year oscillation, 5 year running mean of cyclone frequency and the linear trend are also illustrated. The average number of cyclones has decreased from about 6 in 1890s to nearly 4 in the recent decades. Similar to the decadal oscillations in monsoon depressions, frequency of tropical cyclones also shows multidecadal oscillations with period close to four decades as earlier shown by Joseph and Xavier (1999). The FDO in tropical cyclones has a High Frequency Period (HFP) followed by a Low Frequency Period (LFP).

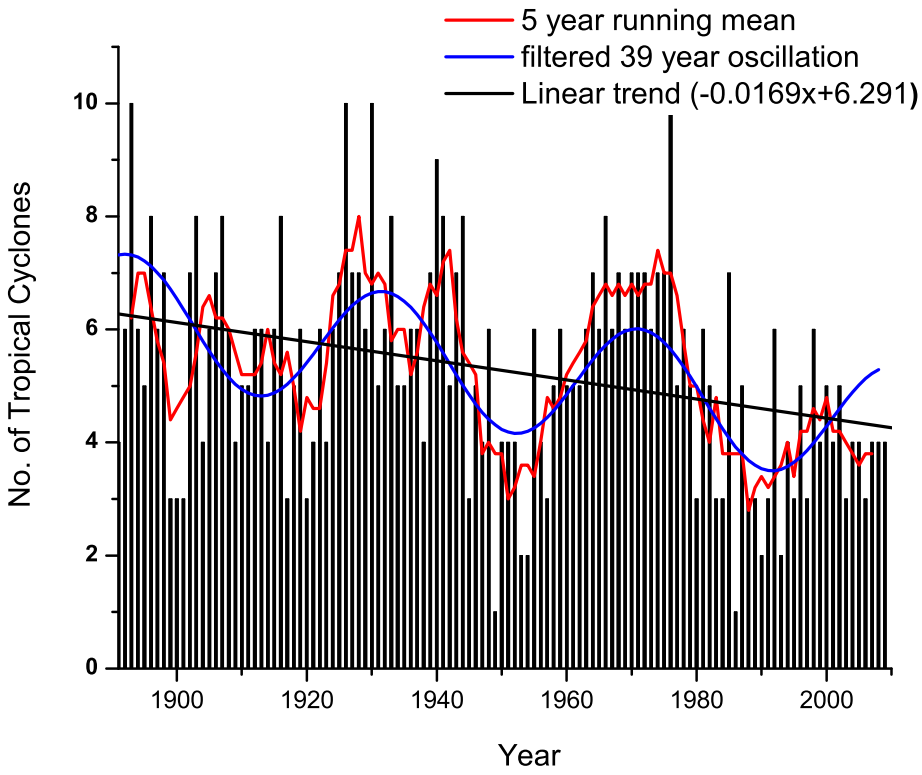

Figure 5.5: Annual frequency of tropical cyclones from 1891 to 2009.

Similar to monsoon depressions, the FDO signal in tropical cyclones is also having amplitude of about 1 cyclone above or below its mean. In the recent years FDO had its HFP in the decade 1965-1974 and LFP during 1985-1994. These two decades are well covered with the reanalysis datasets and satellite observations.

Although there are multi-decadal modes in the frequency of tropical cyclones reported in other ocean basins, related to Pacific decadal oscillations, Atlantic multidecadal oscillation, and North Atlantic oscillations, none of these is related to the frequency of tropical cyclones and monsoon depressions of North Indian Ocean. The temporal phases of tropical cyclones and monsoon depressions, both are close to each other; there is only a small phase difference of about 4 years, with tropical cyclones leading monsoon depressions as can be seen in figure 5.6 which gives the third harmonic of frequencies of both these systems.

Xavier and Joseph (2000) reported a decadal scale variation in VWS over

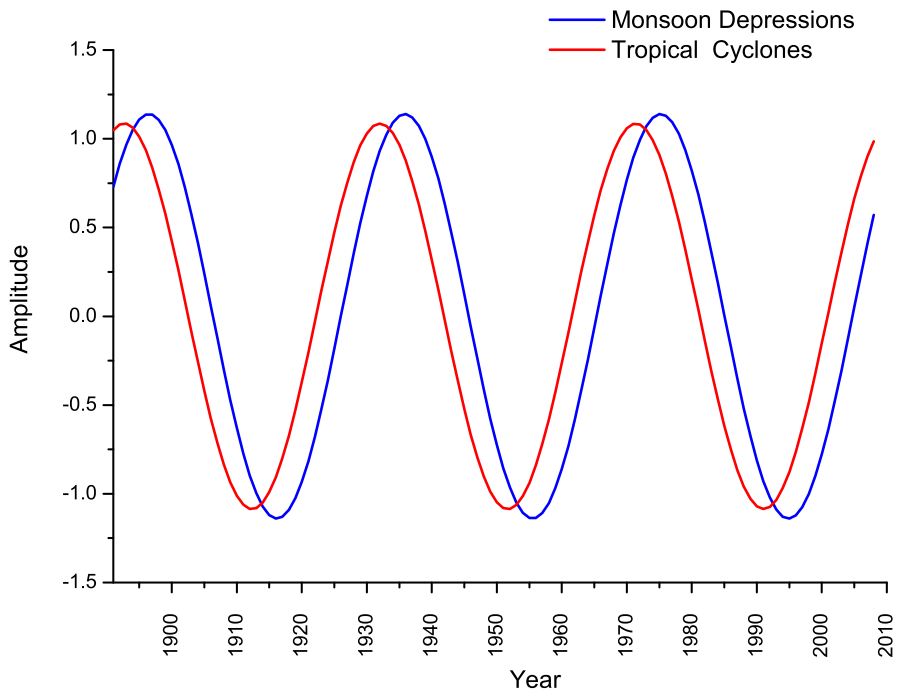

Figure 5.6: Third harmonics of annual frequency of monsoon depressions and tropical cyclones.

North Indian Ocean which possibly influences the decadal oscillation in frequency of tropical cyclones. Pattanaik (2005) found that it is not SST but the large scale atmospheric circulation that is responsible for the interdecadal variability of cyclones of North Indian Ocean. The FDO in tropical cyclone frequency was studied in detail by considering the variations in Gray (1979) parameters associated with cyclogenesis. Cyclogenesis parameters such as SST, wind at 850 hPa and 200 hPa, VWS, vorticity at 850 hPa, divergence at 200 hPa, and humidity at different levels were analysed. The cyclogenesis parameters were analysed for the area bounded by latitudes 7.5°N-15°N and longitudes 80°E-92.5°E. The cyclogenesis parameters were analysed for this area for the October-December season of 1948 to 2009. Among these variables, VWS and vorticity at 850 hPa has shown a multi-decadal oscillation consistent with the FDO in tropical cyclones. The decadal oscillation in VWS was further analysed for Bay of Bengal considering a larger area bounded by latitudes 7°N-25°N and longitudes 80°E-100°E.

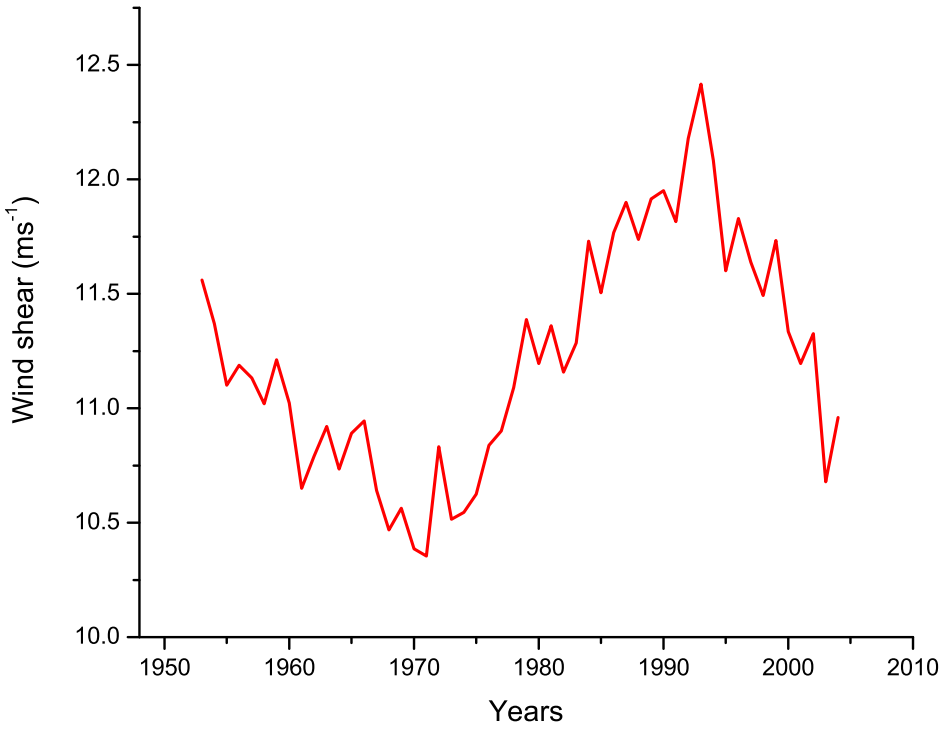

Figure 5.7: The 11-year moving average of VWS over Bay of Bengal (7°N-25°N, 80°E-100°E).

The 11-year running mean of VWS over this area is depicted in figure 5.7. This clearly shows a decadal oscillation in the VWS in phase with the observed FDO in tropical cyclone frequency.

In order to understand the decadal variation in 850 hPa wind flow and vorticity, composites of the parameters are analysed for the HFP and LFP. The difference in 850 hPa wind field between the composites of HFP and LFP is shown in figure 5.8. The normal 850 hPa wind pattern over Indo-Pacific region has westerlies over equatorial Indian Ocean region and easterlies over the equatorial Pacific Ocean which is the lower tropospheric part of the Walker circulation. But from the difference between HFP and LFP (HFP - LFP) (see figure 5.7), it can be seen that the equatorial westerlies over the Indian Ocean region are stronger during HFP compared to the LFP. The equatorial wind averaged over an area bounded by latitudes 2.5°S to 7.5°N and longitudes 50°E to 100°E (marked by a

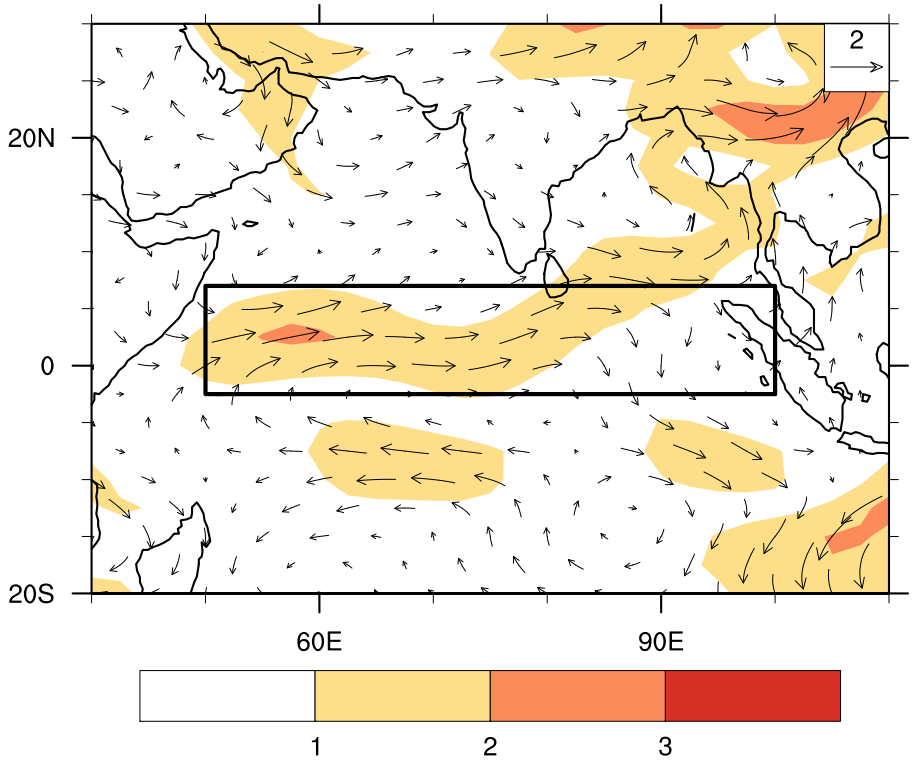

Figure 5.8: The difference in 850 hPa circulation between HFP (1965 -1974) and LFP (1985-1994).

box in figure 5.8) shows an FDO in-phase with the tropical cyclone frequency and the vorticity in the cyclone genesis region. The 11 year moving average of North Indian Ocean tropical cyclone frequency, 850 hPa wind over the equatorial Indian Ocean and vorticity at 850 hPa over the cyclone genesis region are shown in figure 5.9. All these parameters are having the same phase. The cyclone genesis region is located just to the north of the area of the equatorial westerly wind which is the cause of the cyclonic vorticity over the genesis region.

The multi-decadal variability in the equatorial westerlies over North Indian Ocean has been analysed in relation to the variations in SST over a large area of the Indian Ocean. The difference between SST of two areas, box-A (5°N- 20°N , 80°E- 100°E) and box-B (10°S- 5°N, 50°E-70°E) (marked in figure 5.10 on either side of the anomalous equatorial westerly wind was calculated. It is hypothesized

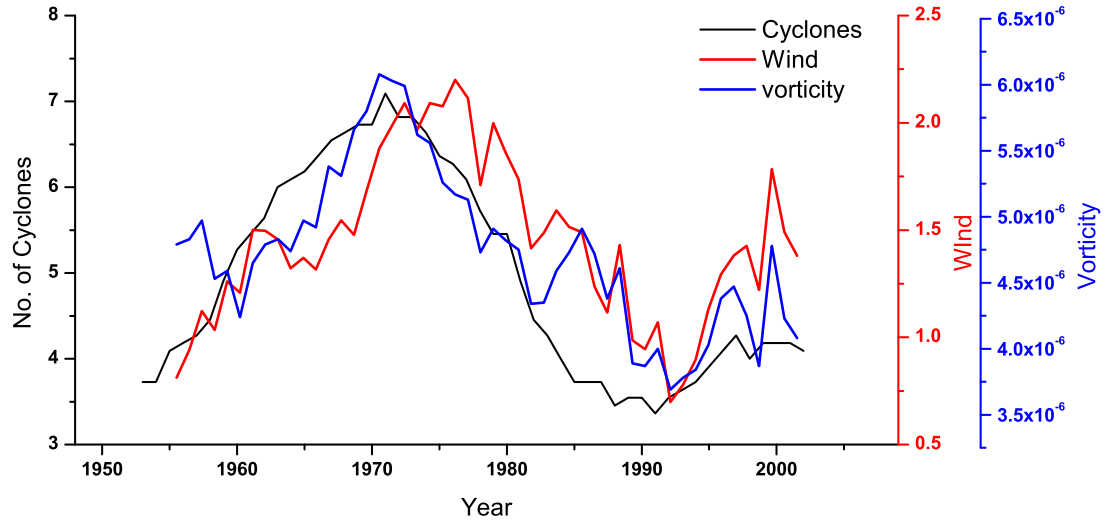

Figure 5.9: The 11-year running mean of tropical cyclone, equatorial Indian Ocean westerlies and vorticity over the genesis region.

that higher SST values over box-A can cause an increase in convection over box-A compared to box-B, which in turn can enhance the westerly flow over the equatorial Indian Ocean. The SST differences between the boxes using HadISST as well as ERSST have been calculated. The 11 year moving averages of the SST difference between the two boxes for the season October-December of 1891 to 2009 are shown in figure 5.11. It can be seen that the SST difference is also showing a decadal oscillation almost similar to the FDO in tropical cyclones. The three cycles of the FDO in tropical cyclones are thus associated with the SST. Accordingly, there is a possibility that the SST difference is forcing decadal changes in atmospheric circulation over North Indian Ocean causing the decadal variation in tropical cyclones. The cause of the FDO in the SST difference between boxes A and B is however not known.

5.2.4 Decadal changes in intensity of tropical cyclones

The long-term trends in the intensity of tropical cyclones are a matter of debate because of the data reliability issues. Although certain studies have shown an increase in intensity of tropical cyclones over the years in some ocean basin

(Emmanuel, 2005; Webster, 2005), reliability of the observed long-term data is a matter of concern. Knapp and Kossin (2007) observed that, Indian Ocean has been poorly monitored until the launch of the MeteoSat-7 satellite in 1998 and the view-angle between the existing satellites and storms in Indian Oceans was often highly oblique. Also studies reveal that the existing global hurricane records are too inconsistent to accurately measure trends from the data (Kossin et al, 2007). Using the available tropical cyclone intensity data from India Meteorological Department, the variations in the intensity of North Indian Ocean tropical cyclones are analysed. Based on the maximum sustained wind associated with the cyclone, two categories of tropical cyclones were studied; cyclonic storms (with maximum sustained wind between 34 and 47 knots) and severe cyclonic storms (with maximum sustained wind above 48 knots).

In order to investigate the climate change in the intensity, ratio of the annual frequencies of severe cyclonic storms to the cyclonic storm of North Indian Ocean basin has been calculated from 1891 to 2009. This ratio and its 5 year moving average are given in figure 5.12. The linear trend of this ratio for the full period 1891 to 2009 is marked in this figure. Linear trends representing two different

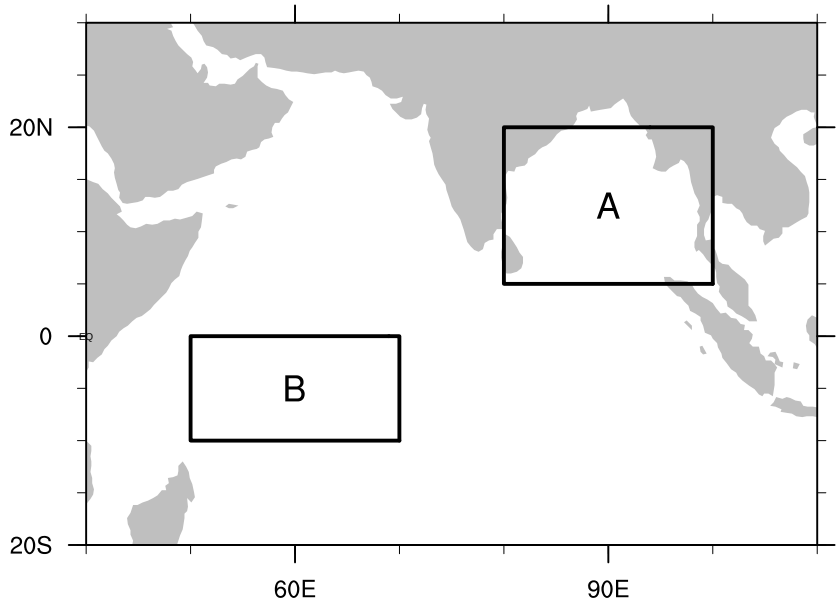

Figure 5.10: The two areas (A and B) chosen for SST studies.

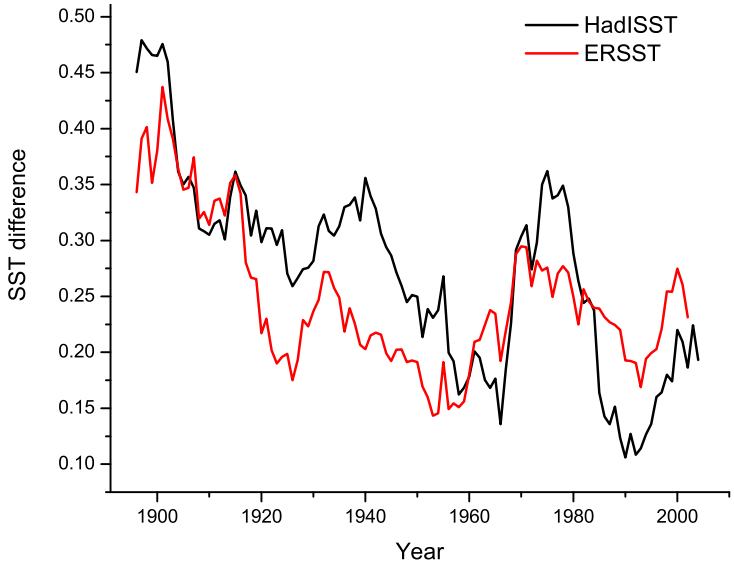

Figure 5.11: The SST difference between the two areas during October to December.

periods; (a) from 1891 to 1964 where satellite observations were not available and (b) from 1965 to 2009 where satellite data was used in determining the intensity of the cyclone are also shown in the figure.The ratio varied between 20% and 50% in the earlier period. It increased to 50% to 80% in the later period. The observed shift in the intensity of tropical cyclones around 1965 may be due to the better monitoring capabilities of the satellite era. Even in the satellite era, studies (Landsea et al, 2006) have questioned the possibility of false trends arising due to the methods of intensity estimation using Dworak technique, since in the earlier stages of satellite era there were only few satellites with very low resolution.

5.3 Conclusion

Tropical cyclone frequency of North Indian Ocean basin is small compared with other ocean basins,but these cyclones have caused large loss of life to those living around the Indian Ocean. Monsoon depressions are important rain producing systems of the monsoon. An attempt is made to study the multidecadal oscillations and long-term trends in the occurrence of these systems using the historical

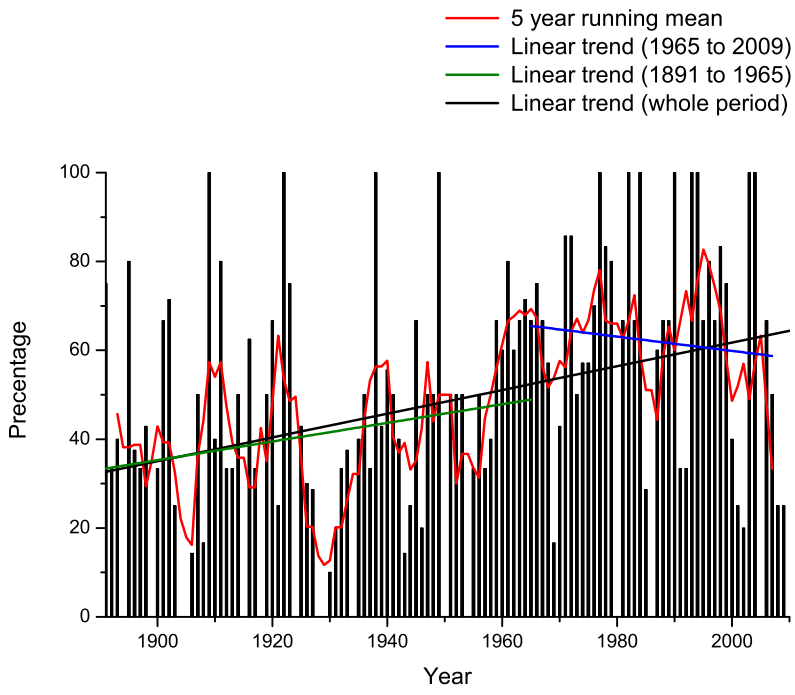

Figure 5.12: The ratio of cyclones to severe cyclones.

datasets archived by the India Meteorological Department. Although the long-term trend in both tropical cyclones and monsoon depressions shows a decrease in their annual frequency, decrease of monsoon depression frequency is large and statistically significant. The multidecadal variation in both tropical cyclones and monsoon depressions has a Four Decade Oscillation (FDO) with almost the same amplitude and temporal phase. Since the two systems tropical cyclones and monsoon depressions occur in different seasons and with mostly different atmospheric and oceanic environment, the physical parameters related to these systems were studied separately.

Of the several parameters analysed, it is found that the intensity of the monsoon LLJ is the main factor affecting the variability in monsoon depression frequency. The weakening of meridional monsoon Hadley circulation associated with the rapid warming of the equatorial Indian Ocean has been found related to the weakening the monsoon LLJ. This weakening is a most likely cause of the decreasing trend in the frequency of monsoon depressions. Also, the FDO in the

frequency of monsoon depressions is found to be related to the decadal changes in the strength of LLJ passing through peninsular India and the Bay of Bengal. In order to study the multidecadal variations in tropical cyclones, the cyclogenesis parameters were analysed for the October-December season, which is the primary season for tropical cyclone activity in North Indian Ocean. For tropical cyclones the rate of decrease in annual frequency is small compared with that of monsoon depressions. But the predominant variation is a multidecadal variability (FDO). FDO in tropical cyclone frequency are not shown by the cyclogenesis parameters of Gray (1979) except the vertical wind shear (VWS) between 850 hPa and 200 hPa and the 850 hPa vorticity over the tropical cyclone genesis region of Bay of Bengal.

The VWS averaged over an area bounded by latitudes 7°N-25°N and longitudes 80°E-100°E shows a multidecadal oscillation which has the same phase as the FDO in tropical cyclones. The decadal oscillation in 850 hPa vorticity is found to be associated with the changes in atmospheric circulation patterns. An area of anomalous equatorial westerly wind flow exists during the High Frequency Period (HFP) of tropical cyclones over the equatorial Indian Ocean which is causing the FDO in vorticity over the tropical cyclone genesis region. The multidecadal variability in the difference of SST between two areas in the eastern and western parts of North Indian Ocean, shows a irregularity which seems to be causing the FDO in the equatorial westerlies. The three major FDO cycles in the annual frequency of tropical cyclones can be clearly seen in the decadal variations of the SST difference between the two areas.

Chapter 6

Intensity of North Indian Ocean Tropical Cyclones

6.1 Introduction

Intensity of tropical cyclones is dependent on several parameters both thermodynamic and dynamic. It includes thermodynamic factors like SST, depth of warm ocean layer at the top, and dynamic factors like VWS and cyclone translation speed. Apart from this several other parameters are identified in subsequent studies such as changes in internal dynamics, translational speed interaction with the upper troposphere and regional influences of individual basins like dry air layer advection and oceanic heat anomaly regions. As pointed out by Emmanuel (2000), the lack of understanding the tropical cyclone dynamics and their interaction with the underlying ocean is a cause for the poor forecasting skill of the cyclone intensity. Kotal et al (2009) studied the relation between cyclone intensity and SST of North Indian Ocean basin and derived an empirical relation between SST and MPI of tropical cyclones over the Bay of Bengal using a sample of 60 cyclones. They found that relation between SST and MPI was linear. Their result showed that about 18% of cyclones reached more than 80% of their MPI and about 38% of cyclones reached more than 50% of their MPI at their peak intensity.

In this study, using 21 years (1990-2011) of daily data, with a sample of 77 cyclones from IBtRACS-WMO data, the factors influencing the intensification of North Indian Ocean tropical cyclones are analysed. The details of the tropical cyclones selected for the study are given in table 6.1

Table 6.1: Details of 77 cyclones considered in the study.

Year	**Period**	**Initial lat/lon**	**maximum sustained wind (msw)(knots)**
1990	4 May-10 May	8.5°N/87°E	127
1990	14 Dec-18 Dec	7°N/88.5°E	55
1991	24 Apr-30 Apr	8.5°N/89°E	127
1991	31 May-2 Jun	13.5°N/90.5°E	45
1991	11 Nov-15 Nov	10°N/91.5°E	45
1992	15 May-19 May	9.5°N/89°E	35
1992	8 Jun-12 Jun	11.5°N/60°E	45
1992	1 Oct-3 Oct	16°N/67°E	45
1992	20 Oct-22 Oct	18°N/88.5°E	35
1992	3 Nov-7 Nov	15°N/90°E	45
1993	12 Nov-16 Nov	11°N/69.5°E	65
1994	29 Apr-2 May	8.5°N/92°E	115
1994	5 Jun-9 Jun	15.5°N/73°E	55
1994	29 Oct-31 Oct	9.5°N/85°E	60
1994	15 Nov-20 Nov	10°N/66°E	65
1995	12 Oct-17 Oct	16.5°N/70°E	45
1995	7 Nov-10 Nov	11°N/91.5°E	77
1995	21 Nov-25 Nov	6.5°N/91°E	102
1996	12 Jun-16 Jun	11°N/86°E	45
1996	17 Jun-20 Jun	17.5°N/69.5°E	60
1996	22 Oct-27 Oct	14°N/69°E	60
1996	4 Nov-7 Nov	16°N/88°E	77
1996	28 Nov-6 Dec	11.5°N/86.5°E	65
1997	15 May-19 May	6.5°N/90.5°E	90
1997	23 Sep-27 Sep	15.5°N/82.5°E	55
1998	17 May-20 May	14.5°N/88°E	60
1998	4 Jun-10 Jun	10.5°N/69.5°E	90
1998	11 Oct-17 Oct	14°N/67.5°E	35

Continued on next page

Table 6.1 – *Continued from previous page*

Year	Period	Initial lat/lon	msw
1998	13 Nov-16 Nov	13°N/87.5°E	77
1998	13 Dec-17 Dec	11°N/68.5°E	55
1999	1 Feb-3 Feb	9°N/89°E	50
1999	16 May-22 May	12.5°N/72°E	105
1999	15 Oct-19 Oct	13.5°N/92.5°E	90
1999	25 Oct-31 Oct	12°N/98.5°E	140
2000	27 Mar-30 Mar	7.5°N/90°E	45
2000	15 Oct-19 Oct	14.5°N/88.5°E	35
2000	25 Oct-29 Oct	13.5°N/93°E	35
2000	26 Nov-30 Nov	8.5°N/91.5°E	102
2000	23 Dec-29 Dec	8°N/86°E	90
2001	21 May-29 May	13.5°N/69°E	115
2001	24 Sep-27 Sep	17°N/69.5°E	35
2001	8 Oct-10 Oct	18.3°N/71°E	35
2001	14 Oct-16 Oct	13.5°N/84°E	35
2002	6 May-10 May	11°N/67°E	35
2002	10 Nov-12 Nov	12°N/82.5°E	55
2002	23 Nov-28 Nov	10°N/87°E	35
2002	21 Dec-25 Dec	4°N/77°E	35
2003	10 May-19 May	6°N/90.5°E	75
2003	12 Nov-15 Nov	6.5°N/61.5°E	55
2003	11 Dec-16 Dec	4.5°N/90.5°E	55
2004	5 May-10 May	11.5°N/73.5°E	55
2004	16 May-19 May	17°N/91.5°E	90
2004	30 Sep-3 Oct	16°N/69°E	55
2004	29 Nov-2 Dec	3.5°N/64°E	55
2005	13 Jan-17 Jan	5.5°N/87°E	35
2005	17 Sep-21 Sep	20°N/90.5°E	35
2005	28 Nov-2 Dec	10.5°N/90.5°E	45
2005	6 Dec-10 Dec	10.5°N/89.5°E	45
2006	25 Apr-29 Apr	9.5°N/90.5°E	100
2006	21 Sep-24 Sep	19.5°N/66°E	55
2006	29 Oct-30 Oct	14°N/80.5°E	35
2007	12 May-14 May	15°N/90.5°E	45
2007	1 Jun-7 Jun	15°N/68°E	127
2007	25 Jun-26 Jun	23.5°N/67.5°E	35
2007	11 Nov-16 Nov	10°N/92°E	115
2008	27 Apr-3 May	12°N/87°E	90

Continued on next page

Table 6.1 – *Continued from previous page*

Year	Period	Initial lat/lon	msw
2008	25 Oct-27 Oct	16.5°N/86.5°E	45
2008	13 Nov-16 Nov	11.5°N/85.5°E	40
2008	25 Nov-27 Nov	8.5°N/81°E	45
2009	14 Apr-17 Apr	12.5°N/88°E	40
2009	23 May-26 May	16.5°N/88°E	60
2009	9 Nov-11 Nov	11°N/72°E	45
2009	10 Dec-15 Dec	6.5°N/85°E	45
2010	19 May-22 May	10.5°N/54°E	40
2010	17 May-21 May	10.5v/88.5°E	55
2010	31 May-7 Jun	15°N/64°E	85
2010	20 Oct-23 Oct	17.5°N/91.5°E	105

6.2 Results and discussion

6.2.1 Thermodynamic conditions

6.2.1.1 Sea surface temperature

The maximum intensity of a tropical cyclone is known to have a direct relationship with SST (Palmen, 1948). The earlier maximum potential intensity theories used only SST as the parameter related to intensity (Merrill, 1988; DeMaria and Kaplan, 1994; Whitney and Hobgood, 1997). The relation between the observed maximum intensity of North Indian Ocean tropical cyclones with SST at the location of maximum intensity is studied and a scatter between these two parameters is depicted in figure 6.1. It is seen that the SST distribution has a broad range from 25°C to 32°C for the North Indian Ocean cyclones. The correlation between cyclone intensity and SST is 0.237 for the full range of SST.

When the maximum attained tropical cyclone wind speeds are below 64 knots, the SST is mainly in the range of 25.5°C and 29.5°C, with more cyclones forming with higher SST environment. For cyclones of intensity 64 knots and above, the SST range is found to be 28°C to 31°C and for this range the correlation coefficient between SST and cyclone intensity is 0.43. In other ocean basins like

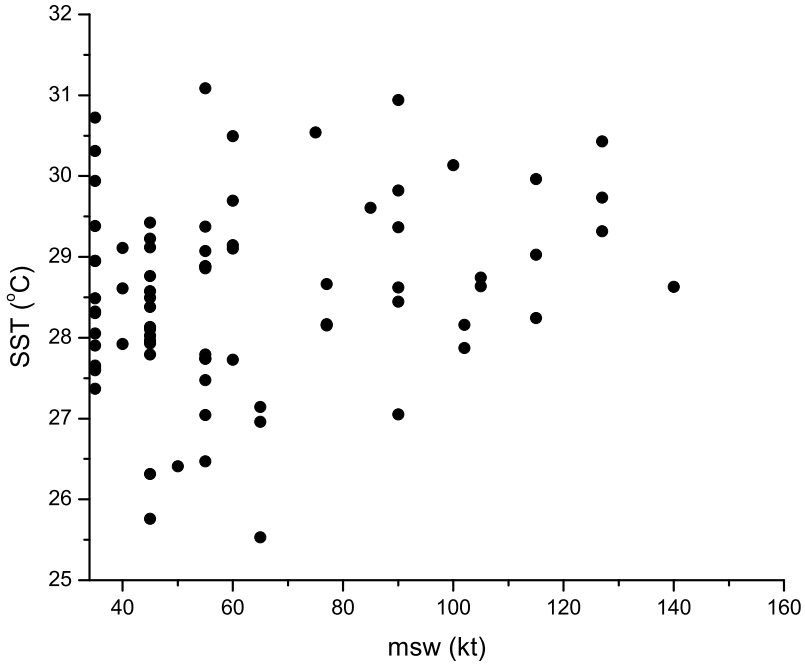

Figure 6.1: Scatter diagram with intensity (maximum sustained wind speeds in knots) and associated Sea surface temperature (°C) of the 77 tropical cyclones.

Atlantic and Pacific the SST associated with cyclones cover a wide range from 15°C to 31°C and many cyclones become extra tropical vortices in their lifetime (Whitney and Hobgood, 1997; Zeng et al, 2007). North Indian Ocean basin is land locked except to the south and this result in short cyclone tracks and many cyclones have landfall as they intensify and they do not reach high intensities.

6.2.1.2 Thermodynamic efficiency

Thermodynamic conditions are mainly dependent on the SST and upper tropospheric outflow layer of the atmosphere. The combined effect of SST and temperature of outflow layer is considered by Emmanuel (1986) and he proposed a thermodynamic efficiency term ε

$$\varepsilon = \sqrt{\frac{T_S - T_0}{T_S}} \tag{6.1}$$

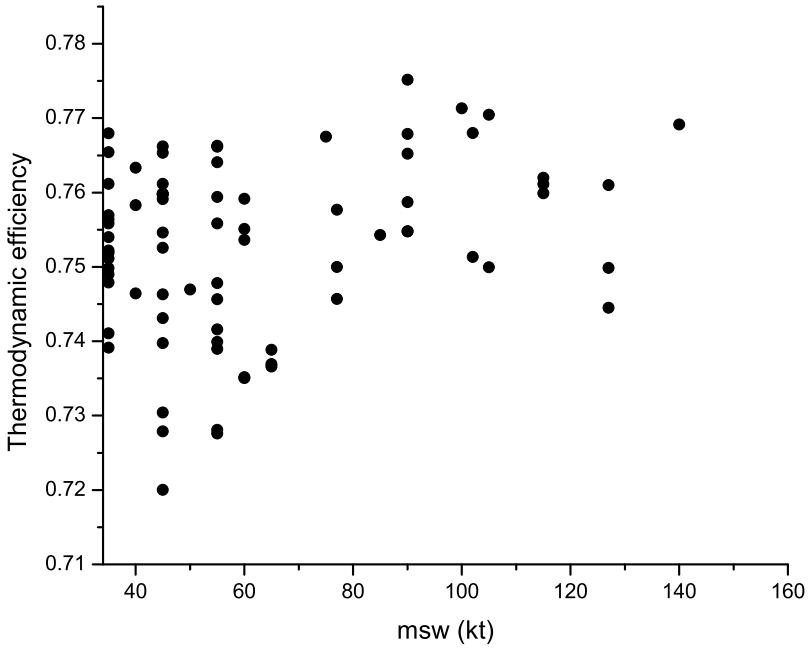

Figure 6.2: Scatter diagram with intensity (maximum sustained wind speeds in knots) and associated thermodynamic efficiency of the 77 tropical cyclones

where T_S is the SST and T_0 is the temperature at outflow layer of the atmosphere.

A scatter plot against thermodynamic efficiency and maximum wind speed is shown in figure 6.2. It is found that the thermodynamic efficiency values are between 0.75 and 0.77 for cyclones with maximum wind speed 64 knots and above and the range is higher for weaker cyclones. North Indian Ocean is thermodynamically favourable for a tropical cyclone to attain its maximum intensity most of the time. The relative contributions of dynamic factors are described in the following sections.

6.2.1.3 Thermodynamic maximum potential intensity

On a given thermodynamic condition, the maximum potential intensity which a tropical cyclone can attain is derived by Emmanuel (1995). Thermodynamic maximum potential intensity is calculated for each day following Emmanuel (1995) (EMPI hereafter) and is given as

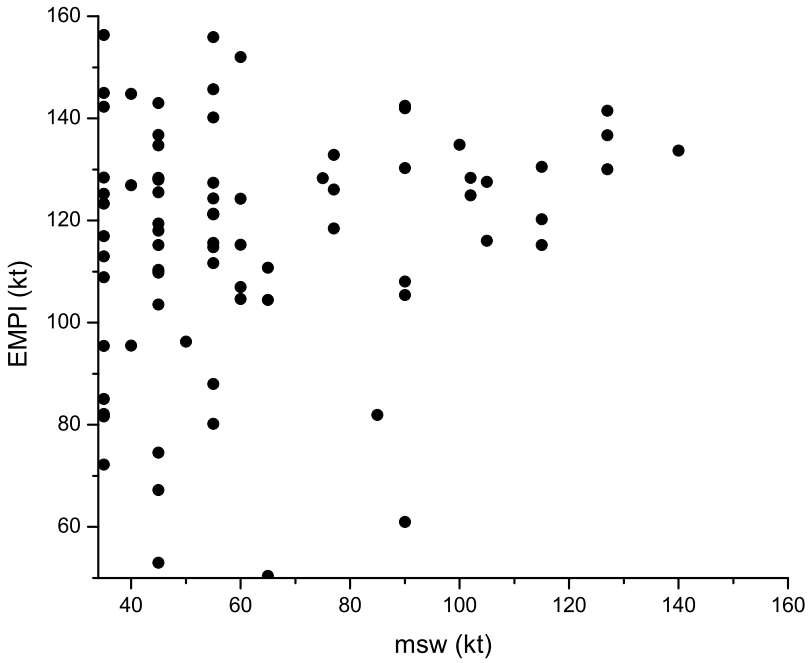

Figure 6.3: Scatter diagram with intensity (maximum sustained wind speeds in knots) and associated calculated thermodynamic maximum potential intensity (knots) of the 77 tropical cyclones

$$V_{max} = \sqrt{\frac{T_S}{T_0} - \frac{C_K}{C_D}\left(CAPE^* - CAPE\right)_m} \tag{6.2}$$

where T_S is the SST, T_0 is the mean outflow temperature (temperature at the level of neutral buoyancy), C_K is the exchange coefficient for enthalpy, C_D is a drag coefficient, CAPE* is the convective available potential energy of air lifted from saturation at sea level in reference to the environmental sounding, and CAPE is that of boundary layer air.

A scatter diagram of observed maximum intensity against the EMPI is shown in figure 6.3. The intensity values remain highly scattered for the low intensity cyclones. The correlation between the two for the full range is 0.16 and for cyclones with maximum wind 64 knot and above, the correlation is 0.45. For higher intensity levels, EMPI is mainly between 100 knots to 140 knots. With-

Table 6.2: Correlation coefficient between intensity (maximum sustained wind speeds in knots) and other parameters

	SST	Thermodynamic efficiency	VWS	Dynamic Efficiency	EMPI	MMPI[a]
All	.237[b]	.228[b]	-.215	.226[b]	.163	.208
64> knots	.431[b]	.266	-.445[b]	.419[b]	.450[b]	.530[c]

[a]Modified Maximum Potential Intensity (discussed later in section 6.2.3)
[b]Correlation is significant at the 0.05 level (2-tailed)
[c]Correlation is significant at the 0.01 level (2-tailed)

out the inclusion of other dynamical parameters, the calculated intensity shows larger values compared with the actual observed intensity especially in the lower intensity categories.

6.2.2 Dynamic conditions

6.2.2.1 Translational speed

Tropical cyclone must move with an optimum speed over the ocean in order to ensure the proper exchange of heat and moisture fluxes between the ocean and the atmosphere. Since the North Indian Ocean basin is bounded by land region to the north, tropical cyclone with high translational speed will make landfall faster than a slow moving cyclone. Thus fast motion will limit the maximum intensity the cyclone can attain. Another factor is the negative feedback from the ocean which becomes important for slow moving cyclones. In other ocean basins such as Western North Pacific and Atlantic, a translation speed of 3 to 8 ms^{-1} is the most favourable range for intensification (DeMaria and Kaplan, 1994; Whitney and Hobgood, 1997; Zeng et al, 2007). In this study, the translation speeds of tropical cyclones are calculated by finding the great circle distance between two consecutive observations. From figure 6.4, it is observed that the maximum favourable translation speed of tropical cyclones over North Indian Ocean is in the range of 2 to 6 ms^{-1}. It is found that the range of translational speed narrows for higher intensity tropical cyclones.

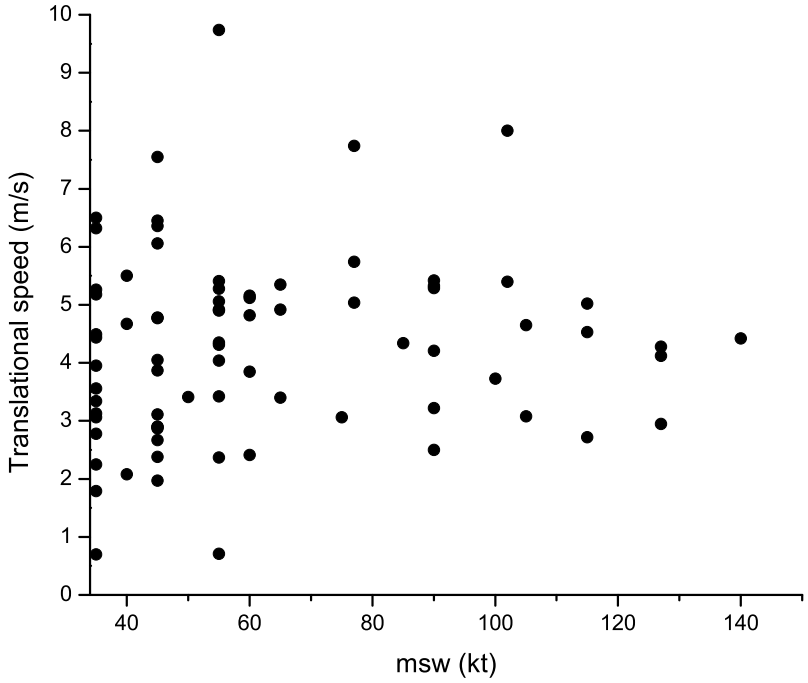

Figure 6.4: Scatter diagram with intensity (maximum sustained wind speeds in knots) and associated translational speed of tropical cyclones (ms^{-1}) of the 77 tropical cyclones

6.2.2.2 Vertical wind shear

The scatter plot between VWS and observed maximum wind is shown in figure 6.5. The correlation between VWS and maximum wind is -0.21 for the full range of intensities and for storms of maximum wind 64 knots and above -0.45 significant at .05 level. The maximum intensity of the tropical cyclones increases with decreasing VWS. Cyclones of maximum wind speed 64 knots and above are associated with VWS between 5 and 15 ms^{-1} (between levels 850 and 200 hPa).

6.2.2.3 Dynamic efficiency

An empirical method for determination of dynamic efficiency using VWS and translational speed was given by Zeng et al (2007) for Western North Pacific. Yu and Wang (2009) subsequently used this index to study the changes in North

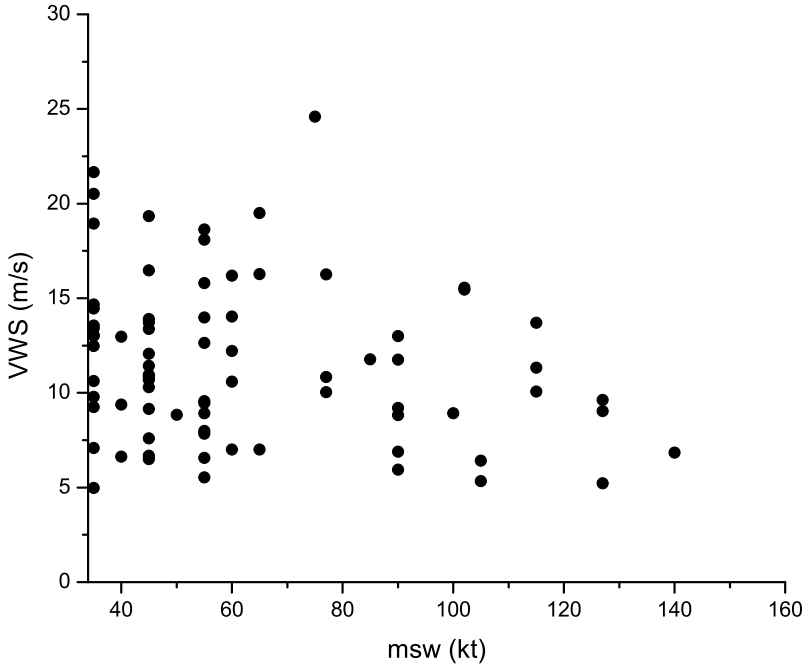

Figure 6.5: Scatter diagram with intensity (maximum sustained wind speeds in knots) and associated vertical wind shear (ms^{-1}) of the 77 tropical cyclones

Indian Ocean tropical cyclone potential intensity in a global warming scenario. The dynamical efficiency is defined as

$$\eta = \frac{1}{1 + U_{ST}/U_0} \tag{6.3}$$

where

$$U_{ST} = \sqrt{0.6V_{shear}^2 + (V_{trans} - 5)^2} \tag{6.4}$$

where V_{shear} is the VWS defined as the difference of wind speeds between 200 hPa and 850 hPa, and V_{trans} is the translational speed of the targeted tropical cyclone and $U_0 = 60$ ms^{-1} as given by Yu and Wang (2009). The average translational speed of the cyclones for the entire lifetime is used for calculating the dynamical

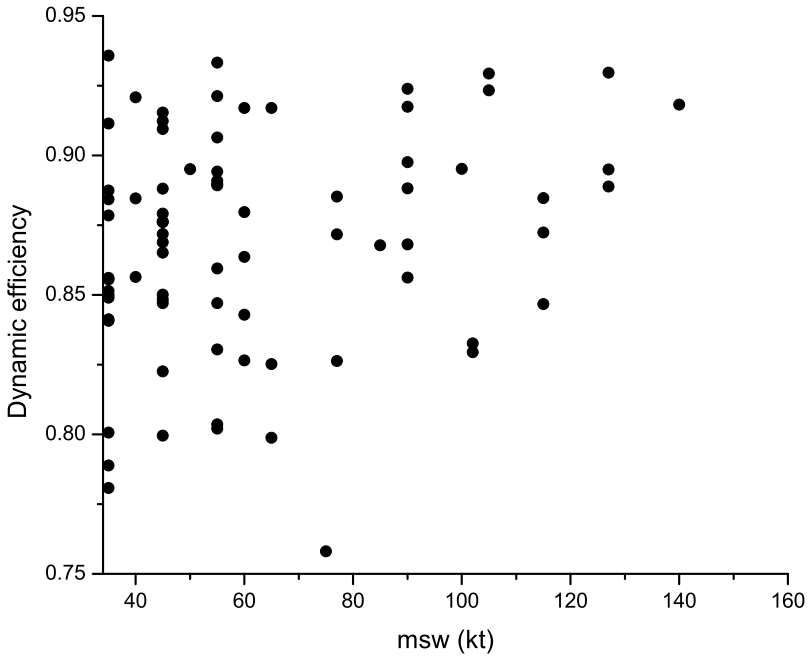

Figure 6.6: Scatter diagram with intensity (maximum sustained wind speeds in knots) and associated dynamical efficiency of the 77 tropical cyclones

efficiency. The variation in dynamic efficiency with the maximum intensity of the cyclones are given in figure 6.6. The dynamic efficiency is highly dependent on the VWS of the environment. In this analysis values in the range of 0.75 to 0.95 are observed in North Indian Ocean for the tropical cyclones. If the dynamic efficiency is maximum, tropical cyclones will be able to reach its maximum EMPI. For cyclones below 64 knots the lower limit of dynamic efficiency is 0.77. But for tropical cyclones above it the dynamic efficiency are in the range of 0.85 to 0.95. As seen in the case of VWS, the net dynamic efficiency is favouring high intensity cyclones. The correlation between maximum cyclone intensity and dynamical efficiency for the full range of cyclone intensity is 0.23 and for cyclones with maximum wind speed 64 knots and above the correlation coefficient is 0.26.

6.2.3 Modified maximum potential intensity

Accounting for both the changes in thermodynamic and dynamic parameters for maximum potential intensity of tropical cyclones, Zeng (2007) and Yu and Wang (2011) proposed a modified index. The modified maximum potential intensity (MMPI) of the tropical cyclones including the dynamical efficiency parameter is calculated as

$$MMPI = \eta.V_{max} \tag{6.5}$$

where V_{max} is the thermodynamic maximum potential intensity (EMPI). The variation of MMPI with the observed maximum intensity is given in figure 6.7. The MMPI calculated is scaled by the dynamic factor and in most cases it leads to a reduction in EMPI. It is observed that some of the lower intensity tropical cyclones are not accounted even after the inclusion of dynamic factors. Thus the maximum intensity of the North Indian Ocean tropical cyclones cannot be completely accounted by the parameters considered. The correlation between the observed intensity and MMPI is only 0.21 for the entire range of intensities. But if we consider only cyclones with maximum intensity above 64 knots, the correlation values increases up to 0.53 and is significant at 0.01 level. There is thus a possibility that the life span of the tropical cyclone and thermal structure of the upper ocean may also have a significant role in modulating the maximum intensity of the tropical cyclones.

6.2.4 Relative intensity

The observed intensity and the calculated intensity both with and without dynamic factors show some relations. To quantify this relation a relative intensity is defined which is the ratio of calculated intensity to the observed maximum intensity. Thus it will give a measure of the total percentage of available intensity a cyclone attained. .e.

$$RI = \frac{ObservedIntensity}{CalculatedIntensity} * 100 \tag{6.6}$$

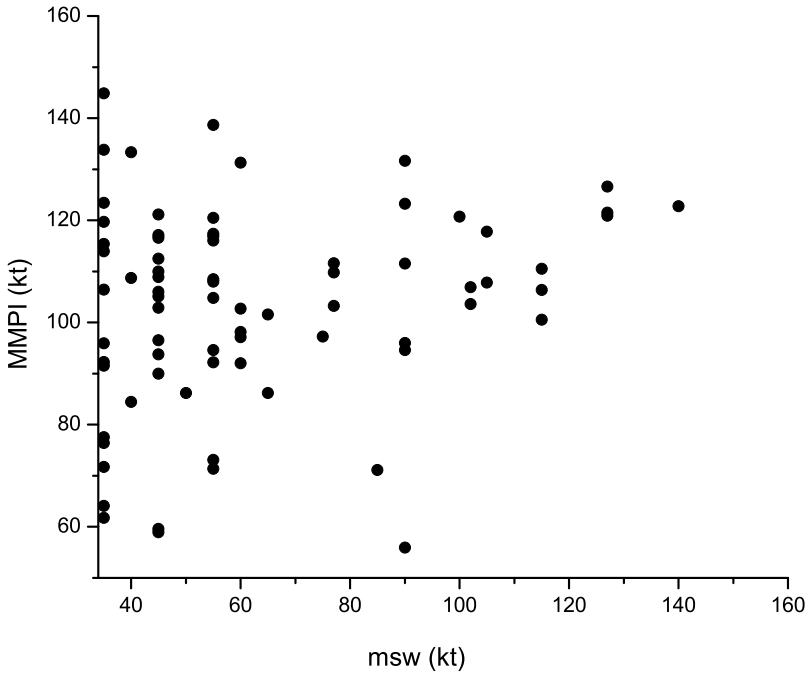

Figure 6.7: Scatter diagram with intensity (maximum sustained wind speeds in knots) and associated modified maximum potential Intensity (knots) of the 77 tropical cyclones

A scatter diagram of the intensity of the 77 cyclones with the relative intensity is depicted in figure 6.8. The black dots represent the relative intensity with respect to the EMPI and the red triangles represent those calculated with the modified index. It is observed that the relative intensity increases linearly with the observed intensity in both the cases. Lower intensity cyclones are able to attain only 20-60 % of its MPI. The relative intensity then increases linearly and attains 80-120% of its MPI in cases above 100 knots. Inclusion of dynamic factors has slightly modified the index but is unable to account for the inability of cyclones to reach their MPI.

6.2.5 Life span of tropical cyclones

For the steady development and intensification, tropical cyclones must stay over the warm ocean surface. This ensures the inflow of maximum heat and

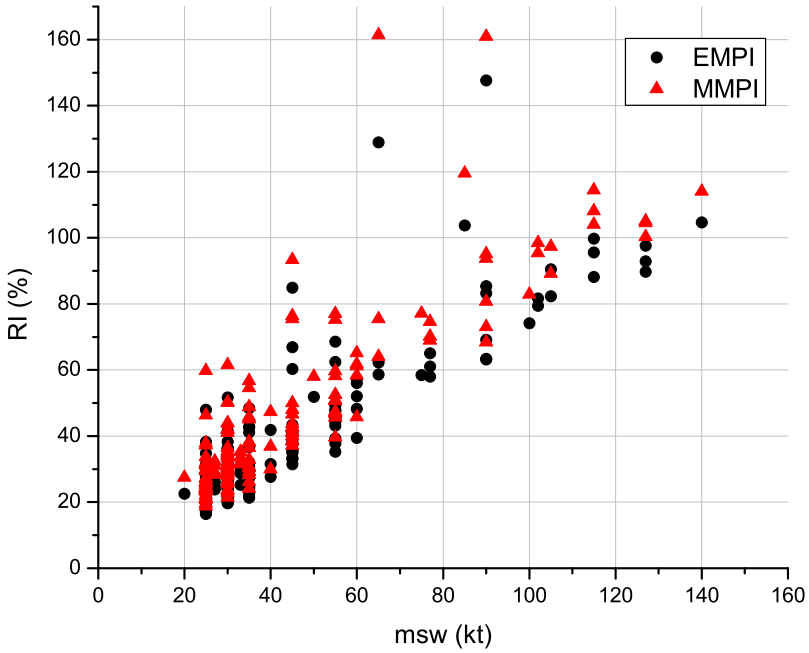

Figure 6.8: Scatter diagram with intensity (maximum sustained wind speeds in knots) and associated relative intensity of the 77 tropical cyclones

moisture fluxes into the cyclone which helps the intensification process. Figure 6.9 depicts the life time of tropical cyclones under consideration. For the cyclones considered in this study the life time ranges from 1 to 10 days. It can be seen that the maximum intensity of the tropical cyclones shows a linear increase with the life time. Below the 64 knot intensity category the life span of tropical cyclones is about 2 to 5 days. But for tropical cyclone above 64 knots the life span increases. Thus even though the environmental conditions are favourable, the tropical cyclones must stay for sufficient time in order to intensify. In a warm ocean basin like North Indian Ocean, the life span has more importance. Figure 6.10 represents the variation in tropical cyclones intensity with the SST, VWS, EMPI and MMPI with life span included. The color of the dots represents the life span of the tropical cyclone in days. From earlier sections, we have seen that although the environment is favourable and sufficient energy is available, some tropical cyclones do not intensify much. In figure 6.10a it can be seen that although SST values are high, lower intensity cyclones are not intensifying due

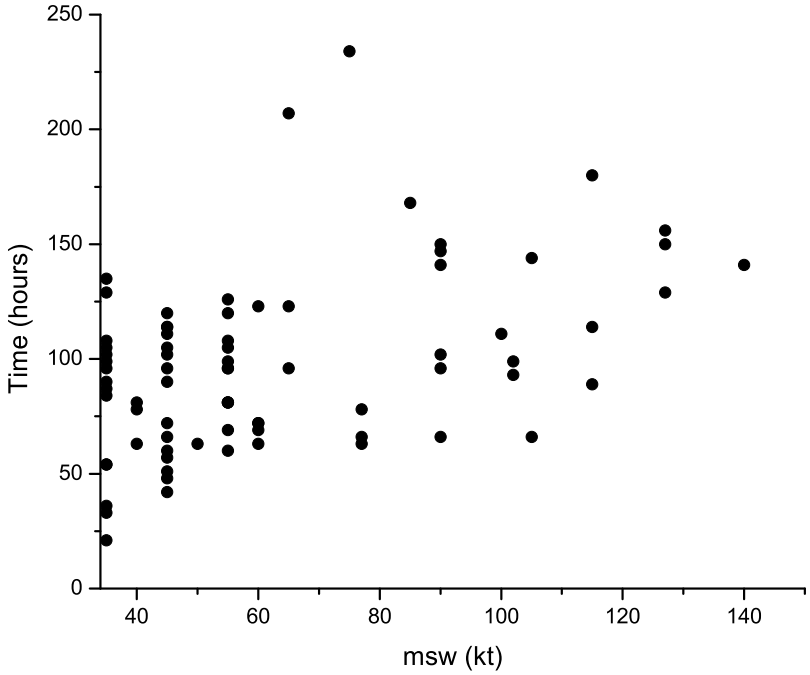

Figure 6.9: Scatter diagram with intensity (maximum sustained wind speeds in knots) and associated life time (hours) of the 77 tropical cyclones.

to shorter life span (usually less than 4 days). Similarly for VWS, in spite of the lower VWS values, due to the shorter life span the cyclones are not intensifying. In the calculated intensities also a similar pattern is seen. Table 6.3 represents the correlation values when the tropical cyclones with life span less than 4 days are excluded. There is significant and high correlation between the environmental parameters and the intensity of the cyclones.

Table 6.3: Correlation values when cyclones with lifetime less then 4 days removed

SST	Thermodynamic efficiency	VWS	Dynamic Efficiency	EMPI	MMPI
0.339	0.449	-0.430	0.286	0.362	0.437

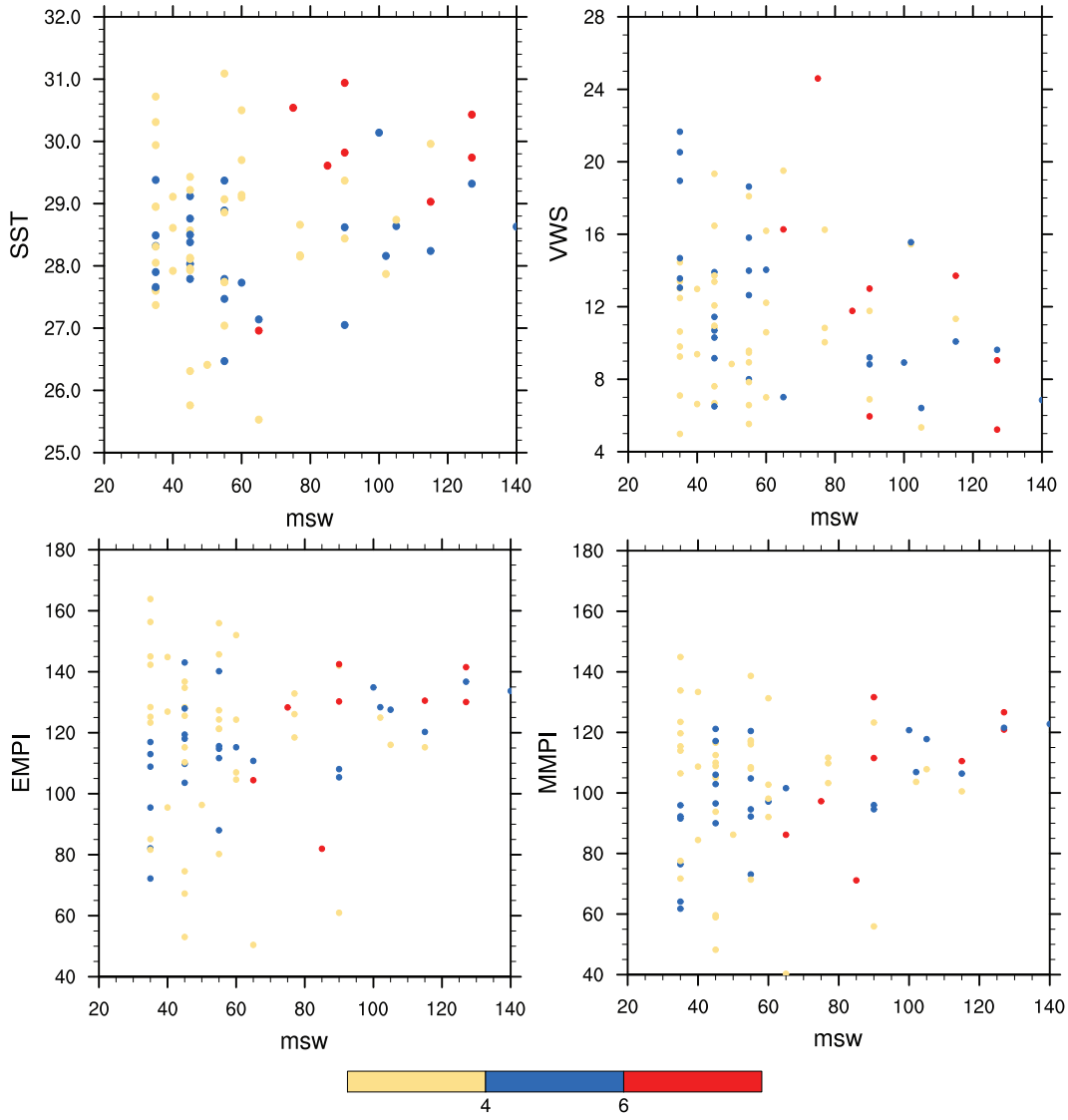

Figure 6.10: Scattered plot between intensity (maximum sustained wind speeds in knots) and a) SST b) VWS c) EMPI and d) MMPI. The colours of the dots represents the lifetime of the cyclones in days.

6.3 Conclusion

Using 21 years data, the observed maximum intensity of North Indian Ocean tropical cyclones are analysed. Environmental conditions leading to the intensification of these cyclones are then analysed by calculating the maximum potential

intensity (MPI) possible. The MPI values are calculated thermodynamically and analysed with and without the inclusion of dynamic factors. Both the thermodynamic efficiency and dynamic efficiency favours the intensification process. SST values of 28°C and above are found to be associated with tropical cyclones with intensity more than 64 knots. Thermodynamic efficiency values are also favouring the tropical cyclone intensification although the variations in this parameter are small for North Indian Ocean. Only a small fraction of the North Indian Ocean tropical cyclones are found to have attained its maximum available intensity. The optimum value of translation speed of North Indian Ocean is found to be 2 to 6 ms^{-1} for the proper intensification.

Dynamical efficiency showed similar trend like thermodynamic efficiency but the values were in the range 0.75 to 0.95. The trend in dynamical efficiency is highly influenced by the relative influence of VWS. A value of VWS below 15 ms^{-1} is another important contribution which is essential for the intensification process. The final modified potential intensity which is the product of dynamical efficiency and the thermodynamic potential intensity showed only a small variation when the entire range of intensities are considered. But for cyclones with maximum intensity above 64 knots, the correlation between observed and calculated intensities are high (0.53). Thus even with the inclusion of dynamic factors the entire intensity range is not accounted. This is evident from the relative intensity values where only cyclones with lower intensities attain 20 to 60% of the calculated intensity.

The life span of the tropical cyclones is found to have a large importance in the intensification of North Indian Ocean tropical cyclones. Cyclones with a life time above 4 days are found to have better relationship with the calculated intensity and there is high correlation between the observed intensity and the parameters considered. Thus although the environment is favourable, the lower intensity cyclones are unable to intensify due to their shorter life span.

Chapter 7

Rapid Intensification of Tropical Cyclone *Gonu* over the Arabian Sea in June 2007

7.1 Introduction

In the year 2007 southwest monsoon set in on 28 May over Kerala located at the south peninsular part of the Indian subcontinent. The track of cyclone Gonu which formed and moved over the Arabian Sea from June 1-7 is illustrated in figure 7.1 (data from IMD sources). On 01 June there was an area of active convection over south-east Arabian Sea north of a well formed monsoon LLJ. A low-pressure area formed in the area of active convection on the cyclonic shear side of the LLJ on the morning of 01 June 2007. By 1800 UTC of that day, this system was declared a depression by the India Meteorological Department when its center lay at 15.0°N, 68.0°E. It intensified into a cyclonic storm and was named Gonu by 0700 UTC of 02 June with its center at 15.0°N, 67.0°E. According to Dvorak classification it then had a T-number of 2.5. Moving northwards, by 00 UTC of 3 June Gonu had intensified into a severe cyclonic storm (T 3.5) centered at 15.4°N, 66.6°E. By 1800 UTC of 03 June the system intensified into a very severe cyclonic storm (hurricane intensity) with T number 4.0. It rapidly intensified and by 1200 UTC of 4 June became a super cyclone (T 6.5) and was located at 19.9°N, 64.1°E. Thus within 18 hours (1800 UTC of 3 June to 12 UTC

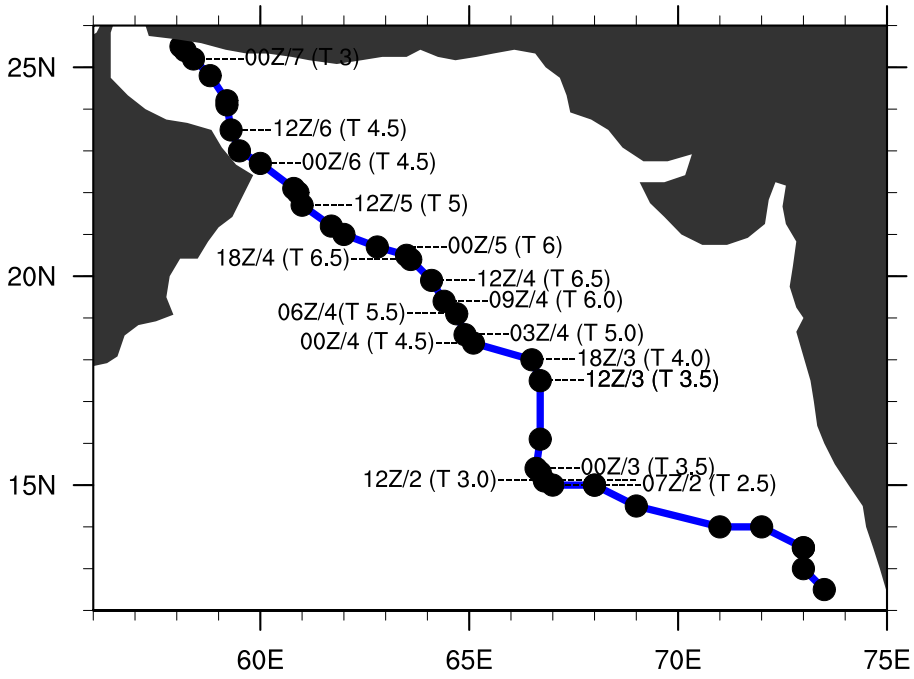

Figure 7.1: Track of cyclone Gonu from 1 June to 7 June 2007. Dots represent positions of center of cyclone as determined by IMD. The T numbers showing the intensity of the cyclone are also marked.

of 4 June) the cyclone intensity increased by 2.5 T numbers on the Dvorak scale (T 4.0 to T 6.5). A detailed description of Gonu and its intensification into a super cyclone may be seen in Tyagi et al (2010). According to them numerical cyclone models could not forecast the intensification of Gonu to a super cyclone.

Dvorak's (1975) study has shown that 70% of the cyclones in Atlantic and Pacific Oceans intensify through one T-number in 24 hours. Thus Gonu's intensification rate was 3 times higher than that of a typical cyclone. By 2000 UTC of 4 June, Gonu weakened to T-number 6.0. Continuing to weaken, the system had intensity of T 5.0 at 12 UTC of 5 June and T 4.5 at 00 and 12 UTC of 6 June when its center moved through the Gulf of Oman, very close to the coast of Oman. By 00 UTC of 7 June the system further weakened into a cyclonic storm and it crossed the Mekran coast along longitude 58°E by 03 UTC of 7 June. According to IMD, the lowest estimated central pressure of the cyclone was 920 hPa and the estimated maximum sustained wind speed was 127 knots (65 ms^{-1}).

Cyclonic storm Gonu is reported to be the worst natural disaster on record in Oman. Strong waves and heavy rain caused severe damage along the Oman coast. In Muscat winds reached 54 knots (28 ms^{-1}). As per IMD and also Tyagi et al (2010) Gonu is the first reported super cyclone in the Arabian Sea. This devastating cyclone killed 49 persons and 27 were reported missing. Over 20,000 people were adversely affected by cyclone Gonu and the damage in Oman was estimated to be close to 4 billion US dollars. *(Source - Wikipedia report on super cyclone Gonu).*

Available studies show that the upper bound of the intensity of a cyclone is a function of SST, relative humidity of the atmospheric column and temperature in the atmospheric outflow layer. Studies by Demaria and Kaplan (1994), Schade and Emanuel (1999) pointed out that even though SST is important in tropical cyclone intensification, the heat content of the ocean mixed layer must be considered. Accurate prediction of hurricane intensity requires accurate measurements of upper ocean thermal structure ahead of the storm (Emanuel,1999).

As a cyclone moves along a warm oceanic surface, it causes turbulent mixing in the oceanic mixed layer. This cools the oceanic mixed layer. This is treated as a negative feedback when considering the intensification of a cyclone. But if the warm water is deep (usually determined by the depth of 26°C isotherm), the oceanic heat content may be large (Leipper and Volgenau, 1972) and the cooling of the mixed layer is inhibited leading to the intensification of cyclone. A good example is the hurricane Opal (Shay et al, 2000), which rapidly intensified from a central pressure of 965 hPa to 916 hPa in 14 hours as it crossed a warm ocean eddy in the Gulf of Mexico.

Similar studies done on hurricanes Opal, Bret, Mitch and Typhoon Imbedo (Goni and Trinanes, 2003), Supertyphoon *Meami* (Lin et al, 2005) and cyclone *Nargis* (Lin et al, 2009) have shown the presence of warm oceanic eddies in the path of these cyclones. Preliminary results show that the intensification of most hurricanes in the tropical Atlantic and Gulf of Mexico during the period 1993-2000 are linked to the variability of the integrated vertical temperature of the top layer of the ocean in the storm track (Goni et al, 2000). Numerical simulations of hurricane *Meami* and Opal by Wu et al (2007) showed that interaction of warm eddies with tropical cyclones are critical for rapid intensification of the cyclone.

Further studies by Wada and Usui (2007) and Mainelli et al (2008) explained the role of upper ocean thermal structure in intensification of cyclone in numerical experiments.

7.2 Results and discussion

7.2.1 Genesis of GONU

Daily 850 hPa wind field over Arabian Sea for 01 to 06 June 2007 are given in figure 7.2. Since monsoon set in over Kerala on 28 May, a well-formed LLJ (Findlater, 1969; Joseph and Sijikumar, 2004) was present in the Arabian Sea south of latitude 10°N on 01 June 2007 when a feeble cyclonic circulation formed over south east Arabian Sea which intensified into a cyclonic storm Gonu on the afternoon of 2 June. The vortex associated with Gonu and the maximum organization of the vortex when the system was declared as a super cyclone is presented figure 7.2 in which LLJ can be clearly observed. During the formation of Gonu the LLJ was to its south and Gonu grew in intensity on the cyclonic shear side of the LLJ in an environment of large cyclonic vorticity in the atmospheric boundary layer.

The wind flow at 200 hPa during the cyclone is depicted in figure 7.3. STJ present over the latitude belt 20°N to 30°N moved towards north from 3 June. Consequent to this, the VWS over the north Arabian Sea decreased considerably as shown in figure 7.5. On 1st and 2nd June, the low VWS zone was between 10°N and 20°N. The SST field on 1 to 6 June 2007 is given in figure 7.4. Monsoon onset over Kerala is associated with very warm SST (of the order of 31°-32°C) in Southeast Arabian Sea (Joseph et al, 2006). In the case of Gonu also the SST over this part of the Arabian Sea was very high. The convective activity associated with monsoon onset occurs over the SST gradient area south of the axis of maximum SST. It is seen that Gonu had it genesis over the Southeast Arabian Sea in the SST gradient area of the warm pool. The high SST in this region and the cyclonic shear vorticity associated with the LLJ have been favourable factors for the genesis of cyclones in south-east Arabian sea at the time of monsoon onset over Kerala.

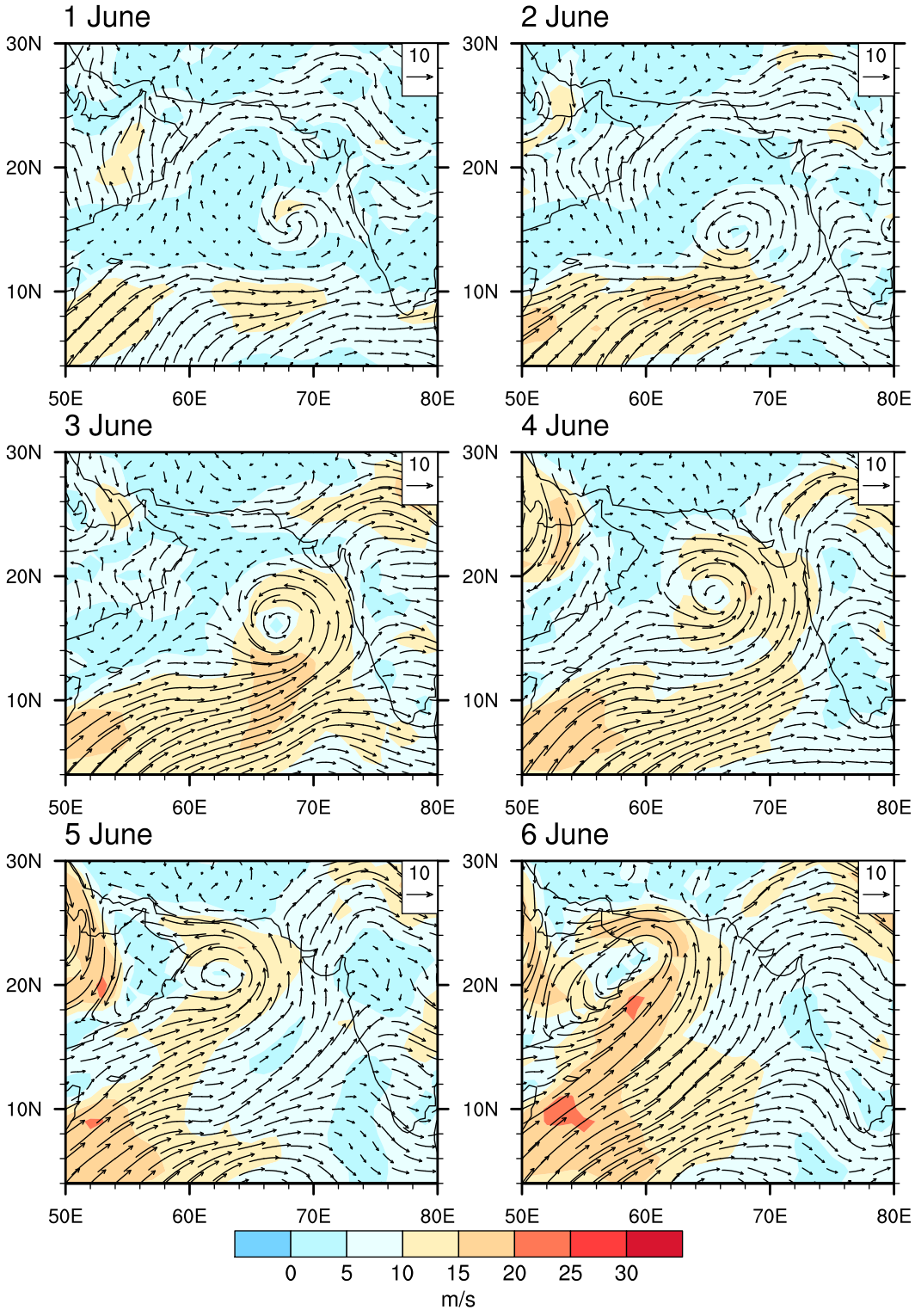

Figure 7.2: Daily horizontal variations in the 850 hPa wind associated with the development of Gonu from 1 June to 6 June 2007.

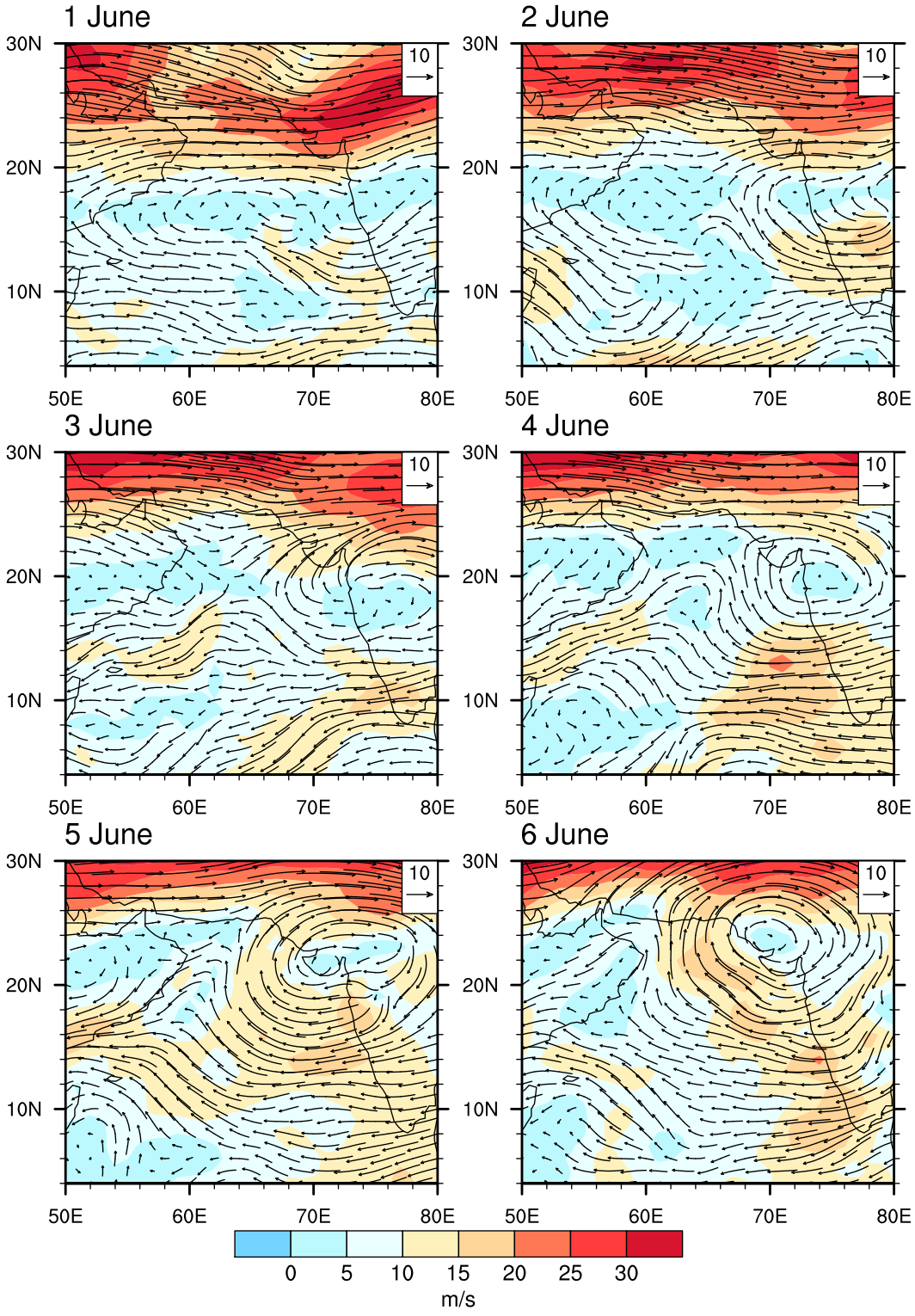

Figure 7.3: Daily horizontal variations in the 200 hPa wind associated with the development of Gonu from 1 June to 6 June 2007.

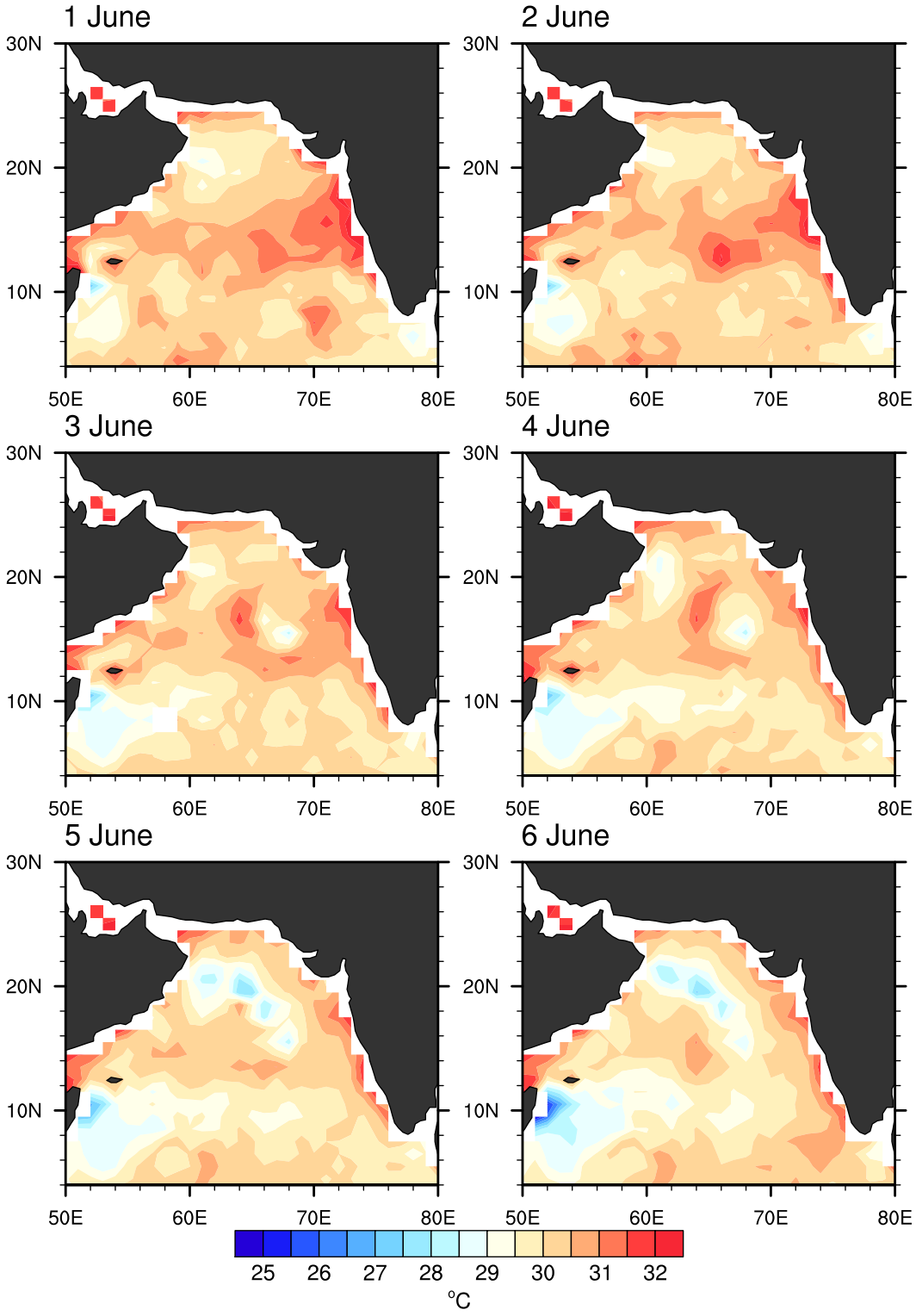

Figure 7.4: Daily horizontal variations in the SST associated with the development of Gonu from 1 June to 6 June 2007.

7.2.2 Intensification of GONU

A comparison of the mean intensity of the recent 30 cyclones of the north Indian Ocean as derived by Bhowmik et al (2007) at 6 hour intervals with that of Gonu has been made and the intensity variations are depicted in figure 7.6. It is evident that the intensity of Gonu was below the average cyclonic intensity in this region in the first 30 hours. In the next 30 hours the intensity of Gonu is on par with that of an average cyclone. After Gonu attained hurricane intensity (T 4) its rate of intensification became much higher than that of the average cyclone in north Indian Ocean. During the 78-84 hours of its formation Gonu attained the peak intensity much above that of an average cyclone.

Tropical cyclone is known to pump upwards large amounts of moisture into the troposphere and even into the lower stratosphere. Daily variations of vertically integrated moisture and the wind divergence at 200 hPa are shown in figure 7.7. Figure 7.7 shows that a large area of high vertically integrated moisture (VIM) was associated with the cyclone. From figure 7.7 it can be seen that monsoon current (LLJ) to the south of Gonu is also feeding moisture into it. LLJ is found to be associated with high values of VIM. Thus LLJ with high values of VIM advecting moisture into the cyclone field and the vertical pumping of moisture from oceanic boundary layer to the higher levels within the cyclone has ensured high moisture content in the cyclone field, which is necessary for cyclone intensification. It is one of the important factors that led to the rapid intensification of Gonu. Such a condition should normally be available for cyclones forming on the cyclonic shear side of LLJ.

On 3rd and 4th of June, with the northward movement of the STJ, low VWS was present around the cyclone area (see figure 7.5, particularly the map of 4 June with the track of Gonu marked on it) helping it to intensify fast.

The most important factor that must have created the rapid intensification of Gonu to a super cyclone on 4th June 2007 was the availability of large heat storage in the top layer of the Arabian Sea around Gonu on that day. Figure 7.8 shows the daily sea surface height anomaly during 1 to 6 June 2007. The track of Gonu is also shown in the figure for 4th June along with SSHA. The blue lines drawn to the north and south of the track are 150 km from the cyclone track.

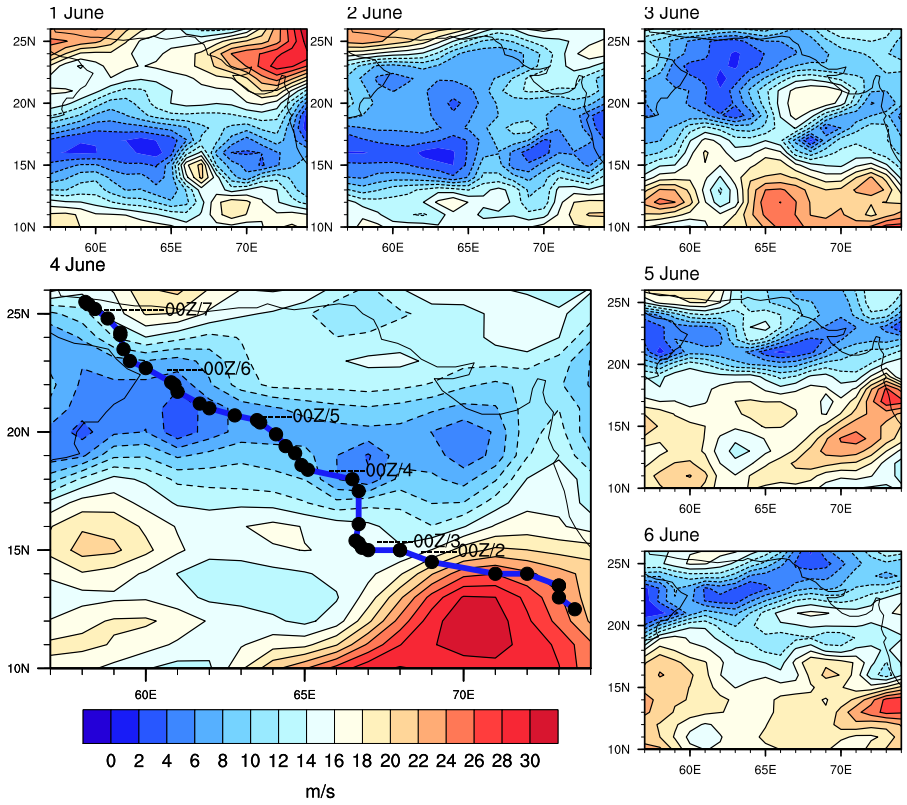

Figure 7.5: Daily vertical wind shear from 1 June to 6 June 2007. The blue shaded areas are having VWS (between 200 hPa and 850 hPa) of 12 ms^{-1} or less at intervals of 2 ms^{-1}. The track of Gonu is also marked in the figure for 4 June.

Between these lines there are a few warm ocean eddies with high SSHA and also a cold eddy in the track of Gonu. The area of active convection in a tropical cyclone is within a radius of about 300 km from the cyclone center (Gray, 1979). The maximum of convective activity is within a radius of 100 km, which includes the eye wall cloud convection. The effect of high heat storage in the warm ocean eddies is to increase convection in the wall cloud and the spiral bands within a radius of 300 km. Figure 7.9 gives the 6 hourly maximum wind of Gonu from 2 to 7 June 2007 as derived from the T numbers of cyclone intensity provided by IMD, using the conversion table provided by Dvorak (1975). The other three curves in the figure give the mean of SSHA averaged over latitude-longitude squares

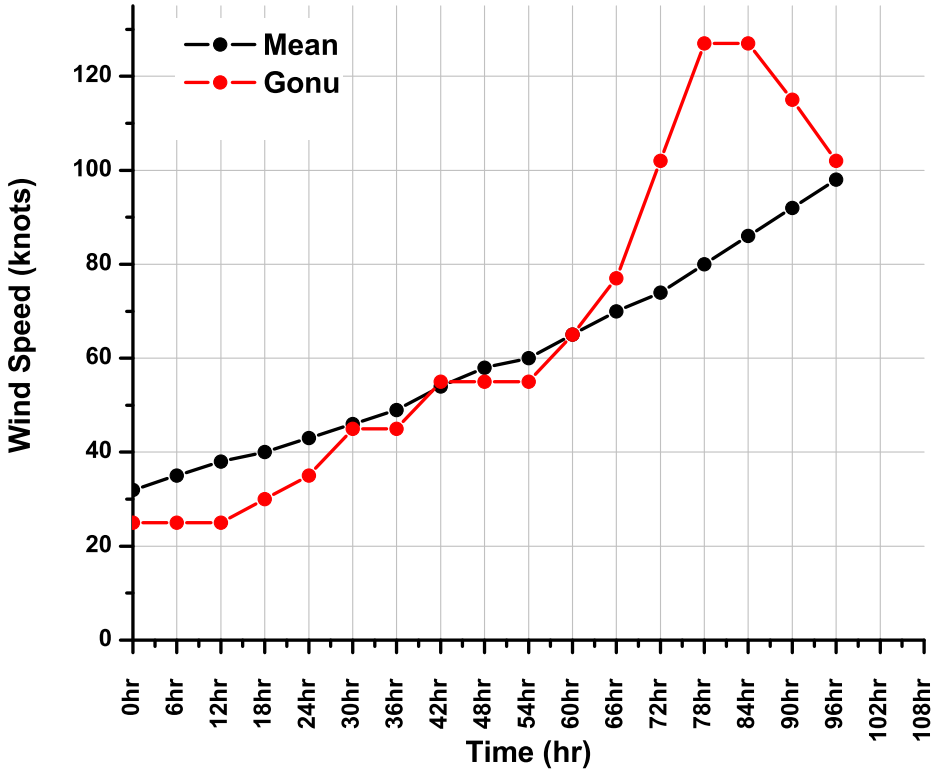

Figure 7.6: Six hourly intensities of Gonu and of an average cyclone over North Indian Ocean as derived by Bhowmik et al (2007). After reaching hurricane intensity (T 4) Gonu intensified rapidly.

around the 6 hourly position of the cyclone center 1, 1.5 and 2 degrees around the cyclone center. It is a simple area average giving equal weightage to all data points in the area. It is found that all the curves are found to follow the intensity changes of the cyclone but the maxima are displaced 6 to 12 hours in the first two curves. The average of 2 degrees around the cyclone center is found to follow best the intensification and decay of Gonu particularly in the time of occurrence of maximum intensity. By the averaging process adopted in our study the effects of the positive and negative anomaly areas in a specified area around the cyclone center are taken into consideration. It is interesting to note that the depth of 26°C isotherm and the TCHP above the 26°C isotherm in the Arabian Sea were very high around cyclone Gonu on 4 June 2007 (figures not shown in the paper,

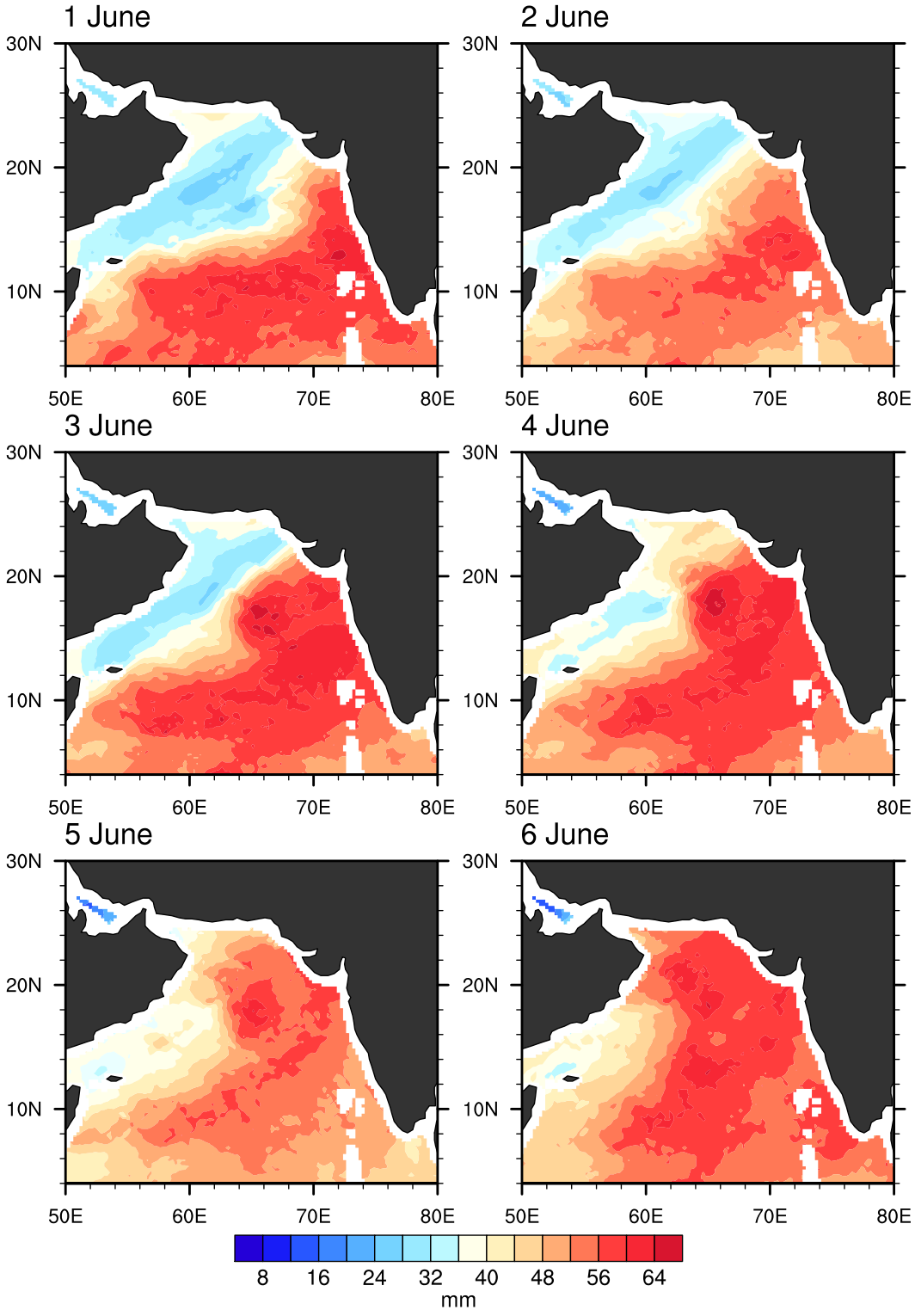

Figure 7.7: Daily horizontal variations in vertical integrated moisture associated with the development of Gonu from 1 June to 6 June 2007

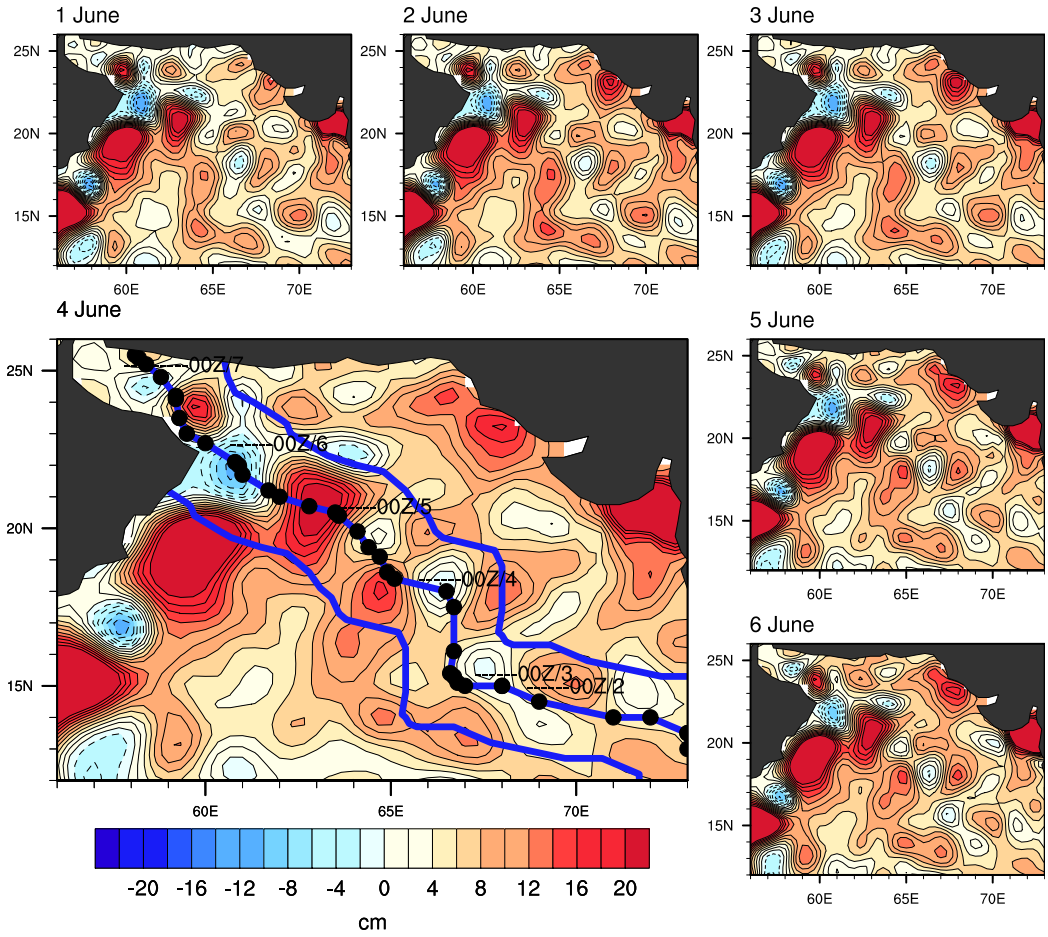

Figure 7.8: Daily SSHA from 1 June to 6 June 2007 at intervals of 2cm. The blue shaded areas are having negative SSHA. The track of Gonu is also marked in the figure for 4 June. The blue lines are at distance of 150 km from the centers of Gonu.

but are available at the website *http://www.aoml.noaa.gov/phod/cyclone/data/*).

7.3 Conclusion

The study has shown that in the rapid intensification phase of Gonu (from the hurricane stage T 4.0 to the super cyclone stage T 6.5), the central region

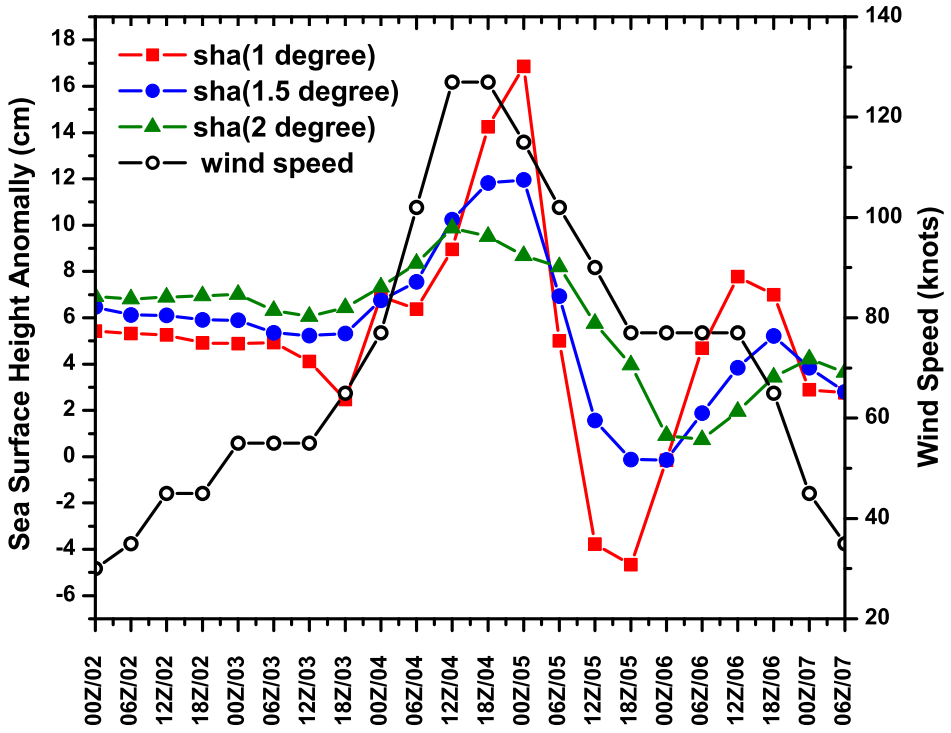

Figure 7.9: The black line gives the 6 hourly intensity of cyclone Gonu in terms of the maximum wind (derived from the T-number). The other lines give the area averaged SSHA for lat-lon squares of side 1 degree (100 km), 1.5 degree (150 km) and 2 degree (200 km) centered on the cyclone center.

of the cyclone was situated in an area with (a) low VWS and (b) positive upper tropospheric divergence (at 200 hPa). These factors are known to be favourable for intensification of a cyclone. The rate of intensification of the cyclone appears to be related to the heat storage in the upper layer of the ocean over which the central region of intense convection associated with the cyclone moved. Areas of positive SSHA (eddies) are assumed to be areas of large heat storage in the ocean. Since these eddies are small in horizontal dimensions and the heat from the ocean surface layer is extracted and fed to the deep moist convection in the cyclone central region, we used an area average of the SSHA around the cyclone center as described earlier.

The convection in a cyclone is high in an area of 100 km around the eye wall cloud and decreases outwards rapidly to become practically zero about 300 km from the cyclone center. The SSHA averaged in boxes of side 200 km and 300 km around the cyclone center follow the intensity of the cyclone but with a lag of 6 to 12 hours. The zero lag intensity curve is for an average of the SSHA for a box around the cyclone center of side 400 km. Such an area covers most of the areas of intense convection in the cyclone.

Chapter 8

Interaction of Bay of Bengal Tropical Cyclones with the Subtropical Jetstream

8.1 Introduction

Upper tropospheric circulation and the STJ are important for tropical cyclones of the North Indian Ocean as they provide a channel for the mass outflow from the systems. Tropical cyclone intensification is a result of complex interactions between different dynamical and thermodynamical parameters. In this chapter the role of the STJ and the high speed center embedded in it (the Asian high speed center) have been studied. Tropical cyclones posses high inertial stability in the lower troposphere and hence it is resistive to the horizontal forcing by external weather systems. But since the inertial stability does not extend up to the upper troposphere, the upper part of a tropical cyclone is vulnerable to the influences of upper tropospheric environment (Holland and Merrill, 1984). Upper level forcing for tropical cyclone intensification is mainly focused on two concepts; enhancement of tropical cyclone outflow by pre-existing outflow channels in the upper troposphere and the intensity changes induced by dynamic forcing from upper troposphere involving eddy flux convergence of angular momentum (EFC) in regions of weak inertial stability or superposition of potential vorticity anomalies over the cyclone.

Significant relationships between upper tropospheric outflow channel in the intensification of tropical cyclones were identified by Cheng and Gray (1984) during First Garp Global Experiment (FGGE). For North Indian Ocean tropical cyclones, Lee et al (1989) showed an increase in intensity of the tropical cyclone under the influence of an upper tropospheric outflow channel. Studies such as Challa and Pfeffer (1980), DeMaria et al (1993), Hanley et al (2001) and Yu and Kwon (2005) found that positive EFC of angular momentum is a favourable factor for tropical cyclone intensification. When an upper troposphere trough becomes superposed with the warm outflow from the tropical cyclone, a positive eddy momentum flux convergence contributes to a cyclonic spin-up of the inner vortex leading to a favourable condition for cyclone intensification (Hanley et al, 2001). Molinari et al (1998) found that the super-position of positive upper tropospheric potential vorticity anomaly contributes to the intensification of tropical cyclone along with the EFC.

Another approach has focused on the divergence field associated with the upper troposphere troughs and high speed centers in Jetstreams. High speed centers (HSC) of Jetstreams are known to have divergence in the right entrance

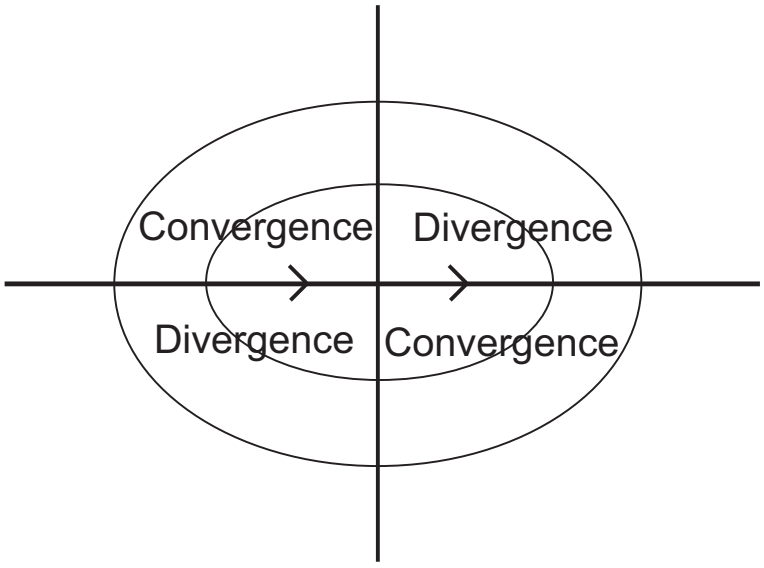

Figure 8.1: The convergence and divergence patterns associated with the four quadrents of a westerly high speed center

and left exit regions and convergence in the left entrance and right exit regions (Bebee and Bates, 1955; Uccellini and Johnson, 1979, Shapiro and Kennedy, 1981; Ziv and Padlor, 1999; Webster and Fasullo, 2003), see also figure 8.1. Upward motions are associated with divergent regions and downward motions are associated with convergent regions of HSCs. The divergence field around a HSC depends on the structure of the jet, whether it is a straight or a curved one. For a HSC with cyclonic or anticyclonic curvature the divergence field is much different than that of a straight jet (Bebee and Bates, 1955). When the center of the tropical cyclone is located in the right-entrance region of a HSC, the upward motion enhances the deep convection associated with the central region of the cyclone leading to its intensification. In addition, the pre-existing outflow channel in the upper troposphere (for North Indian Ocean the STJ) creates favourable outflow channel for the tropical cyclone mass flux which also is a factor favouring intensification of the cyclone.

Although upper troposphere Jetstream HSCs influence weather systems like tropical cyclones, these systems in turn are found to modify the strength of the Jetstream while interacting with it. Convective heating associated with tropical cyclone involving latent heat release intensifies the HSC (Maddox, 1979; Keyser and Johnson, 1984; Uccellini and Kocin, 1987; Market, 1999). The Jetstream which contributes to the upper tropospheric activity in North Indian Ocean basin is the subtropical Jet stream (STJ) during the north Indian Ocean tropical cyclone seasons March to May and October to December. Its maximum wind is close to the 200 hPa level.

The three wave pattern of the global winter STJ has been studied by Krishnamurthi (1961) and shown in figure 8.2. The climatological STJ has three troughs and three high speed centers associated with it. STJ over Asian continent has a well defined trough over the Arabian Sea and a high speed center near Japan (the Asian HSC). It is a semi-permanent feature but its maximum winds in the Asian HSC have large temporal fluctuations. North Bay of Bengal is situated in the divergent region of the Asian HSC (right entrance). The Asian HSC has the maximum wind speed of the STJ system.

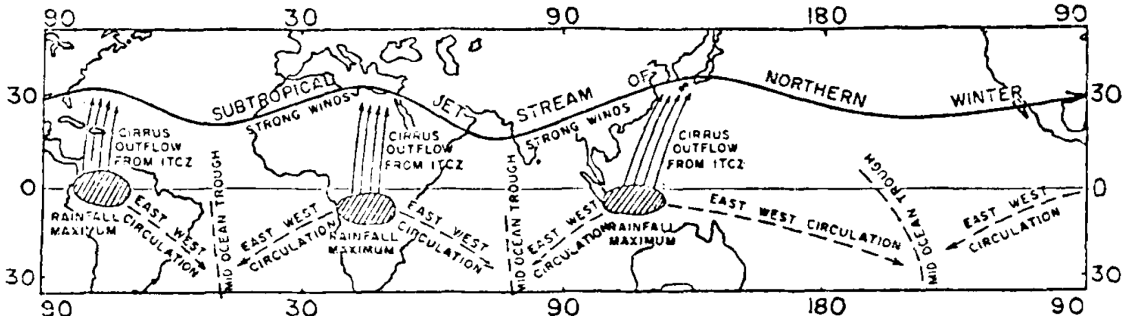

Figure 8.2: A schematic illustration of Subtropical westerly Jetsterams and associated high speed centers during northern hemispheric winter; from Krishnamurthi (1979).

8.2 Results and discussion

For the analysis of the interaction between the Asian HSC and the tropical cyclones of Bay of Bengal , 30 years of tropical cyclone data (1979 to 2008) from IBtRACS have been used. Only the tropical cyclones formed over Bay of Bengal which reached their maximum intensity north of latitude 15°N are considered in this study. Three categories of tropical cyclones are studied; those with maximum wind speed between 34 to 47 knots (category-1; Cat-1 hereafter), 48 to 63 knots (category-2; Cat-2 hereafter) and above 64 knots (category-3; Cat-3 hereafter). For these 30 years, there were 34 tropical cyclones which satisfied the above criteria. Out of these, 8 tropical cyclones were in Cat-1 and 12 each in Cat-2 and Cat-3. The details of the individual storms are given in figure 8.3 and table 8.3, 8.2 and 8.1. Figure 8.3 shows the tracks of each tropical cyclone in these categories where the red dots represent the location at which the tropical cyclone attained its maximum intensity.

The upper tropospheric circulation and STJ associated with each category of cyclones are studied by compositing 200 hPa winds form ERA interim reanalysis data. For each category of tropical cyclone, composites are made for the period 5 days before (t-5) to the day (t), t being the day when the cyclone reached its maximum intensity (red dots in figure 8.3). The 200 hPa composite wind field showing the STJ and its HSC for the three categories of cyclones are shown in

Table 8.1: Details of the 8 cyclones under category 1

Year	Period	Day of max intensity	location of max intensity (lat/lon)	MSW
1990	13 Dec-19 Dec	17 Dec	16.75°N/86.6°E	47.3
1991	30 May-3 Jun	2 Jun	22.27°N/91°E	44.5
1992	15 May-20 May	19 May	18.43°N/93.54°E	46.1
1992	14 Jun-18 Jun	17 Jun	20.4°N/87°E	39.6
1992	24 Jul-28 Jul	26 Jul	20.3°N/86.4°E	35.2
1996	11 Jun-18 Jun	15 Jun	17.1°N/83.55°E	42.3
1996	21 Oct-29 Oct	27 Oct	17°N/86.11°E	34.8
2008	24 Oct-27 Oct	26 Oct	21°N/89.3°E	39.8

Table 8.2: Details of the 12 cyclones under category 2

Year	Period	Day of max intensity	location of max intensity (lat/lon)	MSW
1982	30 May-4 Jun	3 Jun	19.9°N/86.9°E	51.7
1983	5 Nov-9 Nov	9 Nov	19°N/90.5°E	51.7
1985	22 May-25 May	25 May	22.5°N/91.2°E	56.4
1986	4 Nov-9 Nov	9 Nov	21.8°N/89°E	50
1987	30 May-5 Jun	4 Jun	21°N/90.5°E	49.2
1988	14 Nov-18 Nov	18 Nov	19.7°N/93°E	51.7
1989	23 May-27 May	26 May	21.3°N/87.3°E	51.7
1995	5 Nov-10 Nov	8 Nov	16.7°N/84.7°E	63.3
1997	19 Sep-27 Sep	27 Sep	22.7°N/91.3°E	57.2
1998	13 May-20 May	20 May	21.7°N/91.5°E	60.8
2002	9 Nov-12 Nov	12 Nov	20.9°N/87.4°E	51.7
2007	13 May-15 May	14 May	21.4°N/92°E	51.1

Table 8.3: Details of the 12 cyclones under category 3

Year	Period	Day of max intensity	location of max intensity (lat/lon)	MSW
1981	17 Nov-20 Nov	19 Nov	17.5°N/90.7°E	70.5
1981	5 Dec-10 Dec	9 Dec	16.9°N/86.7°E	70.5
1988	22 Nov-29 Nov	29 Nov	21.8°N/89°E	103.4
1991	22 Apr-30 Apr	29 Apr	20.5°N/90.6°E	125.1
1994	27 Apr-3 May	2 May	19.6°N/91.6°E	106
1995	18 Nov-25 Nov	24 Nov	16.5°N/86.4°E	97.2
1997	13 May-20 May	19 May	20.8°N/91.1°E	95.6
1998	13 Nov-16 Nov	15 Nov	17.6°N/82.8°E	74.8
1999	25 Oct-3 Nov	28 Oct	19.2°N/87.1°E	131.6
2004	14 May-19 May	19 May	20.3°N/92.9°E	73.6
2007	10 Nov-16 Nov	15 Nov	19.4°N/89.1°E	119.1
2008	25 Apr-4 May	2 May	15.9°N/93.5°E	95.6

figure 8.4, 8.5 and 8.6. Some of the common climatological features of the upper troposphere are seen in these figures. The Jetstream axis is at latitude around 30°N. Two features are prominent (a) an anticyclone over the Bay of Bengal and

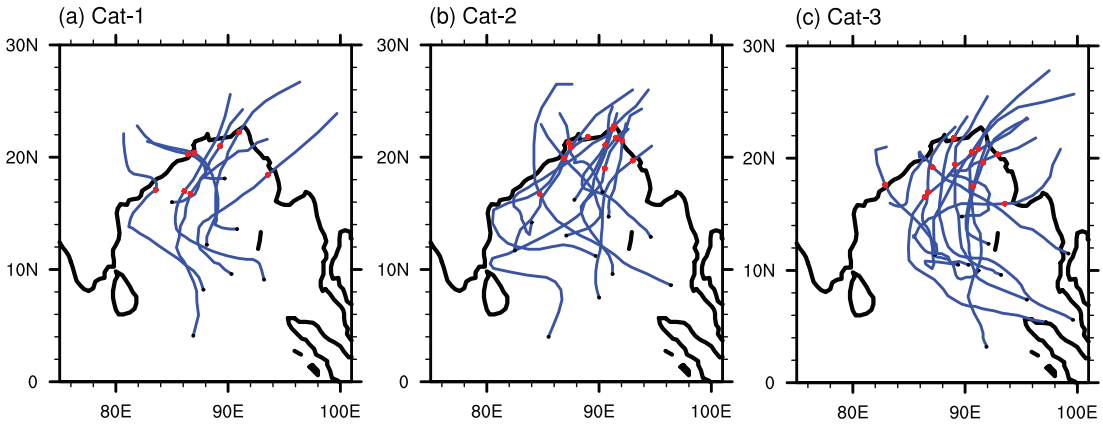

Figure 8.3: Tracks (Blue lines) and location of maximum intensity (Red dots) of tropical cyclones in the three categories a) Cat-1 b) Cat-2 and c) Cat-3.

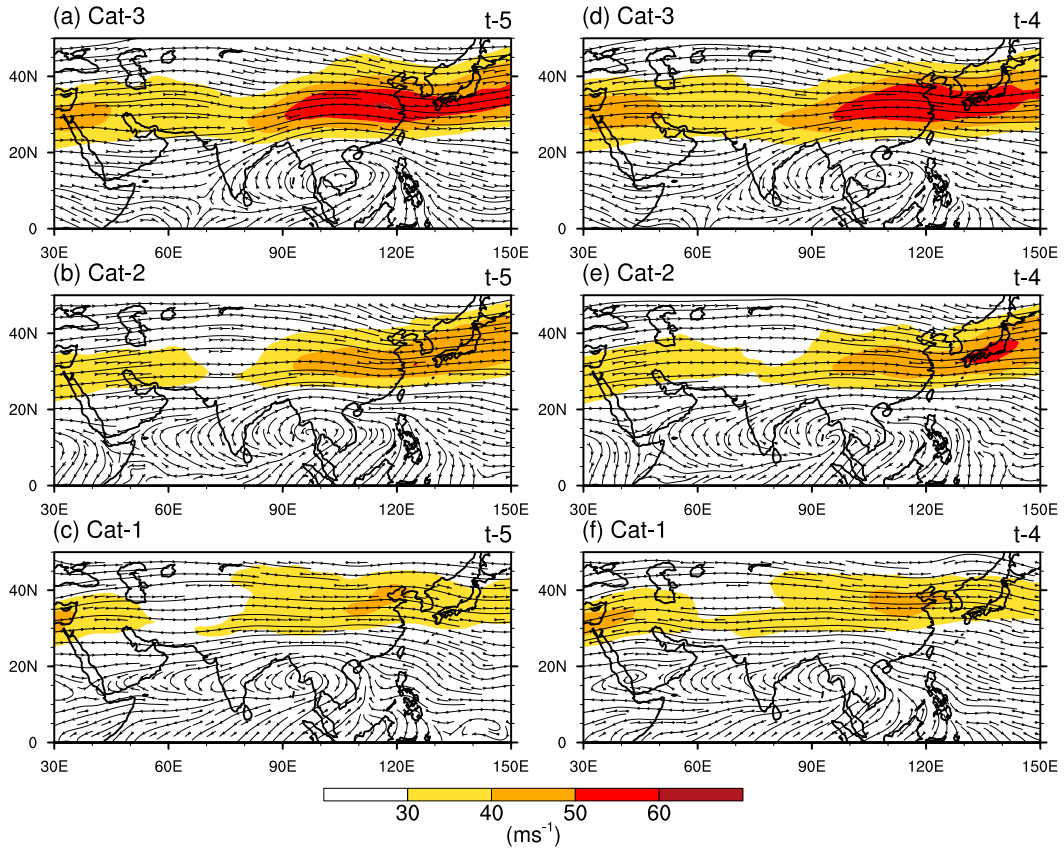

Figure 8.4: Composite of 200 hPa wind for t-5 and t-4 days for a) Cat-3, b) Cat-2 and c) Cat-1. The wind magnitude is given as shaded contours.

the adjoining Southeast Asia with its ridge line at about latitude 15°N and (b) the STJ with a trough over south Asia located near the longitude 70°E where the wind field of the Jet-stream is weak and a high speed center to its east which has very high wind speed of the order of 60 to 70 ms^{-1}. Bay of Bengal cyclones with their centers located north of the ridge line have an environment of winds towards northeast which make them move in a north-northeast direction. All the cyclones in this study fall under this category.

It is observed that the 200 hPa wind field shows a clear distinction in the strength of HSCs in the three categories of tropical cyclones. The differences in the strength of core winds of the HSC are evident even 5 days ahead of the day of maximum intensity (t) for all the three categories of cyclones. For Cat-3 cyclones

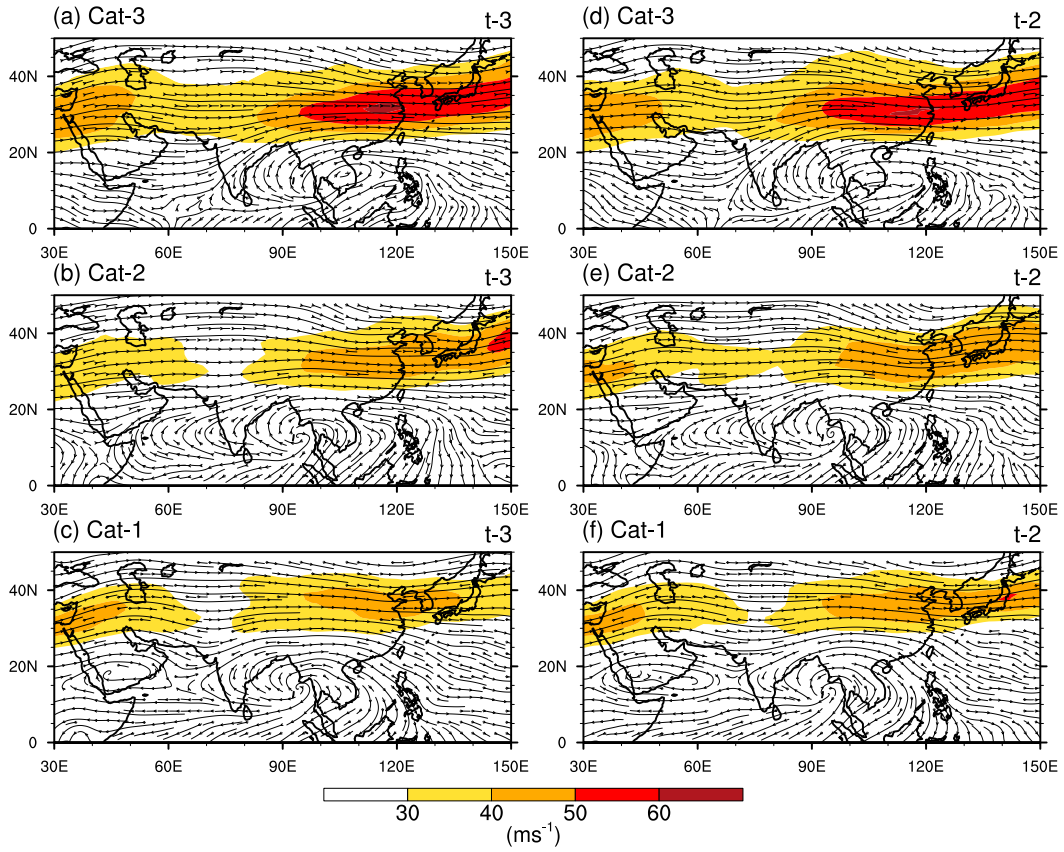

Figure 8.5: Composite of 200 hPa wind for t-3 and t-2 days for a) Cat-3, b) Cat-2 and c) Cat-1. The wind magnitude is given as shaded contours.

the composite HSC has a core wind speed of 50 to 60 ms^{-1} 5 days ahead of the day of maximum intensity (t-5). For Cat-2 maximum intensity 5 days ahead is in the range 40 to 50 ms^{-1}. For Cat-1, the strength of the HSC is in comparison low (30 to 40 ms^{-1}) at day t-5.

As the cyclone center approaches the right entrance region of the HSC, the mean intensity of the HSC in STJ is found to increase in all the three categories. For Cat-1, major part of the HSC have wind speeds 30 to 40 ms^{-1} during t-5. A small patch with 40 to 50 ms^{-1} is seen at t-5 which expands by t-3. At t-1 and t, the 40 to 50 ms^{-1} contour is prominent in the core of the HSC. This increase in wind speed is attributed to the interaction with the tropical cyclone. For Cat-2, there is a 40 to 50 ms^{-1} contour for the HSC at t-5. This intensifies to wind

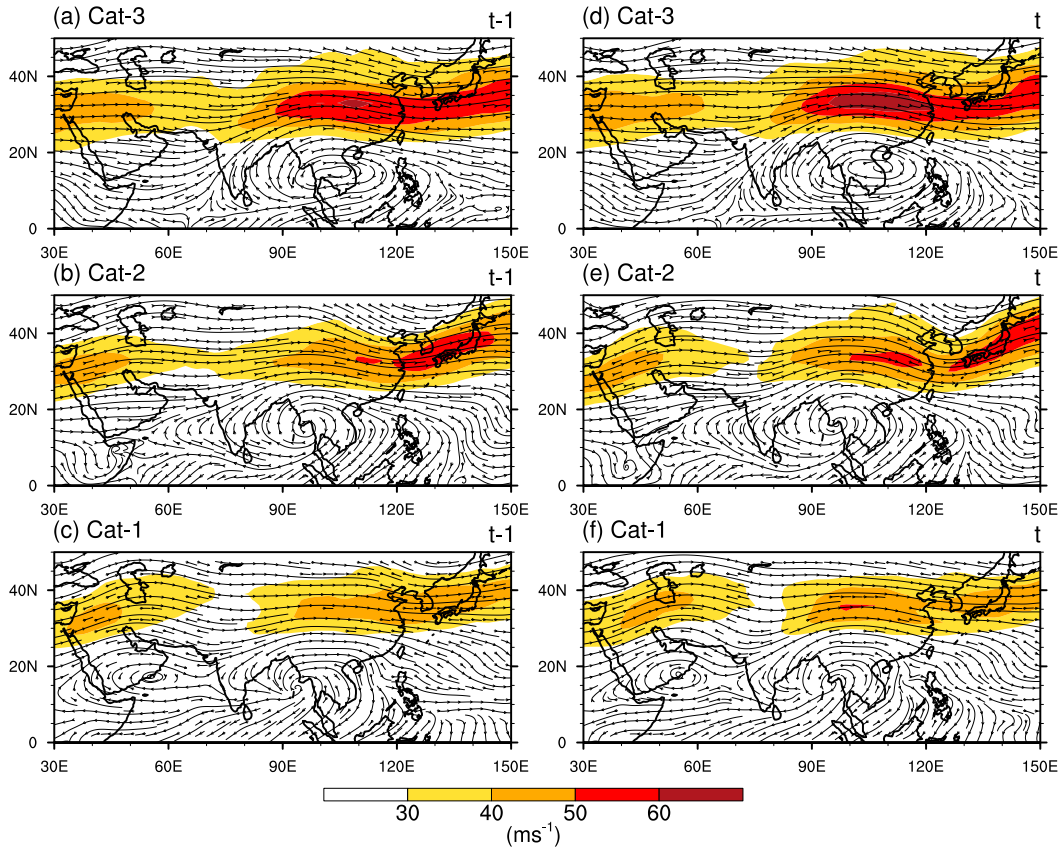

Figure 8.6: Composite of 200 hPa wind for t-1 and t days for a) Cat-3, b) Cat-2 and c) Cat-1. The wind magnitude is given as shaded contours.

speed 50 to 60 ms^{-1} on day t-1. For Cat-3 cyclones the composite has a large area of wind speed 50 to 60 ms^{-1} at day t-5 itself. A small area of winds above 60 ms^{-1} is observed at t-3 to t-1. Then on day of maximum intensity (t), the area with winds 60 ms^{-1} and above has expanded considerably. In general the maximum intensify of the core wind speed of HSC in STJ occurs from day t-3 to t (particularly t-1 to t) when the cyclone is closest to the HSC. It is seen that in the composites the core wind speed of the HSC is related to the intensity category of the cyclone even 5 days ahead of the cyclones maximum intensity. As the cyclone approaches the HSC the core winds of the HSC grows in wind speed. There is thus mutual interaction between the tropical cyclone and the HSC of the STJ.

For the three categories of cyclones the composite 200 hPa meridional profiles

of the wind speed of the are analysed. This profile shows the mean wind speed between longitudes 90°E and 130°E (the core of the HSC) calculated for each latitude. Although there is clear distinction between the strength of the composite HSC from Cat-1 to Cat-3 in all the days from t-5 to t, in each category there is considerable scatter in the strength of the core winds from case to case. As an example the individual cases of cyclones for all the three categories for day t-5 is shown in figure 8.7. Although the scatter is large 60 to 70 % of the cyclones are close to the mean profile as shown by the thick red line showing that there is possibility for forecasting the maximum intensity of a cyclone using the HSC data. The high scatter is expected as the maximum intensity of the cyclone is also controlled by two major factors; the VWS and Ocean surface characteristics.

8.2.1 Case studies

In order to study the mutual interaction process between the tropical cyclone and HSC in detail, case studies are made of two cyclonic storms of the Bay of Bengal, one of the pre-monsoon season and the other of the post monsoon season. The Bay of Bengal cyclone of 22 to 30 April 1991 had maximum wind speed of 125 knots and the Bay of Bengal cyclone (Sidr) 10 to 16 November 2007 which had

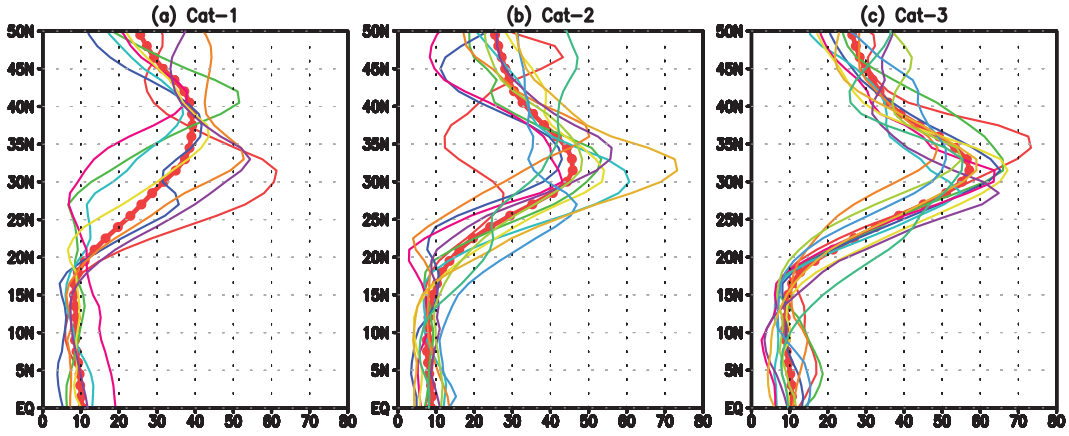

Figure 8.7: Meridionaly averaged profiles of 200 hPa winds 5 days before the maximum intensity (t-5) of the tropical cyclones

a maximum wind speed of 119 knots. The detailed analysis of the 200 hPa wind is done using 6 hourly data at from ERA-interim reanalysis.

8.2.1.1 Tropical cyclone BOB 01 (22 to 30 April 1991)

Figure 8.8 shows the 200 hPa wind at 24 hour interval during the period of intensification of the cyclone. The tropical cyclone symbol on the figure marks the position of the center of the cyclone. The low pressure system associated with the cyclone concentrated into a depression on April 24 at 1800 UTC (t-5) when it was located close to 10.1°N/89°E. The STJ with a distinct high speed center can be observed north of the storm. There was strong westerly flow in the northern side of the cyclone and light easterly wind to its south. At this time the core wind speed of the HSC of STJ was in the range 50 to 60 ms^{-1}. The depression moved in a northwesterly direction intensifying into a cyclonic storm centerd at 11.1°N/88°E on 25 April at1200 UTC. During this period the core of the HSC expanded westward with a large contour of 50 to 60 ms^{-1} north of Bay of Bengal. As the cyclone intensification process occurred the wind speed of the core of HSC further increased and a large area of wind speed 60 to 70 ms^{-1} is may be seen at 1200 UTC on 26 April. The cyclone further moved north intensifying to severe cyclone stage at 0600 UTC 27 April with its center located at 13.4°N/87.2°E. The center of the tropical cyclone was near the divergent right entrance region of the HSC at this time and the core wind speed of the HSC increased to more than 70 ms^{-1}. Recurving to a north-east direction the cyclone intensified into a super cyclone at 0600 UTC on 29 April when its center was located at 19.7°N/89.9°E. The cyclone reached its maximum intensity of 125 knots and the central pressure dropped to 931 hPa at 1200 UTC on 29 April with center at 20.5°N/90.6°E. The intensity of the HSC increased and a large area of core wind speed above 70 ms^{-1} is seen in the figure. The system crossed Bangladesh coast at 29 April midnight and started dissipating. During the intensification process, most of the upper tropospheric outflow occurred through the Jet stream. The changes in VWS around the cyclone center and the intensity of the cyclone (maximum wind) are depicted in figure 8.9 at hourly intervals from 22 to 30 April 1991. From the genesis of the cyclone VWS shows a steady increase. As the cyclone is moving

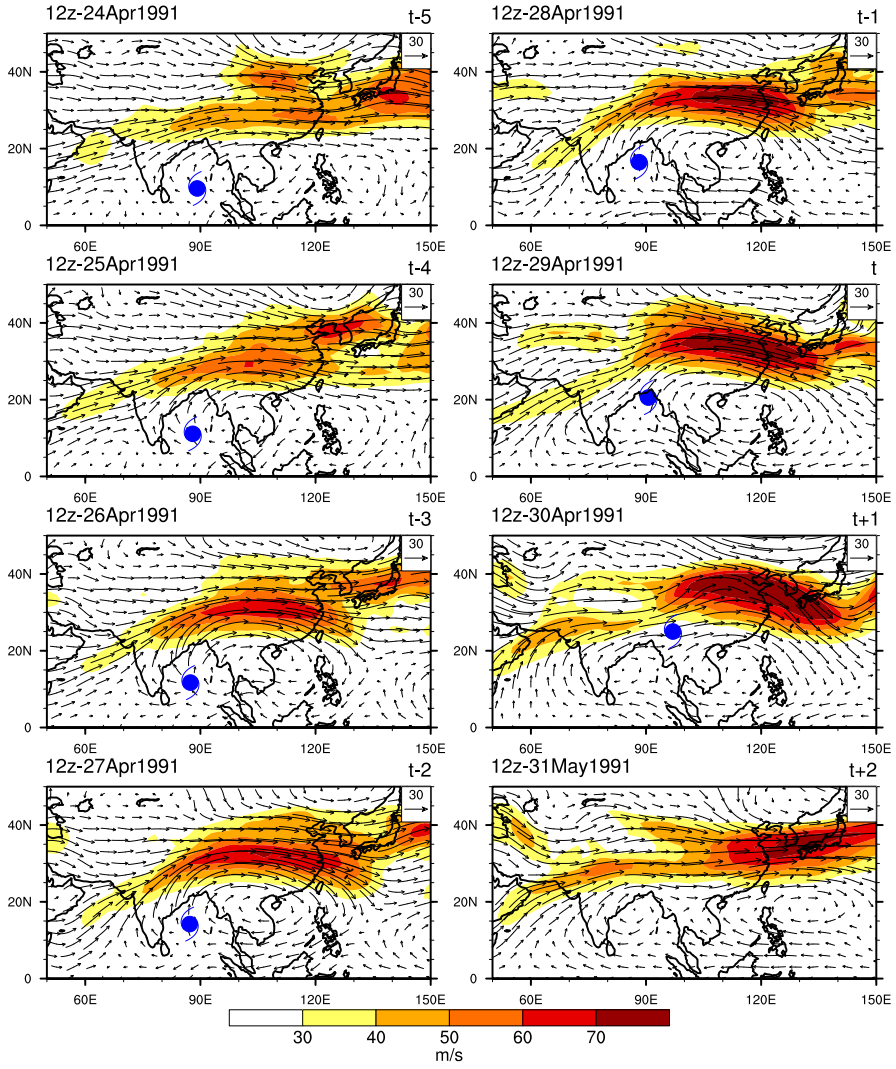

Figure 8.8: 200 hPa wind associated with the April 1991 tropical cyclone from 1200 UTC April 24 to 1200 UTC 01 May at 24 hour intervals. Symbol marks the location of the tropical cyclone.

northward the upper tropospheric wind speed increases and that increases the VWS in its environment. Inspite of the increase in VWS the cyclone steadily intensified possibly helped by the divergent region of the HSC (right entrance).

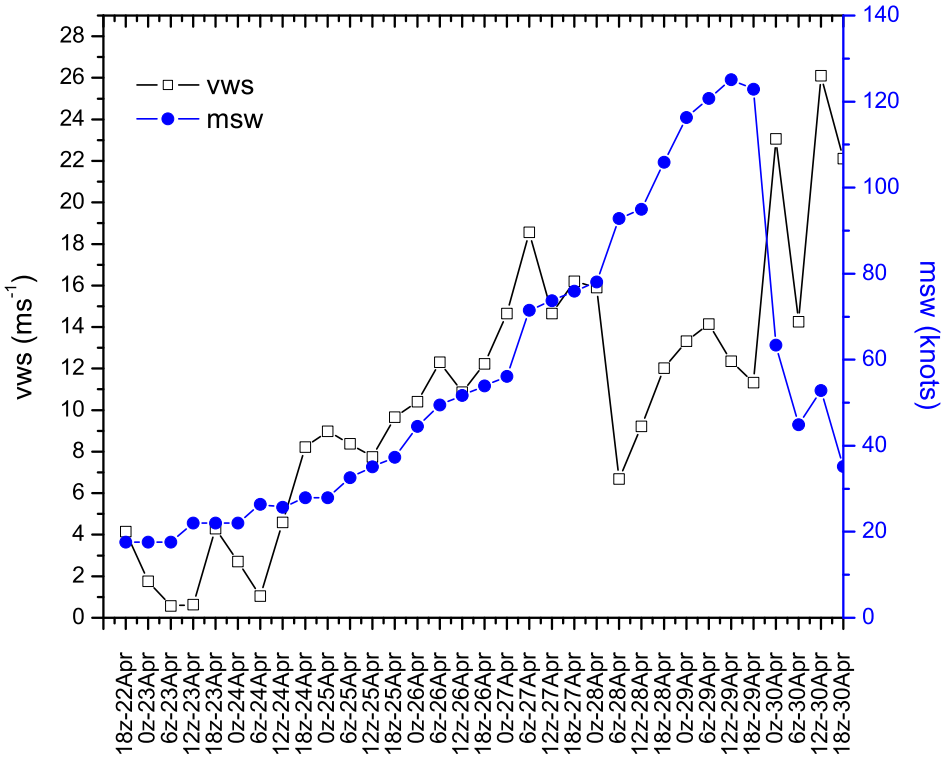

Figure 8.9: The 6 hourly changes in VWS and wind speed associated with April 1991 tropical cyclone.

8.2.1.2 Tropical cyclone Sidr (11 to 16 November 2007)

Figure 8.10 shows the 200 hPa flow at 24 hour intervals for the super cyclone Sidr of Bay of Bengal during 11 to 16 November 2007. Sidr formed over south-east Bay of Bengal and intensified into a depression when its center was located near 10.1°N/92.2°E at 0600 UTC 11 November. In the initial stage itself the main outflow region from the cyclone is via the outflow channel provided by the STJ. On 11 November (t-4) the core wind speed of the HSC was in the range of 60 to 70 ms^{-1}. The system moved north-west and intensified into a cyclonic storm located over 10.3°N/91.4°E at 1800 UTC 11 November. The cyclone moved northwestward and lay centered near 11.3°N/90.1°E when it intensified to a very severe cyclonic storm at 1200 UTC on 12th November. The intensity of HSC also increased and a large area with core wind speed from 60 to 70 ms^{-1} is observed.

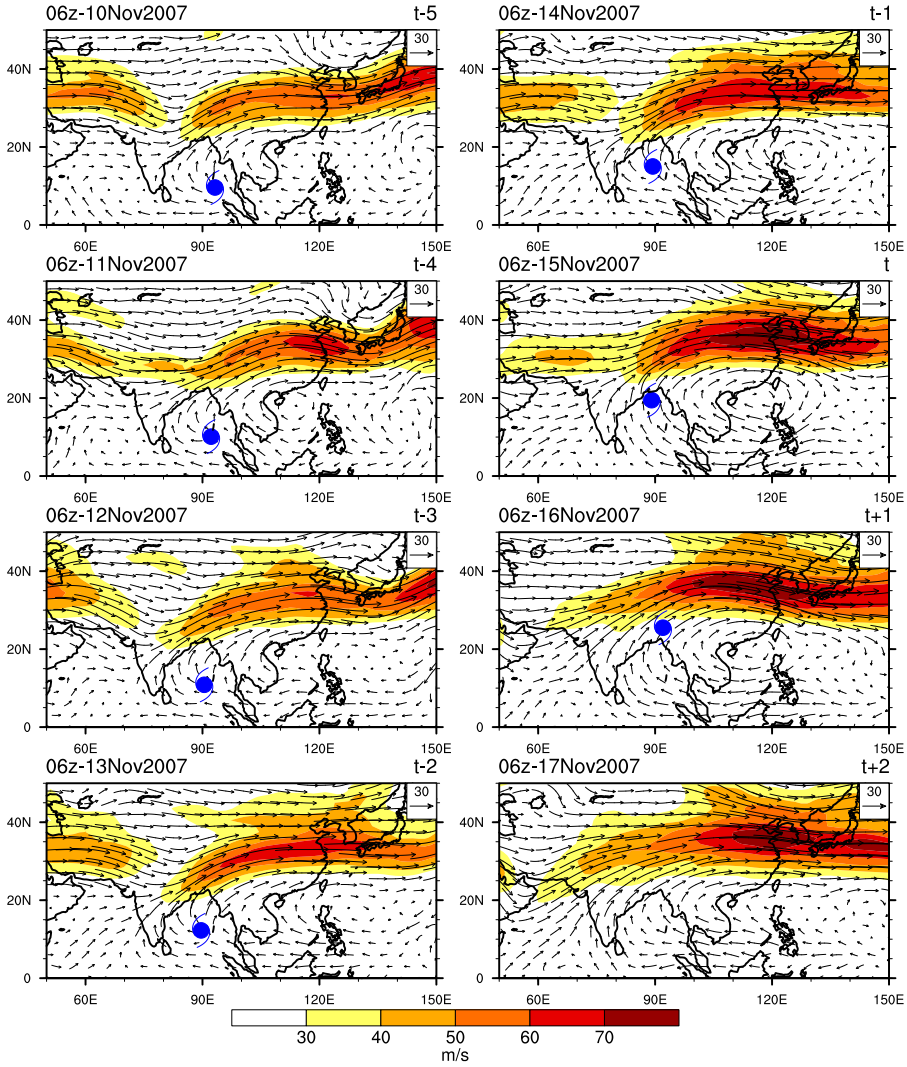

Figure 8.10: 200 hPa wind associated with tropical cyclone *Sidr* from 0600 UTC 11 November to 0600 UTC 17 November at 24 hour intervals. Symbol marks the location of the tropical cyclone.

Further moving north the cyclone intensified into a super cyclonic storm at 0600 UTC of 15 November when it was located near 19.4°N/89.1°E. The cyclone is now close to the HSC and the core wind speed of the HSC increased to more than 70 ms^{-1}. The cyclone moved northeastward and crossed West Bengal- Bangladesh coast around 1600 UTC of 15th November. Moving further north-eastward the system weakened and dissipated. As seen in the previous case the VWS (shown

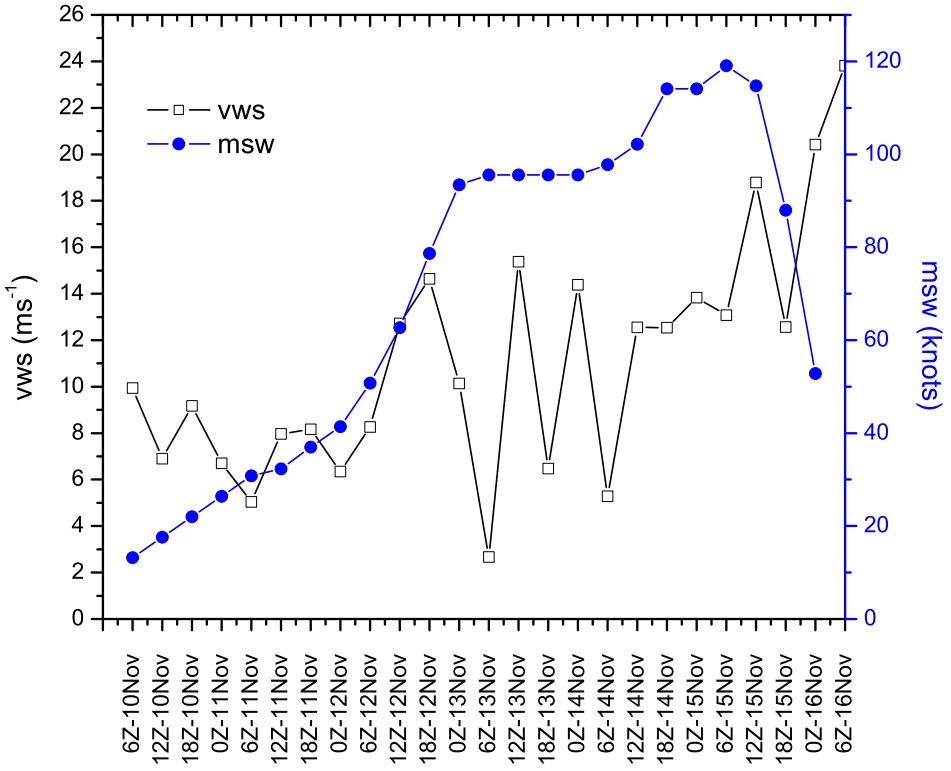

Figure 8.11: The 6 hourly changes in VWS and wind speed associated with tropical cyclone *Sidr*.

in figure 8.11) around the center of the cyclone showed an increase as the cyclone approaches the HSC. Inspite of the higher VWS the cyclone intensified.

8.3 Conclusion

The interaction of Bay of Bengal tropical cyclones which attain their maximum intensity north of latitude 15°N with the Asian high speed center of the STJ is studied in this chapter. Cyclones were divided into three categories with maximum intensity between 34 to 47 knots, 48 to 63 knots and above 64 knots. It is observed that the climatological trough in STJ over south Asia has little effect on the intensity of Bay of Bengal cyclones, but the high speed center of STJ is found to be associated with the maximum intensity of the cyclones. The relation

between the strength of the high speed center and the intensity of the cyclone can be found even five days before the day of maximum intensity of the cyclone. The divergent right entrance region of the High Speed Center of the STJ at 200 hPa has an important role in the intensification of the tropical cyclone. In addition the tropical cyclone and the HSC of STJ are found to mutually interact as the cyclone center approaches the HSC. As the tropical cyclone approaches the HSC the maximum wind of the HSC is found to increase. It is suggested that the strength of the HSC may be considered as a factor in the intensification of a cyclone in addition to other dynamic and thermodynamic parameters. Two case studies are presented; one of a pre-monsoon cyclone (April 1991) and the other of a post-monsoon cyclone (November 2007) to illustrate the interaction between the tropical cyclone and the high speed center of the Jetstream. It is suggested that the findings of this empirical study may be verified using numerical models.

Chapter 9

Summary and Conclusions

Tropical cyclones of North Indian Ocean basin and the environmental factors influencing their frequency of occurrence and intensity have been studied in this thesis. North Indian Ocean is part of the warm pool of the tropical oceans characterised by high sea surface temperatures throughout the year. The eastern part of the warm pool (North-west Pacific Ocean) has produced the maximum number of tropical cyclones in any ocean basin globally (about 26% per year). Cyclones in this basin have their genesis during May to December. In contrast the western part of the warm pool i.e. North Indian Ocean has generated only 6% of the global tropical cyclones annually, but these cyclones have produced maximum human fatalities. One of the main reasons for the low percentage of the global cyclones occurring in the North Indian Ocean basin is the suppression of tropical cyclone genesis there during the Asian summer monsoon season (June to September) due to the prevailing high vertical wind shear in the atmosphere.

This thesis has studied the variability in the frequency of tropical cyclones of North Indian Ocean in the three time scales intra-seasonal, inter-annual and decadal. The environmental factors associated with these variabilities have been investigated. The thesis has also studied the environmental factors in the atmosphere and ocean related to the intensification of tropical cyclones of North Indian Ocean, in particular the roles of sea surface temperature and upper ocean heat content, vertical wind shear in the atmosphere, life duration and translation speed over the ocean of the cyclone and the influence of Sub-tropical westerly Jetstream, particularly its Asian high speed center.

In Chapter-1 is given a summary of the available research literature on global tropical cyclones relevant to this thesis. The data used for the studies presented in this thesis have been described in Chapter-2. Cyclone frequency and intensity data have been taken from IMD sources and the IBtRACS data set. For the environmental parameters, data has been taken from several sources : Daily and monthly wind and humidity data from National Centers for Environmental Prediction/National Center for Atmospheric Research (NCEP/NCAR) Reanalysis; daily fields from European Centre for Medium-Range Weather Forecasts interim reanalysis (ERA-interim) and NCEP FNL analysis; Outgoing Long wave Radiation (OLR) data from National Oceanic and Atmospheric Administration (NOAA); Sea Surface Temperature (SST) data from HadISST and ERSST; SST from NOAA IOSST; SST and Vertically Integrated moisture from TMI; Sea surface height Anomaly (SSHA) data from AVISO are used in the thesis. Available indices such as ENSO index from NOAA-CPC, IOD index from Japan Agency for Marine-Earth Science and Technology (JAMSTEC) and MJO index from Bureau of Meteorology (BOM), Australia are also been used.

Chapter 3 has studied the role of Madden Julian Oscillation in the genesis of North Indian Ocean tropical cyclones. Formation of cyclonic storms over North Indian Ocean during the period 1979 to 2008 have been studied with respect to the eastward passage of Madden-Julian Oscillation. In this study, MJO intensity with amplitude 1 and above only has been examined, which includes 61% days of the whole period. The relationship between these cyclones with the different phases of MJO has been studied. The cyclones are clustered in eight phases P1 to P8 with respect to MJO. The main findings from this study are

- In the three decades (1979-2008), there were a total of 118 cyclones reported in which 96 formed in the region chosen (0-15°N, 60°E-100°E) for the study. Although the percentage of MJO days inducing cyclogenesis is small, it is found that tropical cyclone genesis preferentially occurred during the convective phase of MJO. This accounted for 44 cyclones of the total 54 cyclones (i.e., 81.5%) formed under MJO amplitude 1 and above.

- The study has shown that, when the enhanced convection of MJO is over the maritime continent and the adjoining eastern Indian Ocean, it creates

the highest favourable environment for cyclogenesis in the Bay of Bengal. During this phase, westerlies at 850 hPa are strong in the equatorial region south of Bay of Bengal creating strong cyclonic vorticity in the lower troposphere along with the low vertical wind shear.

- Vertical shear of zonal wind is found to be favourable during the phases P3 and P4 of November-December and May-June which account for the maximum number of cyclone genesis in those phases.

The interannual variation of tropical cyclone activity over North Indian Ocean is studied in Chapter-4. Two major modes of interannual variability in North Indian Ocean are El Nino Southern Oscillation (ENSO) and Indian Ocean Dipole (IOD). From the analysis it is observed that most of the El Nino-0 years are positive IOD years and hence we did not separately study the IOD years. Variations in the genesis, intensity and tracks of the post-monsoon (October-December) North Indian Ocean tropical cyclones with respect to the El Nino-Southern Oscillation were analysed using 30 years of IBtRACS tropical cyclone data. An empirical Genesis Potential Index (GPI) was calculated following Emmanuel and Nolan (2004) in order to analyse the variations associated with cyclogenesis. The main findings in the study are

- There is a net reduction in the intensity and frequency of tropical cyclones formed over the North Indian Ocean during the El Nino-0 years compared with the non El Nino years. Also there is a southward shift in the genesis region during the El Nino-0 years along with a zonal shift towards east.

- Analysis using the GPI shows that anomalous negative values exist over the northern Bay of Bengal during the El Nino-0 years.

- The relative contribution of individual parameters to the GPI are examined and it is found that low values of VWS over southern Bay of Bengal favours the southward shift of genesis region during El Nino-0 years. For La Nina years vorticity and relative humidity parameters are found to be favourable and higher contributions of these parameters are responsible for

the westward shift of mean genesis region over the Bay of Bengal during these years.

- The tropical cyclone tracks are westwards during the El Nino-0 years compared with the northward moving tropical cyclones during La Nina. These are caused by the changes in upper tropospheric circulation patterns. Although the vertical wind shear is less favourable compared with El Nino-0 years, tropical cyclone during La Nina intensifies more since the duration of northward moving tropical cyclone over the oceanic region is more.

Chapter 5 deals with the decadal variation in the intensity and frequency of tropical cyclones and monsoon depressions of North Indian Ocean. The tropical cyclones in the North Indian Ocean, normally occur during the pre-monsoon and the post-monsoon months, differ drastically from the monsoon depressions that form during the summer season in their intensity, asymmetry of winds around the center, tilt of the circulation center with height, vertical wind shear in the environment, etc

- Both the tropical cyclones and the monsoon depressions exhibit four decade oscillations in their annual frequency, which is unique for the North Indian Ocean basin. The four decade oscillations of tropical cyclones and monsoon depressions have very little temporal phase difference.

- Of the six cyclone genesis parameters of Gray, low level vorticity and vertical wind shear are found to have association with the four decade oscillation in tropical cyclones. It has been found that during October to December season, which is highly favourable for the formation of tropical cyclones, the zonal wind at 850 hPa level averaged over an equatorial box bounded by latitudes 2.5°S and 7.5°N and longitudes 50°E and 100°E has a four decade oscillation during 1948 to 2009, which is in phase with that in tropical cyclones.

- Annual frequency of monsoon depressions during 1891-2009 has a large and statistically significant decreasing trend, whereas the tropical cyclones during the same period showed only a small decreasing trend. Four decade

oscillation is superposed on the long term trend for both monsoon depression and tropical cyclone.

- The decreasing trend in the frequency of monsoon depressions and its four decade oscillation are seen related to the strength of the monsoon low level Jetstream passing through peninsular India and Bay of Bengal. The decreasing trend in the strength of low level Jetstream is related to the observed rapid warming of the equatorial Indian Ocean which is hypothesized to weaken the monsoon Hadley circulation.

A comparison between observed maximum intensity attained by North Indian Ocean tropical cyclones and calculated maximum potential intensity (MPI) is made in chapter 6 using 21 years IBtRACS-WMO tropical cyclone data (1990-2010). The dependencies of environmental parameters, both thermodynamic and dynamic components have been analysed. The following is the summary of the findings

- A board range of sea surface temperatures (SST) values from 26 to 31 degrees are observed but the highest intensity storms are associated with the high SST values.
- Vertical Wind Shear values below 12 ms^{-1} is observed associated with very severe cyclonic storms and super cyclones.
- It is found that cyclone translational speed from 2-6 ms^{-1} is associated with with cyclones of high intensity.
- The life span of the tropical cyclones is found to have a large importance in the intensification of North Indian Ocean tropical cyclones.

A case study of tropical tropical cyclone Gonu which formed over the Arabian Sea and rapidly intensified into a super cyclone on 4 June 2007 while it was centered at about 19.90°N, 64.10°E is presented in chapter-7. The factors that caused this rapid intensification from T 4.0 to T 6.5 on the *Dvorak scale* in about 18 hours were investigated in this Chapter. We examined the role of ocean

parameters viz, sea surface temperature (SST), tropical cyclone heat potential above the 26°C isotherm (TCHP) and ocean eddies which are areas of sea surface height anomalies (SSHA) and atmospheric parameters such as vertical wind shear (VWS), vertically integrated moisture (VIM) and upper tropospheric divergence associated with the sub-tropical jetstream in the rapid intensification of Gonu. Positive SSHA which are areas of high heat storage in the top layer of the ocean is found to be important for the rapid cyclone intensification. The heat storage in these warm SSHA eddies are extracted by the deep moist convection in the central region of the cyclone. The main observations from the chapter are

- The upper ocean heat content in the track of tropical cyclone Gonu favoured the rapid intensification process. The SSHA averaged over a radial distance of 2 degrees around the cyclone center appear to give the best measure of the rate of intensification/weakening of the cyclone. By this averaging process the effect of the positive and negative SSHA areas in a specified area around the cyclone center is taken into consideration.

- The rapid intensification process is further assisted by other parameters important for cyclone intensification as assessed qualitatively such as low values of VWS, positive upper tropospheric divergence and high values of VIM.

Chapter 8 discuss the role of Sub Tropical Jetstream in the intensification process of Bay of Bengal tropical cyclones. The Bay of Bengal tropical cyclones which reached maximum intensity north of latitude 15°N is studied with respect to the Sub Tropical Jetstream (STJ). Cyclones were divided into three categories with maximum intensity between 34 to 47 knots, 48 to 63 knots and above 64 knots and the role of upper tropospheric troughs and high speed center associated with STJ in the intensification of cyclones was studied. The study shows that although the climatological trough in STJ has little effect on the maximum intensity of the storms, the high speed center in STJ influence the maximum intensity of the storms.

- The intensity of high speed centre in the STJ shows clear distinction between the three categories of cyclones even 5 days before the cyclone reaches maximum intensity. The divergent right entrance region of the high speed center of the STJ is found to play an important part in the intensification of the tropical cyclone.
- There is a mutual interaction process by which the intensity of HSC increases as the tropical cyclone centre approaches the STJ.

Scope for future Studies

The tropical-ocean atmosphere system has a strong signal of decadal scale variability of period about 60 years the Atlantic Multi-decadal Oscillation, the Pacific Decadal Oscillation and the alternating three decade long Dry and Wet epochs of Indian Summer Monsoon rainfall. The effect of this decadal variability on tropical cyclones may be investigated. North Indian Ocean tropical cyclones and monsoon depressions exhibit a prominent four decade oscillation unique to this ocean basin which has been investigated in this thesis.

In chapter 8 of this thesis is reported an empirical study on the interaction between the Asian high speed center of the Sub Tropical Jetstream and the northward moving tropical cyclones of the Bay of Bengal. A study using numerical models can provide insight into possible mechanisms of this interaction which can lead to formulation of methods to forecast cyclone intensification.

References

Aiyyer A, Thorncroft C (2011) Interannual-to-multidecadal variability of vertical shear and tropical cyclone activity. Journal of Climate, 24:2949-2962.

Alexander MA, Blade I, Newman M, Lanzante JR., Lau N-C, Scott JD. (2002) The Atmospheric Bridge: The influence of ENSO teleconnections on Air-Sea Interaction over the global oceans. Journal of Climate, 15:2205-2231.

Ashok K, Guan Z, Yamagata T (2001) Impact of the Indian Ocean Dipole on the relationship between the Indian monsoon rainfall and ENSO. Geophysical Research Letter, 26:4499-4502.

Atlas IMD, (1979) Tracks of storms and depressions in the Bay of Bengal and the Arabian Sea. India Meteorological Department. New Delhi, India

Beebe RG, Bates FC (1955) A Mechanism For assisting in the release Of convective instability. Monthly Weather Review, 83:1-10.

Belanger JI, Curry JA, Webster PJ (2010) Predictability of north Atlantic tropical cyclone activity on intraseasonal time scales. Monthly Weather Review, 138:4362-4374.

Bell GD, Chelliah M, (2006) Leading tropical modes associated with interannual and multidecadal fluctuations in North Atlantic hurricane activity. Journal of Climate, 19:590-612.

Bessafi M, Wheeler MC (2006) Modulation of south Indian Ocean tropical cyclones by the Madden-Julian oscillation and convectively coupled equatorial waves. Monthly Weather Review, 134:638-656.

Bengtsson L, Hagemann S, Hodges KI, (2004) Can climate trends be computed from reanalysis data? Journal of Geophysical Research, 109, D11111, doi:10.1029/2004JD004536.

Bengtsson L, Hodges MKI, Esch M, Keenlyside N, Kornbleuh L, Luo J-J, Yamagata T (2007) How may tropical cyclones change in a warmer climate? Tellus, 59A: 539-561.

Bhalme HN (1972) Trends and quasi-biennial oscillation in the series of cyclonic disturbances over the Indian region. Indian Journal of Meteorology and Geophysics. 23:354-358.

Bhowmik SKR, Kotal S D, Kalsi SR (2007) Operational tropical cyclone intensity prediction- an empirical technique; Natural Hazards 41:447-455.

Black PG (1983) Ocean temperature changes induced by tropical cyclones. Ph.D. dissertation, Pennsylvania State University

Camargo SJ, Sobel AH, Barnston AG, Emanuel KA (2007) Tropical cyclone genesis potential index in climate models. Tellus A, 59(4):428443.

Camargo SJ, Sobel AH, Barnston AG, Klotzbach PJ (2010) The influence of natural climate variability, and seasonal forecasts of tropical cyclone activity. In: Chan JCL, Kepert JD (ed) Global perspectives on tropical cyclones, from science to mitigation, World Scientific Series on Earth System Science in Asia, 325-360

Challa M, Pfeffer RL (1980) Effects of eddy fluxes of angular momentum on model hurricane development. Journal of the Atmospheric Sciences, 37:1603-1618.

Chan JCL, Shi J (1996) Long-term trends and interannual variability in tropical cyclone activity over the western North Pacific. Geophysical Research Letter, 23:2765-2767.

Chand SS, Walsh KJE (2009) Tropical cyclone activity in the Fiji region: spatial patterns and relationship to large-scale circulation. Journal of Climate, 22(14):3877-3893.

Chang SW, Anthes RA (1979) The mutual response of the tropical cyclone and the ocean. Journal of Physical Oceanography, 9:128-135.

Chen L, Gray WM (1984) Global view of the upper level outflow patterns associated with tropical cyclone intensity changes during FGGE. Preprints, 15th conference on hurricanes and tropical meteorology, Miami, Florida, American Meteorological Society, 224231.

Chu PS, Clark JD (1999) Decadal variations of tropical cyclone activity over the central North Pacific. Bulletin of American Meteorological Society, 80:1875-1881.

Chu PS (2002) Large-scale circulation features associated with decadal variations of tropical cyclone activity over the central North Pacific. Journal of Climate 15:2678-2689.

CPC (2011) Monthly atmospheric and SST indices. (Available online at http://www.cpc.ncep.noaa.gov/products/analysis _ monitoring/ensostuff/ensoyears.shtml)

Dash S, Kumar JR, Shekhar M (2004) On the decreasing frequency of monsoon depressions over the Indian region. Current Science, 86(10):1406-1411.

Demaria M, Kaplan J (1994) Sea surface temperature and the maximum intensity of Atlantic tropical cyclones. Journal of Climate, 7:1324-1334.

DeMaria M, Kaplan J, Baik J-J (1993) Upper-level eddy angular momentum fluxes and tropical cyclone intensity change. Journal of the Atmospheric Sciences, 50:1133-1147.

Diaz HF, Hoerling MP, Eischeid JK (2001) ENSO variability, teleconnections and climate change. International Journal of Climatology, 21, 1845-1862.

Dvorak VF (1975) Tropical Cyclone intensity analysis and forecasting from satellite imagery. Monthly Weather Review, 103:420-430.

Elsner JB, Jagger T, Niu X-F (2000) Changes in the rates of North Atlantic major hurricane activity during the 20th century. Geophysical Research Letter, 27:1743-1750.

Emanuel KA (1986) An air-sea interaction theory for tropical cyclones. Part I: Steady-state maintenance. Journal of the Atmospheric Sciences, 43(6):585-604.

Emanuel KA (1991) The theory of hurricanes. Annual Review of Fluid Mechanics, 23(1):179-196.

Emanuel KA (1987) The dependence of hurricane intensity on climate. Nature, 326(6112):483485.

Emanuel KA (1988) The maximum intensity of hurricanes. Journal of the Atmospheric Sciences, 45(7):1143-1155.

Emanuel KA (1995) Sensitivity of tropical cyclones to surface heat exchange coefficients and a revised steady-state model incorporating eye dynamics. Journal of the Atmospheric Sciences, 52(22):3969-3976.

Emanuel KA (1999) Thermodynamic control of hurricane intensity. Nature, 401:665-669.

Emanuel KA (2000) A statistical analysis of tropical cyclone intensity. Monthly Weather Review, 128:1139-1152.

Emanuel KA (2005) Increasing destructiveness of tropical cyclones over the past 30 years. Nature, 436:686-688.

Emanuel KA, DesAutels C, Holloway C, Korty R (2004) Environmental Control of tropical cyclone intensity. Journal of the Atmospheric Sciences, 61:843858.

Emanuel KA Nolan DS (2004) Tropical cyclone activity and global climate. Preprints, 26th Conference on Hurricanes and tropical meteorology, American Meteorological Society, Miami, Florida, 240-241.

Evans JL (1993) Sensitivity of tropical cyclone intensity to sea surface temperature. Journal of Climate, 6:11331140.

Findlater J (1969) A major low-level air current near the Indian Ocean during the northern summer. Quarterly Journal of the Royal Meteorological Society, 95:362-380.

Frank WM (1987) Tropical cyclone formation, Chapter 3, A global view of tropical cyclones. Office of Naval Research, Arlington, Virginia, 53-90.

Frank WM, Roundy PE (2006) The role of tropical waves in tropical cyclogenesis. Monthly Weather Review , 134:2397-2417.

Gallina GM, Velden CS (2002) Environmental vertical wind shear and tropical cyclone intensity change utilizing enhanced satellite derived wind information, paper presented at 25th Conference on hurricanes and tropical meteorology, American Meteorological Society, San Diego, California.

Girishkumar MS, Ravichandran M (2012) The influences of ENSO on tropical cyclone activity in the Bay of Bengal during October-December. Journal of Geophysical Research, 117. doi:10.1029/2011JC007417

Goldenberg SB, Landsea CW, Mestas-Nunez AM, Gray WM (2001) The recent increase in Atlantic hurricane activity: causes and implications. Science, 293:474-479.

Goni G, Black PG, Trinanes J (2000) Using satellite altimetry to identify regions of hurricane intensification. AVISO Newsletter, 9:19-20.

Goni G, Trinanes J (2003) Ocean thermal structure monitoring could aid in the intensity forecast of tropical cyclones. Eos, 84:573-580.

Gray WM (1968) Global view of the origin of tropical disturbances and storms, Monthly Weather Review, 96(10):669-700.

Gray WM (1975) Tropical cyclone genesis. Department of Atmospheric Science Paper No. 232, Colorado State University, 121.

Gray WM (1979) Hurricanes: Their formation, structure, and likely role in the tropical circulation. In: Shaw DB (ed) Meteorology over the tropical oceans. Royal Meteorological Society, London, pp 155-218.

Gray WM (1984) Atlantic seasonal hurricane frequency. Part1:El Nino and 30mb Quasi-Biennial Influences. Monthly Weather Review, 112:16491668.

Gray WM (1998) The Formation of tropical cyclones. Meteorology and Atmospheric Physics, 67:37-69.

Guptha A, Muthuchami A (1990) El Nino and tropical storm tracks over Bay of Bengal during post monsoon season. Mausam, 42:257-260.

Hall JD, Matthews AJ, Karoly J (2001) The modulation of tropical cyclone activity in the Australian region by the Madden-Julian oscillation. Mon Weather Rev 129: 2970-2982.

Hanley D, Molinari J and Keyser D (2001) A Composite Study of the interactions between tropical cyclones and upper-tropospheric troughs. Monthly Weather Review, 129:2570-2584.

Hartmann DL, Maloney ED (2001) The Madden-Julian Oscillation, barotropic dynamics, and north Pacific tropical cyclone formation. Part II: Stochastic barotropic modeling. Journal of the Atmospheric Sciences, 58:2559-2570.

Henderson-Sellers A, Zhang H, Berz G, Emanuel KA, Gray WM, Landsea CW, Holland GJ, Lighthill J, Shieh S-L, Webster PJ, McGuffie K (1998) Tropical cyclones and global climate change: a post-IPCC assessment. Bulletin of American Meteorological Society, 79:19-38.

Holland GJ (1997) The maximum potential intensity of tropical cyclones. Journal of the Atmospheric Sciences, 54:2519-2541.

Holland GJ, Merrill RT (1984) On the dynamics of tropical cyclone structural changes. Quarterly Journal of the Royal Meteorological Society, 110:723-745.

Jadhav SK, Munot AA (2008) Warming SST of Bay of Bengal and decrease in formation of cyclonic disturbances over the Indian region during southwest monsoon season. Theoretical and Applied Climatology, 96:327-336.

JAMSTEC (2011) Dipole Mode Index. (Available online at http://www.jamstec.go.jp/frcgc/research/d1/iod/HTML/Dipole%20Mode%20Index.html)

Joseph PV, Chakravorty KK (1980) Lower Topographic Temperature Structure of the Monsoon Depression, 11-14 August 1979. Results of summer MONEX field Phase research (Part B), 257-265.

Joseph PV, Raman PL (1966) Existence of low level westerly jet stream over peninsular India during July. Indian Journal of Meteorology and Geophysics. 17:407-410.

Joseph PV, Sabin TP (2008) Trends in SST and reanalysis 850 and 200 hPa wind data of Asian summer monsoon season during the recent six decades. In: Proceedings of 3rd WCRP international conference on reanalysis, Tokyo, Japan,

Joseph PV, Sijikumar S (2004) Intraseasonal variability of the low-level Jet Stream of the Asian summer monsoon. Journal of Climate, 17:1449-1458.

Joseph PV, Simon A (2005) Weakening trend of the southwest monsoon current through peninsular India from 1950 to the present. Current Science. 89:687-694.

Joseph PV, Sooraj KP, Rajan CK (2006) The summer monsoon onset process over South Asia and an objective method for the date of monsoon onset over Kerala. International Journal of Climatology, 26:1871-1893.

Joseph PV, Xavier PK (1999) Monsoon rainfall and frequencies of monsoon depressions and tropical cyclones of recent 100 years and an outlook for the first decades of the 21st century. Meteorology beyond-2000. In: Proceedings of national symposium Tropmet-99, 16-19 February; 364-371.

Kalnay E and Coauthors (1996) The NCEP/NCAR 40-Year Re-analysis Project. Bulletin of American Meteorological Society, 77:437-471.

Kanamitsu M, Kistler RE, Reynolds RW (1997) NCEP/NCAR reanalysis and the use of satellite data. Satellite Data Applications. Weather and Climate, R. G. Ellingson, Ed., Pergamon Press, 481489.

Keyser DA, Johnson DR (1984) Effects of diabatic heating on the ageostrophic circulation of an upper tropospheric jet streak. Monthly Weather Review, 112:1709-1724.

Kikuchi K, Wang B (2010) Formation of tropical cyclones in the northern Indian Ocean associated with two types of tropical intraseasonal oscillation modes. Journal of Meteorological Society of Japan, 88(3):475-496.

Kim JH, Ho CH, Kim HS, Cui CH, Park SK (2008) Systematic variation of summertime tropical cyclone activity in the western North Pacific in relation to the Madden-Julian oscillation. Journal of Climate, 15:1171-1191.

Kistler R and Coauthors (2001) The NCEP-NCAR 50-Year Reanalysis:Monthly means CD-ROM and documentation. Bulletin of American Meteorological Society, 82:247-267.

Klotzbach PJ (2010) On the Madden-Julian Oscillation-Atlantic hurricane relationship. Journal of Climate, 23:282-293.

Knapp KR, Kossin JP (2007) New global tropical cyclone data from ISCCP B1 geostationary satellite observations. Journal of Applied Remote Sensing, 1(1):013505-013505.

Knapp KR, Kruk MC (2010) Quantifying interagency differences in tropical cyclone best-track wind speed estimates. Monthly Weather Review, 138(4):1459-1473.

Knapp KR, Michael CK, David HL, Howard JD, Neumann CJ (2010) The International Best Track Archive for Climate Stewardship (IBTrACS): Unifying tropical cyclone data. Bulletin of American Meteorological Society, 91:363-376.

Kotal SD, Kundu PK, Bhowmik SKR (2009) An analysis of sea surface temperature and maximum potential intensity of tropical cyclones over the Bay of Bengal between 1981 and 2000. Meteorological Applications, 16:169-177.

Kumar KK, Rajagopalan B, Cane MA (1999) On the weakening relationship between the Indian monsoon and ENSO. Science, 284:2156- 2159.

Kumar A, Yang F, Goddard L, Schubert S (2004) Differing trends in the tropical surface temperatures and precipitation over land and oceans. Journal of Climate 17:653-664.

Kumar JR, Dash SK (2001) Interdecadal variations of characteristics of monsoon disturbances and their epochal relationships with rainfall and other tropical features. International Journal of Climatology, 21:759-771.

Knutson TR, Tuleya RE (1999) Increased hurricane intensities with CO2-induced global warming as simulated using the GFDL hurricane prediction system. Climate Dynamics, 15:503-519.

Knutson TR, Tuleya RE, Kurihara Y (1998) Simulated Increase of hurricane intensities in a CO2-warmed climate. Science, 279(5353):10181020

Knutson TR, Tuleya RE, Shen W, Ginis I (2001) Impact of CO2-induced warming on hurricane intensities as simulated in a hurricane model with ocean coupling. Journal of Climate, 14(11):2458-2468.

Knutson TR and Coauthors (2010) Tropical cyclones and climate change. Nature Geoscience, 3:157-163.

Kossin JP, Knapp KR, Vimont DJ, Murnane RJ, Harper BA (2007) A globally consistent reanalysis of hurricane variability and trends, Geophysical Research Letter 34(4):L04185

Koteswaram P (1958) The easterly jet stream in the tropics. Tellus, 10:43-57.

Krishnamurti TN (1961) The subtropical jet stream of winter. Journal of Atmospheric Sciences, 18:172-191.

Krishnamurti TN (1979) Tropical Meteorology. In: Wiin-Nielsen A (ed) Compendium of meteorology I1 WMO-No. 364. World Meteorological Organization, Geneva

Landsea CW (2004) The Atlantic hurricane database re-analysis project: Documentation for the 1851-1910 alterations and additions to the HURDAT database. In: Murname RJ, Liu KB (eds) Hurricanes and typhoons: past, present and future. Columbia University Press, New York, 177-221.

Landsea CW, Harper BA, Hoarau K, Knaff JA (2006) Can we detect trends in extreme tropical cyclones? Science. 313:452-454.

Le Traon P-Y, Dibarboure G (1999) Mesoscale mapping capabilities from multiple altimeter missions. Journal of Atmospheric and Oceanic Technology, 16:1208-1223.

Le Traon P-Y, Dibarboure G, Ducet N (2001) Use of a high-resolution model to analyze the mapping capabilities of multiple-altimeter missions. Journal of Atmospheric and Oceanic Technology, 18:1277-1288.

Lee C-S, Edson R, Gray WM (1989) Some large-Scale characteristics associated with Tropical cyclone development in the North Indian Ocean during FGGE. Monthly Weather Review, 117:407426.

Leipper DF, Volgenau D (1972) Hurricane heat potential of the Gulf of Mexico. Journal of Physical Oceanography, 2(3):218-224.

Leroy A, Wheeler MC (2008) Statistical prediction of weekly tropical cyclone activity in the Southern Hemisphere. Monthly Weather Review, 136:3637-3654.

Liebmann B, Hendon HH, Glick JD (1994) The relationship between tropical cyclones of the western Pacific and Indian Oceans and the Madden-Julian oscillation. Journal of Meteorological Society of Japan 72:401- 412.

Liebmann B, Smith CA (1996) Description of a complete (interpolated) OLR dataset. Bulletin of American Meteorological Society, 77:1275-1277.

Lin II, Chen CH, Pun IF, Liu WT, Wu CC (2009) Warm ocean anomaly, air sea fluxes, and the rapid intensification of tropical cyclone Nargis (2008). Geophysical Research Letter, 36:1-5.

Lin II, Wu CC, Emanuel KA, Lee IH, Wu CR, Pun IF (2005) The Interaction of supertyphoon Maemi (2003) with a warm ocean eddy. Monthly Weather Review, 133:2635-2649.

Madden RA, Julian PR (1971) Detection of a 40-50 day oscillation in the zonal wind in the tropical Pacific. J Atmos Sci 28:702-708.

Maddox RA, (1979) The evolution of middle and upper tropospheric features during a period of intense convective storms. In: Preprints, 11th Conference on severe local storms, Kansas City, American Meteorological Society, 41-48.

Maloney ED, Hartmann DL (2000a) Modulation of eastern North Pacific hurricanes by the Madden-Julian Oscillation. Journal of Climate, 13:14511460

Maloney ED, Hartmann DL (2000b) Modulation of hurricane activity in the Gulf of Mexico by the Madden-Julian Oscillation. Science 287:2002-2004.

Maloney ED, Hartmann DL (2001) The Madden-Julian Oscillation, barotropic dynamics, and North Pacific tropical cyclone formation. Part I: Observations. Journal of the Atmospheric Sciences, 58:2545-2558.

Mainelli M, DeMaria M, Shay LK, Goni G (2008) Application of oceanic heat content estimation to operational forecasting of recent Atlantic category 5 hurricanes. Weather and Forecasting, 23:3-16.

Market PS (1999) Jet Streak modification via diabatic heating during periods of intense, cool season precipiation. Ph.D dissertation, Saint Louis University

Matsuura T, Yumoto M, Iizuka S (2003) A mechanism of interdecadal variability of tropical cyclone activity over the western North Pacific. Climate Dynamics. 21:105-117.

Marshall GJ (2002) Trends in Antarctic geopotential height and temperatures: A comparison between radiosonde and NCEP-NCAR reanalysis data. Journal of Climate, 15:659-674.

McBride JL (1981) Observational analysis of tropical cyclone formation. part I: basic description of data sets. Journal of the Atmospheric Sciences, 38:1117-1131.

McBride JL (1995) Tropical cyclone formation. Global perspectives on tropical cyclones, WMO/TD No. 693, Rep. TCP-38, World Meteorological Organization, Geneva, 63-105.

Menkes CE, Lengaigne M, Marchesiello P, Jourdain NC, Vincent EM, Lefevre J, Chauvin F, Royer JF (2012). Comparison of tropical cyclogenesis indices on seasonal to interannual timescales. Climate Dynamics, 38(1):301321.

Merrill RT (1988) Environmental influences on hurricane intensification. Journal of the Atmospheric Sciences, 45:1678-1687.

Mo KC, Wang XL, Kistler R, Kanamitsu M, Kalnay E (1995) Impact of satellite data on the CDAS-reanalysis system. Monthly Weather Review, 123:124-139.

Molinari J, Skubis S, Vollaro D, Alsheimer F, Willoughby HE (1998) Potential vorticity analysis of tropical cyclone intensification. Journal of the Atmospheric Sciences, 55:2632-2644.

Nakazawa T (1986) Intraseasonal variations of OLR in the tropics during the FGGE year. Journal of Meteorological Society of Japan, 64:17-34.

Nakazawa T (1988) Tropical super clusters within intraseasonal variations over the western Pacific. Journal of Meteorological Society of Japan, 66:823-839.

Ng EKW, Chan JCL (2011) Interannual variations of tropical cyclone activity over the north Indian Ocean. International Journal of Climatology. doi:10.1002/joc.2304

Oouchi K, Yoshimura J, Yoshimura H, Mizuta R, Kusunoki S, Noda A (2006) Tropical cyclone climatology in a global-warming climate as simulated in a 20 km mesh global atmospheric model: Frequency and wind intensity. Journal of Meteorological Society of Japan, 84:259276.

Palmen EN (1948) On the Formation and structure of tropical hurricane. Geophysica, 3:26-38.

Pant GB, Parthasarathy B (1981) Some aspects of an association between the southern oscillation and Indian summer monsoon. Meteorology and Atmospheric Physics, 29(3):245-252.

Pattanaik DR (2005) Variability of oceanic and atmospheric conditions during active and inactive periods of storms over the Indian region. International Journal of Climatology, 25(11):1523-1530.

Pascual A, Faugre Y, Larnicol G, Le Traon PY (2006) Improved description of the ocean mesoscale variability by combining four satellite altimeters. Geophysical Research Letter 33(2):L02611.

Price JF (1981) Upper ocean response to a hurricane. Journal of Physical Oceanography. 11(2):153-175.

Rajeevan M, De US, Prasad RK (2000) Decadal variation of sea surface temperatures, cloudiness and monsoon depressions in the North Indian ocean. Current Science, 79(3):283-285.

Rao YP (1976) Southwest monsoon. meteorological monograph (synoptic meteorology), No.1/1976, India Meteorological Department, New Delhi.

Rao VB, Ferreira CC, Franchito SH, Ramakrishna SSVS (2008) In a changing climate weakening tropical easterly jet induces more violent tropical storms over the North Indian Ocean. Geophysical Research Letter, 35:2-5.

Rayner NA, Parker DE, Horton EB, Folland CK, Alexander LV, Rowell DP, Kent EC, Kaplan A (2003) Global analyses of sea surface temperature, sea ice, and night marine air temperature since the late nineteenth century. Journal of Geophysical Research, 108(D14):4407.

Reynolds RW, Smith TM, Liu C, Chelton DB, Casey KS, SchlaxMG (2007) Daily high-resolution-blended analyses for sea surface temperature. Journal of Climate, 20:5473-5496.

Ritchie EA (2002) Topic 1.2: Environmental effects. topic chairman and rapporteur reports of the fifth WMO international workshop on tropical cyclones IWTC-V, WMO Tech. Doc. WMO/TD 1136.

Roundy PE, Frank WM (2004) A climatology of waves in the equatorial region. Journal of the Atmospheric Sciences, 61:2105-2132.

Roundy PE (2008) Analysis of convectively coupled Kelvin waves in the Indian Ocean MJO. Journal of the Atmospheric Sciences, 65:1342-1359.

Rui H, Wang B (1990) Development characteristics and dynamic structure of tropical intraseasonal convection anomalies. Journal of the Atmospheric Sciences, 47:357-379.

Sadler JC (1976) A Role of the tropical upper tropospheric trough in early season typhoon development. Monthly Weather Review, 104:1266-1278.

Saji NH, Goswami BN, Vinayachandran PN, Yamagata T (1999) A dipole mode in the tropical Indian Ocean. Nature, 401(6751):360-363.

Santer BD and Coauthors (2006) Forced and unforced ocean temperature changes in Atlantic and Pacific tropical cyclogenesis regions. Proceedings of the National Academy of Sciences, 103:13905-13910.

SSALTO/DUACS User handbook (2010), (M)SLA and (M)ADT near-real time and delayed time products, cLS-DOS-NT-06.034.

Schade LR, Emanuel KA (1999) The oceans effect on the intensity of tropical cyclones: Results from a simple coupled atmosphere-ocean model. Journal of the Atmospheric Sciences, 56:642-651.

Shay LK, Goni G, Black PG (2000) Effects of a warm oceanic feature on Hurricane Opal. Monthly Weather Review, 128:1366-1383.

Shapiro MA, Kennedy PJ (1981) Research aircraft measurements of jet stream geostrophic and ageostrophic winds. Journal of Atmospheric Sciences, 38:2642-2652.

Sikka DR (1977) Some aspects of the life history, structure and movement of monsoon depressions. Pure and Applied Geophysics, 115:1501-1529.

Sikka DR (1980) Some aspects of the large-scale fluctuations of summer monsoon rainfall over India in relation to fluctuations in the planetary and regional scale circulation parameters, Proceedings of the Indian Academy of Sciences-Earth and Planetary Sciences, 89(2):179-195.

Simmons A, Uppala S, Dee D, Kobayashi S (2006) ERA-Interim: New ECMWF reanalysis products from 1989 onwards. ECMWF Newsletter 110:26-35.

Singh OP (2007) Long-term trends in the frequency of severe cyclones of Bay of Bengal: observations and simulations. Mausam, 58:59-66.

Singh OP (2008) Indian ocean dipole mode and tropical cyclone frequency. Current Science, 94(1):29-32

Singh OP, Ali Khan TM, Rahman MS (2000) Changes in the frequency of tropical cyclones over the North Indian Ocean, Meteorology and Atmospheric Physics, 75(1-2):11-20.

Smith TM, Reynolds RW (2003) Extended reconstruction of global sea surface temperatures based on COADS data (1854-1997). Journal of Climate, 16:1495-1510.

Smith TM, Reynolds RW, Peterson TC, Lawrimore J (2008) Improvements to NOAA's historical merged land-ocean surface temperature analysis (1880-2006). Journal of Climate, 21:2283-2296.

Solomon S, Qin D, Manning M, Chen Z, Marquis M, Averyt KB, Tignor M, Miller HL (2007) IPCC Climate Change 2007: The physical science basis. Contribution of Working Group I to the Fourth Assessment Report of the Intergovernmental Panel on Climate Change, Cambridge University Press, Cambridge, United Kingdom and New York, NY, USA (2007).

Sugi M, Noda A, Sato N (2002) Influence of the global warming on tropical cyclone climatology: An experiment with the JMA global climate model. Journal of Meteorological Society of Japan, 80:249-272.

Tippett MK, Camargo SJ, Sobel AH (2011). A Poisson regression index for tropical cyclone genesis and the role of large-scale vorticity in genesis. Journal of Climate, 24(9):2335-2357.

Trenberth KE, Stepaniak DP, Hurrell JW, Fiorino M, (2001) Quality of Reanalyses in the Tropics. Journal of Climate, 14:14991510.

Tyagi A, Mohapatra M, Bandyopadhyay BK, Singh C, Kumar N (2010) The first ever super cyclonic storm GONU over the Arabian Sea during 1-7 June 2007: A case study. In: Charabi Y (ed) Indian Ocean tropical cyclones and climate change. Springer Science + Business Media B.V. 305-313.

Uccellini LW, Johnson DR (1979) The coupling of upper and lower tropospheric jet streaks and implications for the development of severe convective storms. Monthly Weather Review, 107:682-703.

Uccellini LW, Kocin PJ (1987) The Interaction of jet streak circulations during heavy snow events along the east coast of the United States. Weather and Forecasting, 2:289-308.

Vecchi GA, Soden BJ (2007) Effect of remote sea surface temperature change on tropical cyclone potential intensity. Nature, 450:1066-1070.

Wada A, Usui N (2007) Importance of tropical cyclone heat potential for tropical cyclone intensity and intensification in the Western North Pacific. Journal of Oceanography, 63:427-447.

Wallace JM, Hobbs PV (2006) Atmospheric science - an introductory survey. Academic Press, 369 pp.

Webster PJ, Fasullo J (2003) Monsoon: dynamical theory. Encyclopedia of atmospheric sciences, Holton J and Curry JA, Eds., Academic Press, 13701386.

Webster PJ, Holland GJ, Curry JA, Chang HR (2005) Changes in tropical cyclone number, duration, and intensity in a warming environment. Science, 309:1844-1846.

Wheeler MC, Hendon HH (2004) An all-season real-time multivariate MJO index: development of an index for monitoring and prediction. Monthly Weather Review, 132:1917-1932.

Whitney LD, Hobgood JS (1997). The Relationship between sea surface temperatures and maximum intensities of tropical cyclones in the Eastern North Pacific ocean. Journal of Climate, 10:2921-2930.

WMO (2006) Atmospheric research and environment programme. Summary statement on tropical cyclones and climate change, http://www.wmo.int/pages/prog/arep/tmrp/documents/iwtcstatement.pdf

WMO (2010) Tropical cyclone operational plan for the Bay of Bengal and the Arabian Sea, Edition 2010. Technical Document WMO/TD-No.84, World Meteorological Organization, Geneva, Switzerland.

Wong MLM, Chan JCL (2004) Tropical cyclone intensity in vertical wind shear. Journal of the Atmospheric Sciences, 61:1859-1876.

Wu CC, Cheng H (1999) An observational study of environmental influences on the intensity changes of typhoons Flo (1990) and Gene (1990). Monthly Weather Review. 127:3003-3031.

Wu CC, Lee CY, Lin II (2007) The effect of the ocean eddy on tropical cyclone intensity; Journal of the Atmospheric Sciences, 64:3562-3578.

Xavier PK, Joseph PV (2000) Vertical wind shear in relation to frequency of monsoon depressions and tropical cyclones of Indian Seas. In: Proceedings.

TROPMET-2000, National symposium on ocean and atmosphere, Cochin, India, Indian Meteorological Society pp 232-245.

Xue Y, Smith TM, Reynolds RW (2003) Interdecadal changes of 30-yr SST normals during 1871-2000. Journal of Climate, 16:1601-1612.

Yoshimura J, Masato S, Noda A (2006) Influence of greenhouse warming on tropical cyclone frequency. Journal of Meteorological Society of Japan, 84:405-428.

Yu H, Kwon HJ (2005) Effect of TC-trough interaction on the intensity change of two typhoons. Weather and forecasting, 20:199-211.

Yu J, Wang Y (2009) Response of tropical cyclone potential intensity over the north Indian Ocean to global warming. Geophysical Research Letters, 36(3):1-5.

Zeng Z, Wang Y, Wu C-C (2007) Environmental dynamical control of tropical cyclone intensity-An observational study. Monthly Weather Review, 135(1):38-59.

Ziv B, Paldor N (1999) The divergence fields associated with time-dependent jet streams. Journal of the atmospheric sciences, 56:1843-1857.

Zehr R (1992) Tropical cyclogenesis in the Western North Pacific, NOAA Technical Report NESDIS 61 pp. 181.

List of Publications

Papers published in Journals and Proceedings

1. Krishnamohan, K. S., Mohanakumar, K., and Joseph, P. V., (2012). ***The influence of MaddenJulian Oscillation in the genesis of North Indian Ocean tropical cyclones.*** Theoretical and Applied Climatology, 109(1), 271282. doi:10.1007/s00704-011-0582-x

2. Krishnamohan, K. S., Mohanakumar, K., and Joseph, P. V., ***Decadal Variation in the Intensity and Frequency of Tropical Cyclones and Monsoon Depressions of North Indian Ocean.*** *(Communicated)*

3. Krishnamohan, K. S., Mohanakumar, K., and Joseph, P. V., ***Rapid intensification of cyclone Gonu over the Arabian Sea in June 2007***. *(Communicated)*

4. Krishnamohan, K. S., Mohanakumar, K., and Joseph, P. V., ***Climate Change in Tropical Cyclones and Monsoon Depressions of North Indian Ocean.*** In:*(Extended Abstracts)* Second WMO International Conference on Indian Ocean Tropical Cyclones and Climate Change, , New Delhi, 2012.

Papers Presented in International Conferences

1. Krishnamohan, K. S., Mohanakumar, K., and Joseph, P. V., ***Climate Change in Tropical Cyclones and Monsoon Depressions of North Indian Ocean.*** Second WMO International Conference on Indian Ocean Tropical Cyclones and Climate Change, New Delhi, 2012.